The Abdus Salam
International Centre
for Theoretical Physics

United Nations Educational, Scientific and Cultural Organization

IAEA International Atomic Energy Agency

The International Union of Geodesy and Geophysics

2373-15

Workshop on Geophysical Data Analysis and Assimilation

29 October - 3 November, 2012

Physical properties of the lithosphere-asthenosphere system

Fabio Romanelli

Department of Mathematics & Geosciences
University of di Trieste/ICTP
Trieste

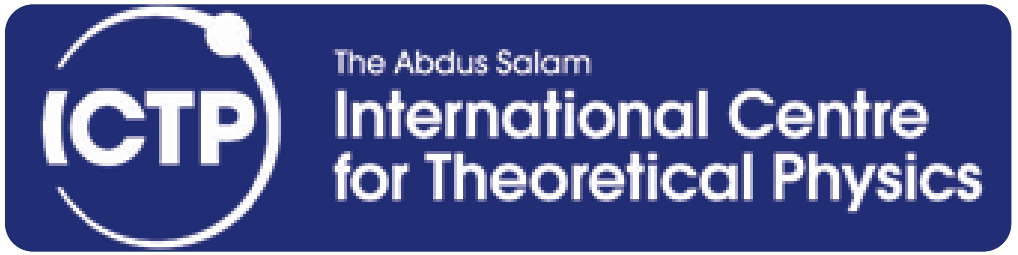

Workshop on Geophysical Data Analysis and Assimilation

Physical properties of the lithosphere-asthenosphere system

Fabio Romanelli

with the contribution of:
(E. Brandmayr, R. Raykova, G. Panza & many others...)

Department of Mathematics & Geosciences, University of di Trieste
SAND Group - ICTP - The Abdus Salam International Centre for Theoretical Physics

romanel@units.it

Rheology

The response of polymeric liquids, such as melts and solutions, to an imposed stress may under certain conditions resemble the behavior of a solid or a liquid, depending on the situation.

Reiner used the biblical expression that "mountains flowed in front of God" to define the DEBORAH number:

$$De = \frac{\text{time of relaxation}}{\text{time of observation}}$$

Solid-like response: $De \rightarrow \infty$

Liquid-like response: $De \rightarrow 0$

Rheology is the science of the deformation and flow of materials.

M. Reiner is credited with naming the Deborah Number after the song of Deborah, Judges 5:5- "The mountains flowed before the Lord"(Fig. 3.10). It was first mentioned in his article "The Deborah Number" in the January 1964 issue of Physics Today.

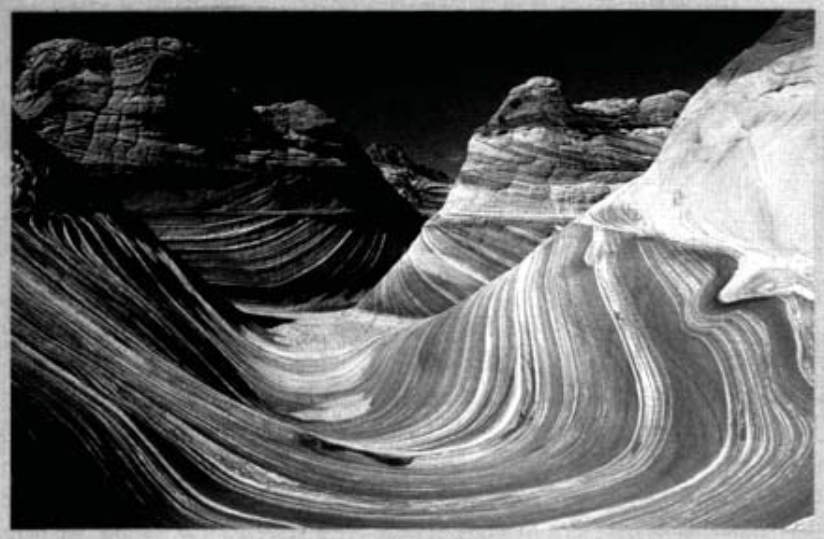

Figure. 3.10 Nestles Canyon, Arizona. Courtesy of Wolfgang Cohnen (©1997)

Earth-deformation Processes - spectrum I

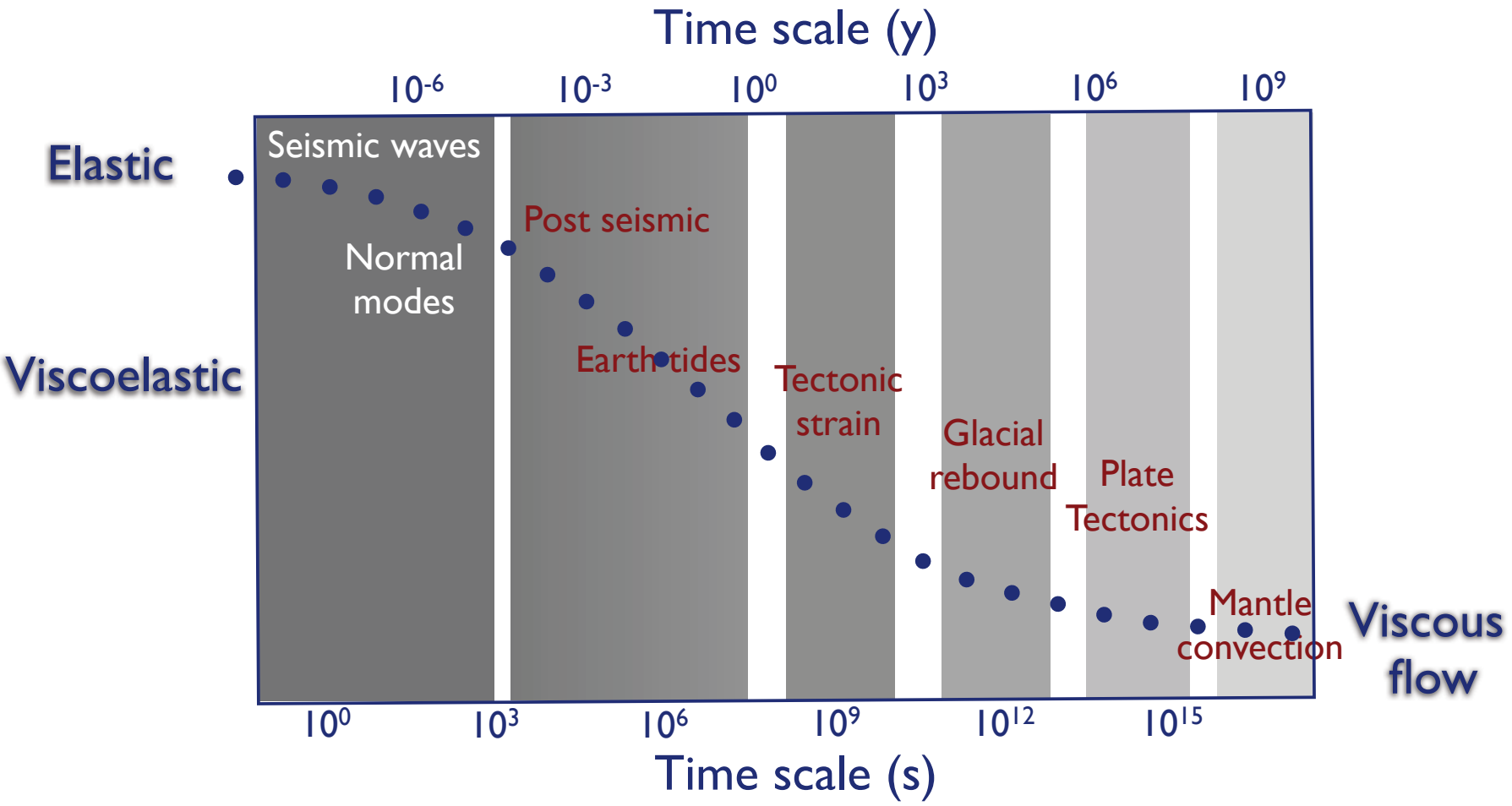

Modified from: Kennett; & Bunge, 2008.
Geophysical Continua: Deformation in the Earth's Interior

Earth-deformation Processes - spectrum II

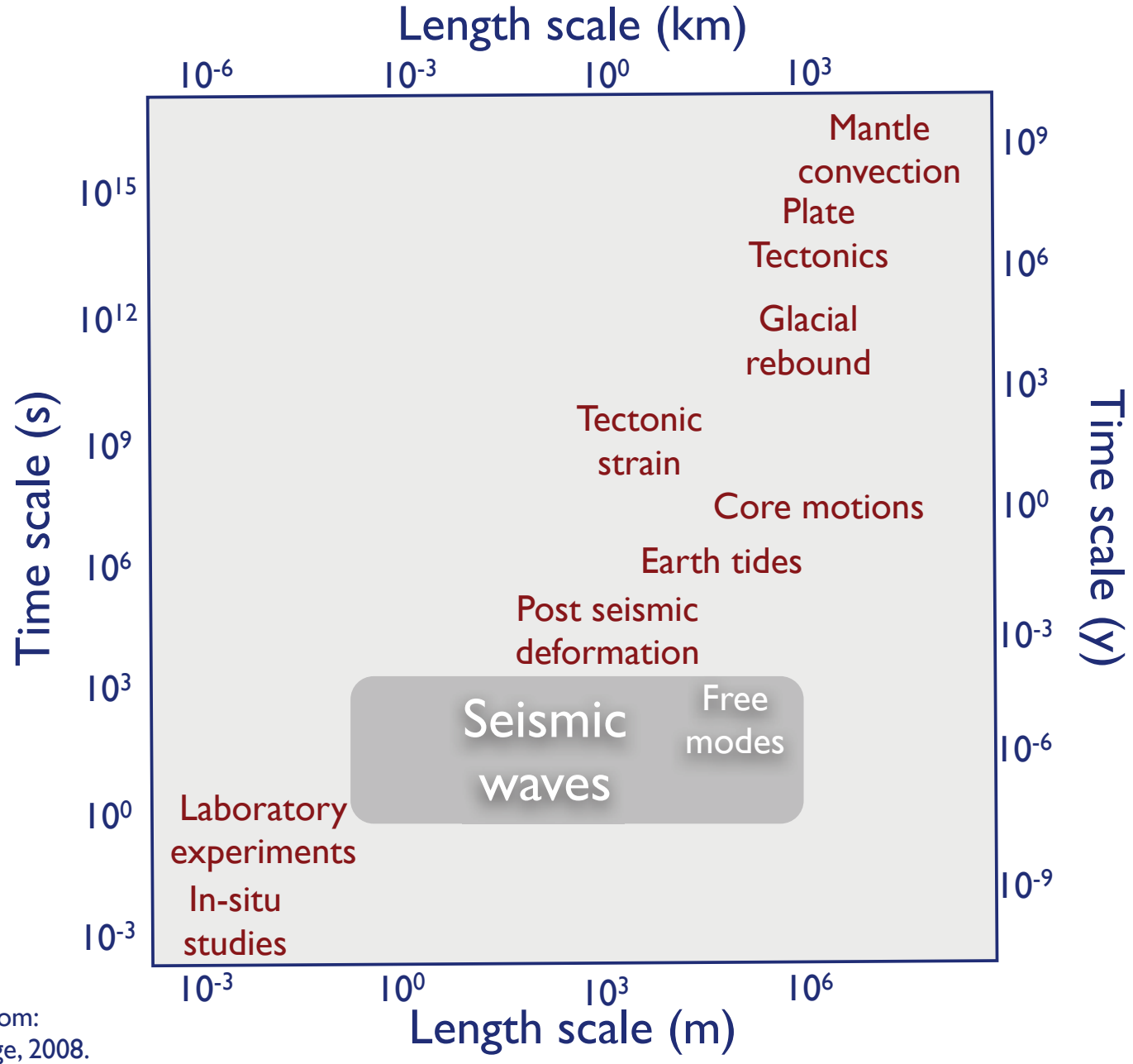

Modified from:
Kennett; & Bunge, 2008.

Elusive lithosphere and its proxies

- The lithosphere–asthenosphere boundary (LAB) is a first-order structural discontinuity that accommodates differential motion between tectonic plates and the underlying mantle. Although it is the most extensive type of plate boundary on the planet, its definitive detection, especially beneath cratons, is proving elusive. Different proxies are used to demarcate the LAB, depending on the nature of the measurement.

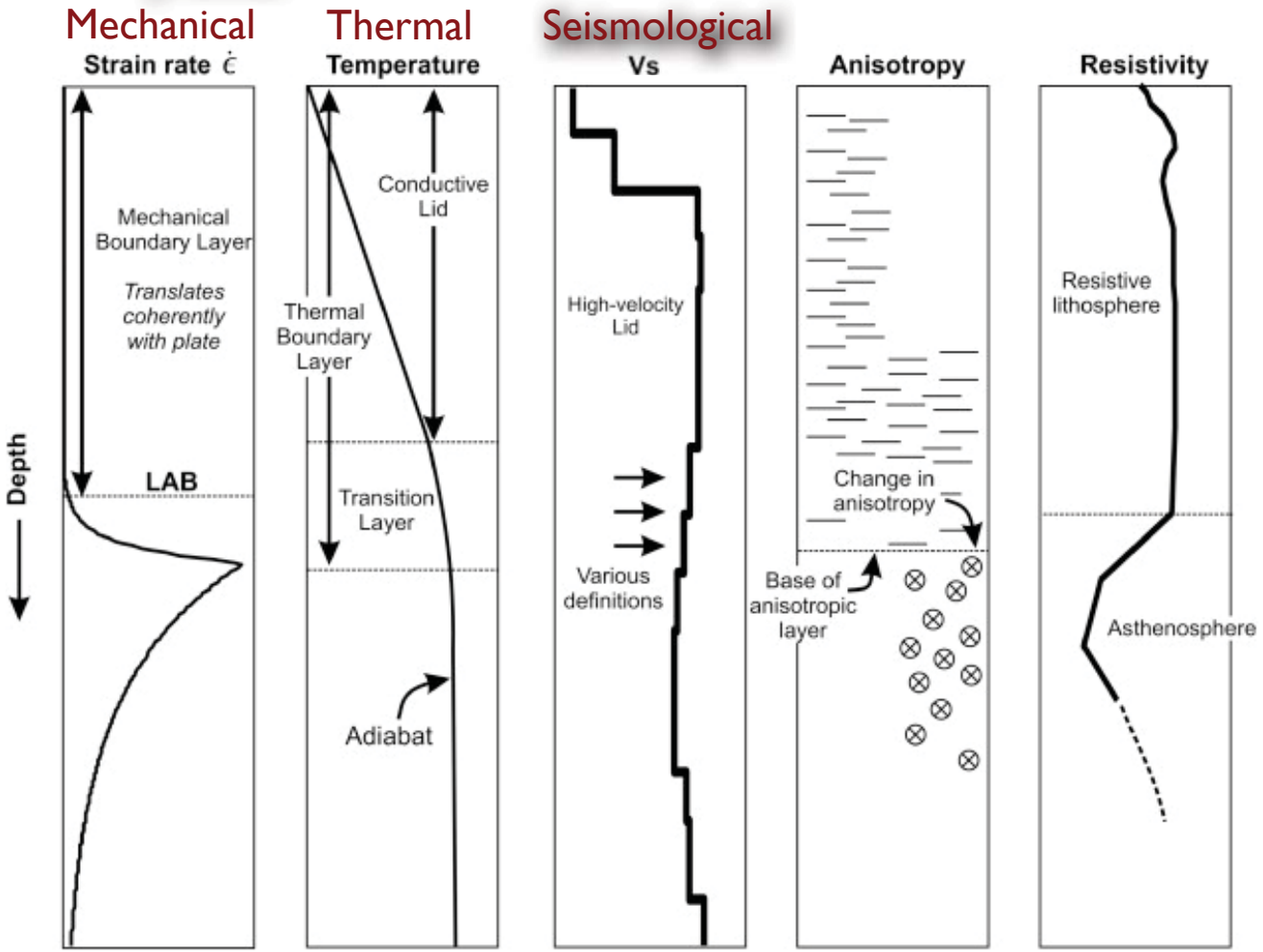

The thermal boundary layer (TBL), containing a conductive lid and a transition layer, represents a near-surface region where temperature deviates from the adiabat. A zone of low seismic shear-wave velocity (Vs) is sometimes detected beneath a high-velocity lid; various definitions have been used to correlate this zone with the LAB. The LAB may also correlate with a downward extinction of seismic anisotropy or a change in the direction of anisotropy and . The electrical LAB is marked by a significant reduction in electrical resistivity.

Eaton et al., 2009

G & seismic rays

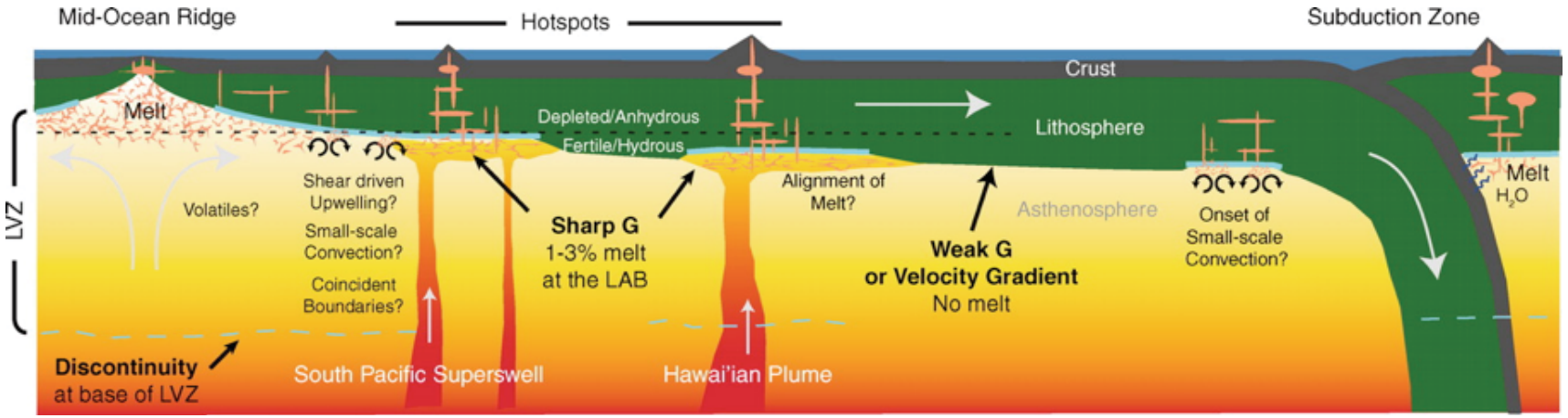

Cross-sectional portrayal of proposed mechanisms for the origin of a high-reflectivity G beneath the Pacific. The reflectivity of the G is enhanced by the stagnation of partial melt at the base of the lithosphere (blue lines).

Another deeper discontinuity (blue dashed lines) predominantly occurs beneath major hotspots, mid-ocean ridges, and subduction zones and lies at the base of the LVZ. Underside reflections from the G do not form where the seismic discontinuity has a weak velocity contrast or a broad velocity gradient.

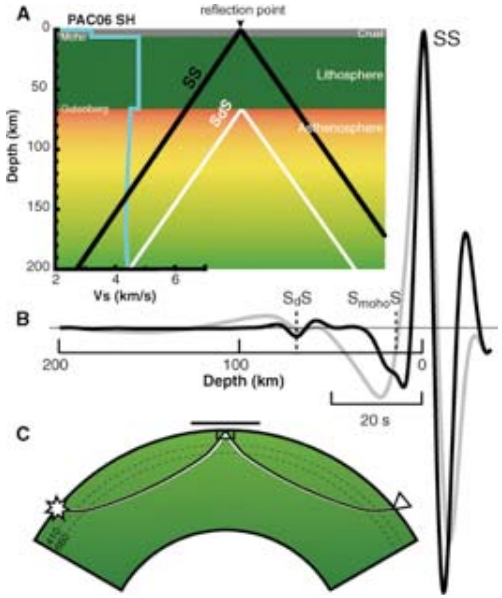

Schmerr, N., (2012), The Gutenberg Discontinuity: Melt at the Lithosphere-Asthenosphere Boundary, Science, 335, 1480-1483.

Road map

- Methodology:
  - Surface wave dispersion analysis
  - Surface wave tomography
  - Non linear inversion of dispersion data
- Cellular models for the lithosphere-asthenosphere system
  - Optimization techniques
  - Scale level I: 1°x1° cells in the whole Italian region
  - Adding other geophysical constraints
  - Selected sections and geodynamic modelling
- Possible applications
  - Joint inversion
  - Seismic hazard studies

Surface waves

On Waves Propagated along the Plane Surface of an Elastic Solid. *By* Lord RAYLEIGH, D.C.L., F.R.S.

[*Read November 12th*, 1885.]

It is proposed to investigate the behaviour of waves upon the plane free surface of an infinite homogeneous isotropic elastic solid, their character being such that the disturbance is confined to a superficial region, of thickness comparable with the wave-length. The case is thus analogous to that of deep-water waves, only that the potential energy here depends upon elastic resilience instead of upon gravity.*

Denoting the displacements by α, β, γ, and the dilatation by θ, we have the usual equations

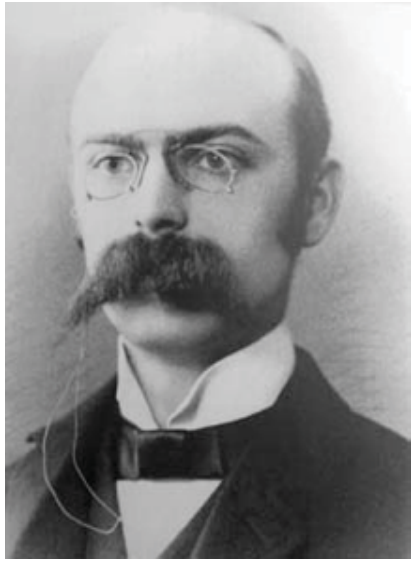

SOME PROBLEMS
OF
GEODYNAMICS

BEING AN ESSAY TO WHICH THE ADAMS PRIZE
IN THE UNIVERSITY OF CAMBRIDGE
WAS ADJUDGED IN 1911

BY

A. E. H. LOVE, M.A., D.Sc., F.R.S.
FORMERLY FELLOW OF ST JOHN'S COLLEGE, CAMBRIDGE
HONORARY FELLOW OF QUEEN'S COLLEGE, OXFORD
SEDLEIAN PROFESSOR OF NATURAL PHILOSOPHY IN THE UNIVERSITY OF OXFORD

Cambridge:
at the University Press
1911

Surface waves - reprised

- Condition of existence:
  - Discontinuity (boundary waves, undispersed: Rayleigh, Stoneley)
  - Waveguide (interferential & dispersed: Love & Rayleigh)

Surface waves - reprised

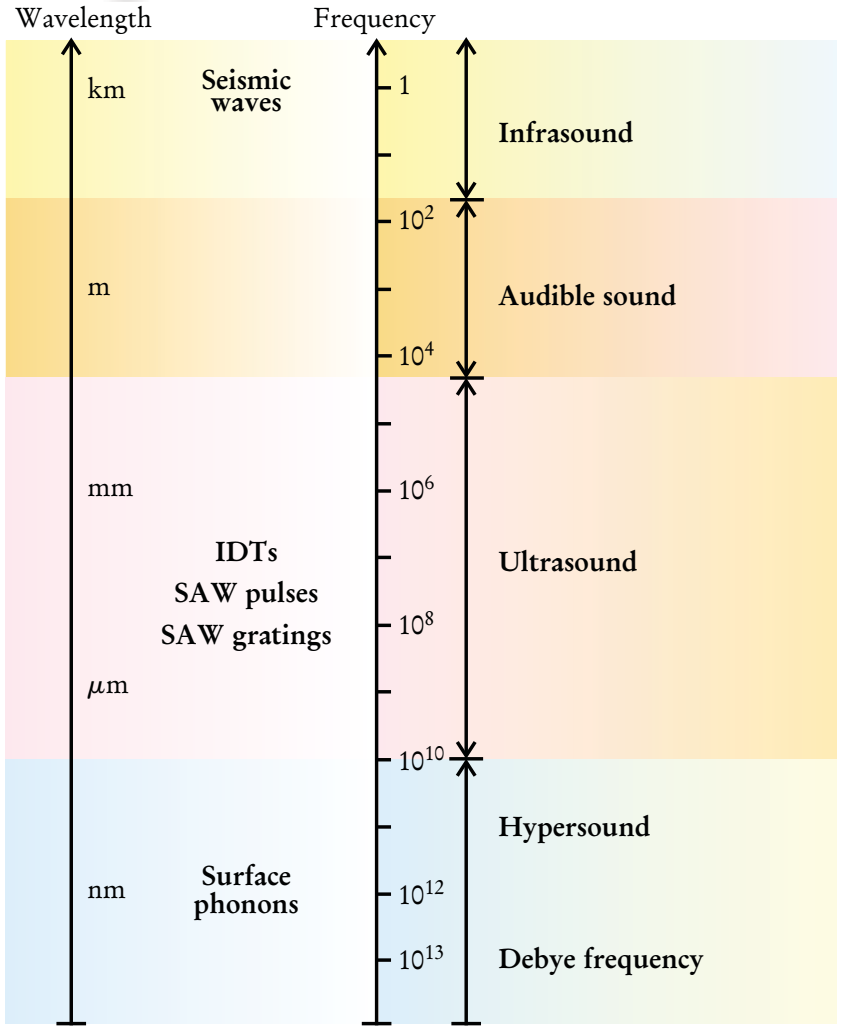

FIGURE 2. SURFACE ACOUSTIC WAVES can be found over a broad frequency spectrum. Current research extends from seismic waves in the infrasound region to interdigital transducers (IDTs) and to laser-generated SAW pulses and transient gratings in the ultrasound region.

Surface waves - reprised

- Condition of existence:
  - Discontinuity (boundary waves, undispersed: Rayleigh, Stoneley)
  - Waveguide (interferential & dispersed: Love & Rayleigh)

T (s)	f (Hz)	λ (km)	c (km/s)	d (km)	application
0.02-0.1	10-50	0.002-0.05	0.1-0.5	0.02	engineering, geophysics
0.2-1	1-5	0.15-1.50	0.1-1.5	0.2	upper sediments
5-10	0.1-0.2	7-30	2-3	5	sedimentary basins
10-35	0.03-0.1	30-100	3.0-3.5	40	crust
35-350	0.005-0.03	200-1000	4-5	300	upper mantle

Dispersion relation

- In physics, the dispersion relation is the relation between the energy of a system and its corresponding momentum. For example, for massive particles in free space, the dispersion relation can easily be calculated from the definition of kinetic energy.

- For electromagnetic waves, the energy is proportional to the frequency of the wave and the momentum to the wavenumber. In this case, Maxwell's equations tell us that the dispersion relation for vacuum is linear: $\omega = ck$.

- The name "dispersion relation" originally comes from optics. It is possible to make the effective speed of light dependent on wavelength by making light pass through a material which has a non-constant index of refraction, or by using light in a non-uniform medium such as a waveguide. In this case, the waveform will spread over time, such that a narrow pulse will become an extended pulse, i.e. be dispersed.

Effect of dispersion...

Demonstration: sum two harmonic waves with slightly different angular frequencies and wavenumbers:

$$u(x, t) = \cos(\omega_1 t - k_1 x) + \cos(\omega_2 t - k_2 x)$$

$$\omega_1 = \omega + \delta\omega \qquad \omega_2 = \omega - \delta\omega \qquad \omega \gg \delta\omega$$

$$k_1 = k + \delta k \qquad k_2 = k - \delta k \qquad k \gg \delta k$$

Add the two cosines:

$$\begin{aligned} u(x, t) &= \cos(\omega t + \delta\omega t - kx - \delta kx) \\ &\quad + \cos(\omega t - \delta\omega t - kx + \delta kx) \\ &= 2\cos(\omega t - kx)\cos(\delta\omega t - \delta kx) \end{aligned}$$

The envelope (beat) has a *group velocity*:

$$U = \delta\omega/\delta k$$

The individual peaks move with a *phase velocity*:

$$c = \omega/k$$

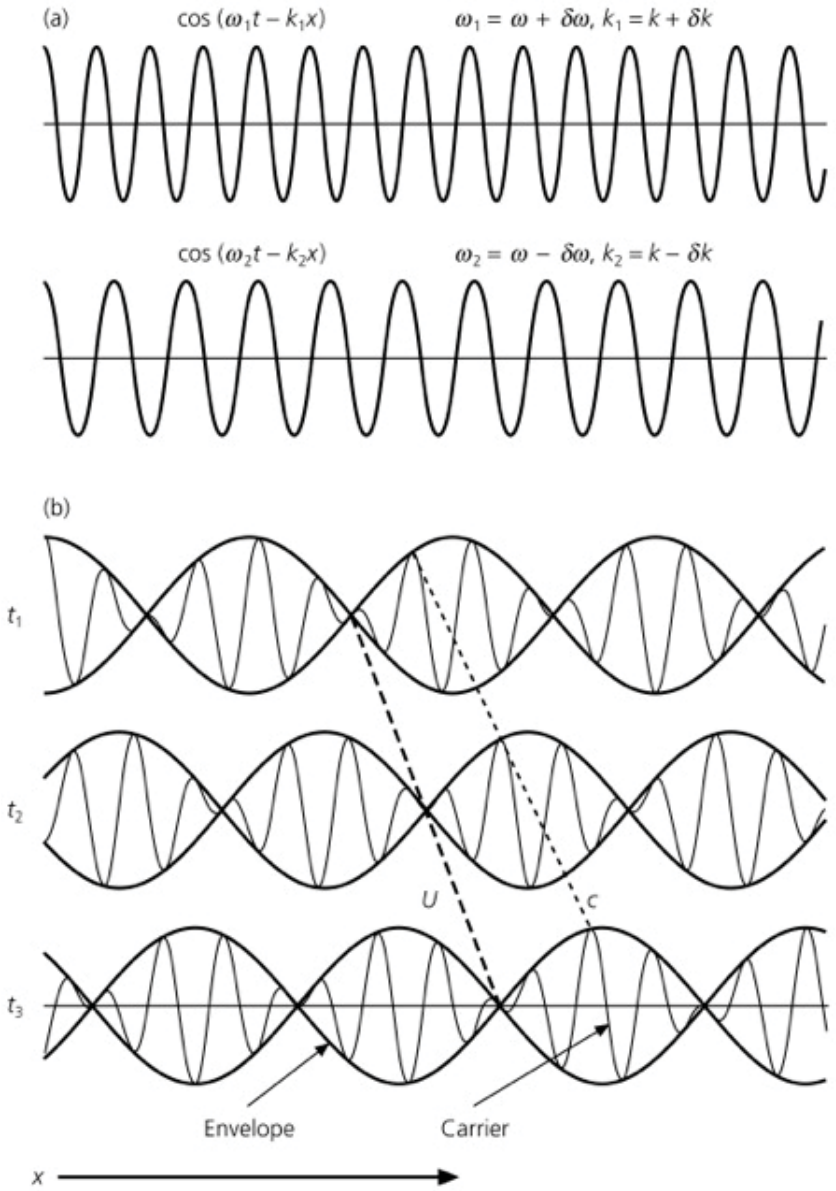

Group velocity

- Another consequence of dispersion manifests itself as a temporal effect. The phase velocity is the velocity at which the phase of any one frequency component of the wave will propagate. This is not the same as the group velocity of the wave, which is the rate that changes in amplitude (known as the envelope of the wave) will propagate. The group velocity vg is related to the phase velocity v by, for a homogeneous medium (here λ is the wavelength in vacuum, not in the medium):

$$v_g = \frac{d\omega}{dk} = \frac{d(vk)}{dk} = v + k\frac{dv}{dk} = v - \lambda\frac{dv}{d\lambda}$$

and thus in the normal dispersion case v_g is always < v !

Dispersion...

- The group velocity itself is usually a function of the wave's frequency. This results in group velocity dispersion (GVD), that is often quantified as the group delay dispersion parameter : If D is < 0, the medium is said to have positive dispersion. If D is > 0, the medium has negative dispersion.

$$D = \frac{dv_g}{d\omega}$$

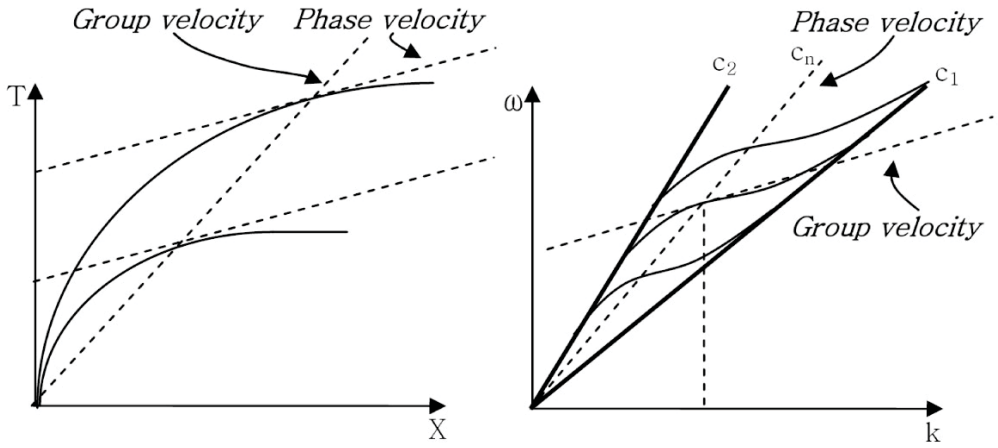

Airy Phase

wave that arises if the phase and the change in group velocity are stationary and gives the highest amplitude in terms of group velocity and are prominent on the seismogram.

Dispersion and structural information

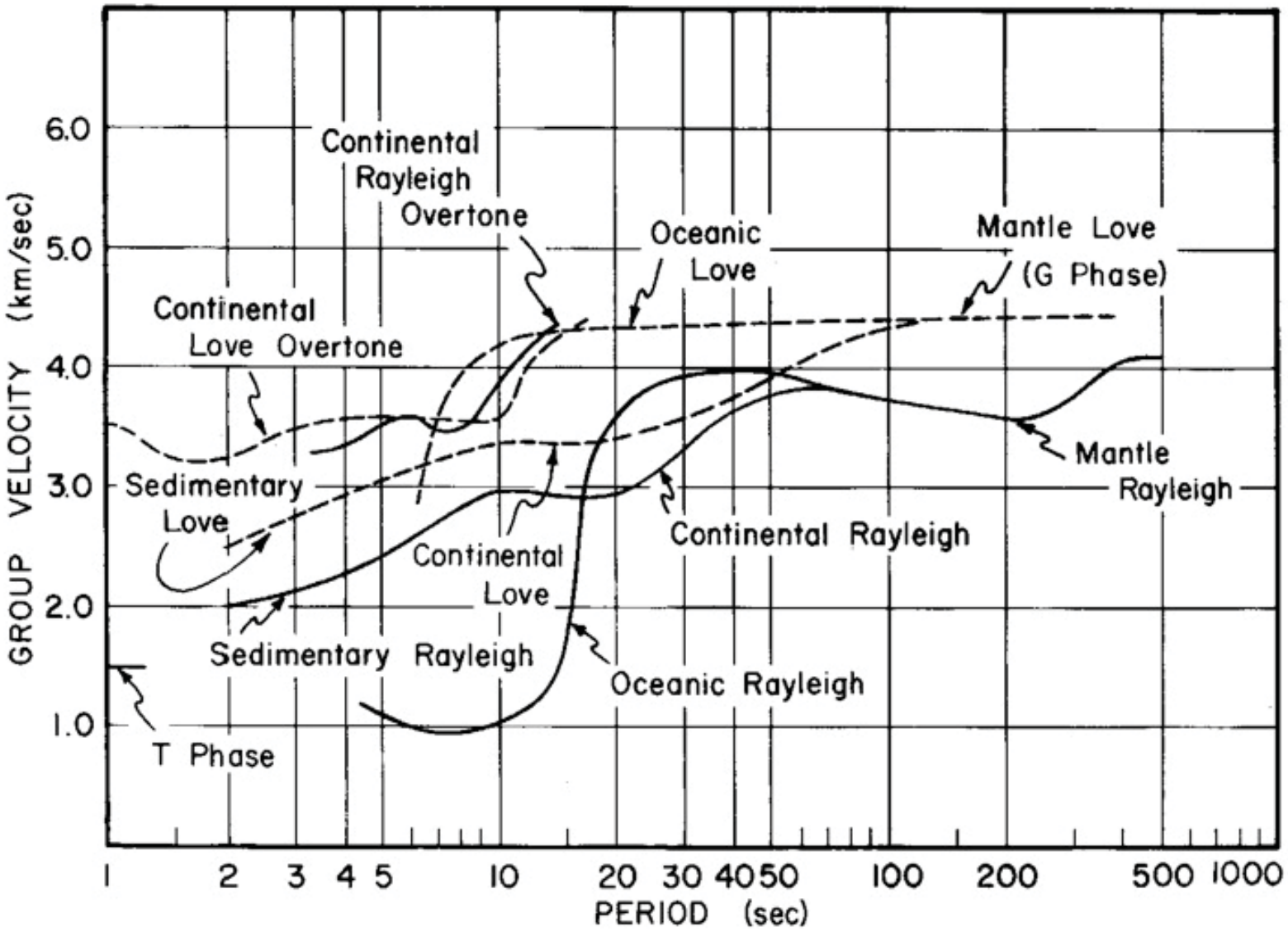

Figure 1.2.1b Composite of dispersion curves for surface waves.

Manual of Seismological Observatory Practice (1979 Edition)

Dispersion

Love wave V_g dispersion shown by a seismogram from a Mongolian eq. recorded in Japan.

From Stein & Wysession, 2003.

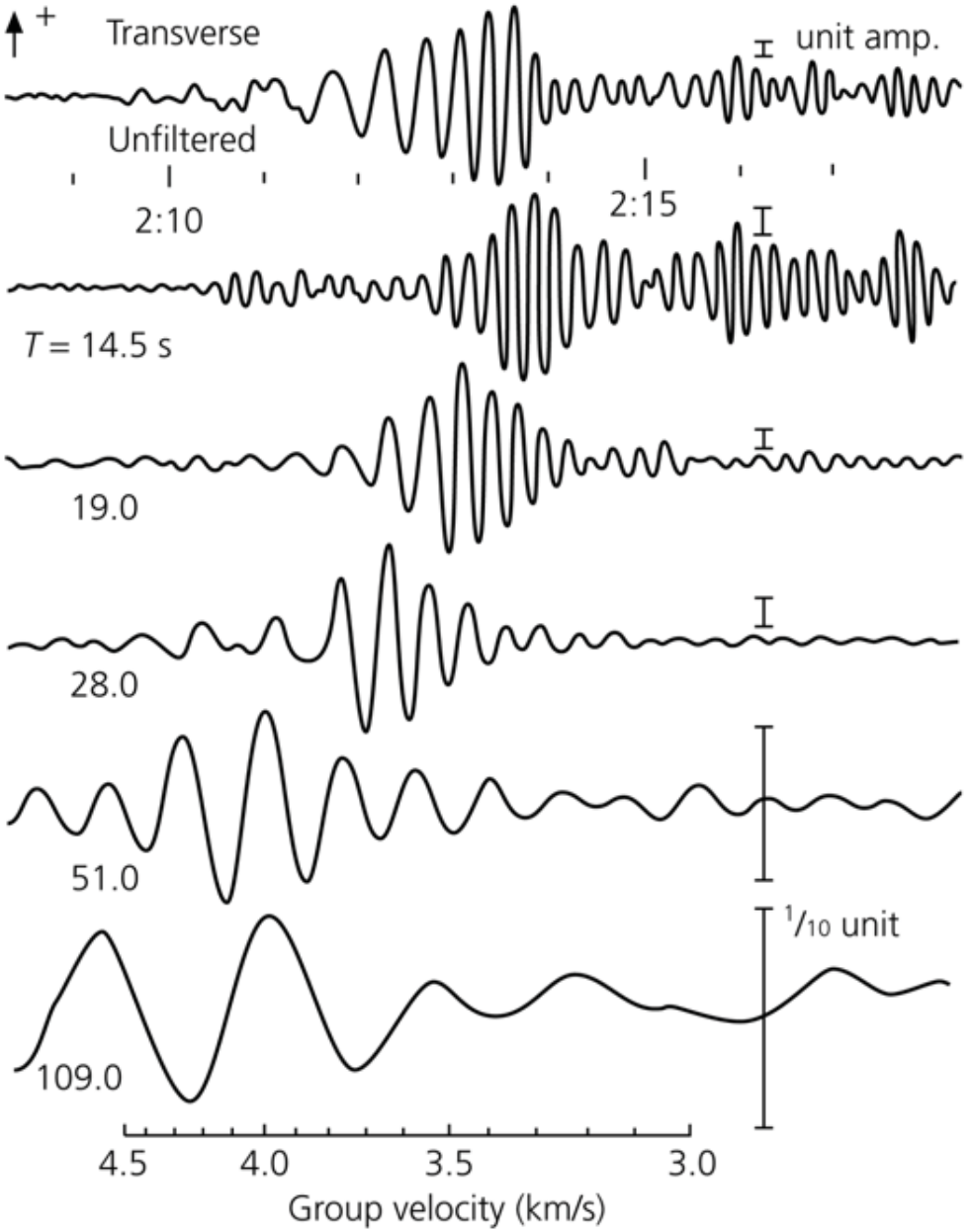

Methodology - Scale level I

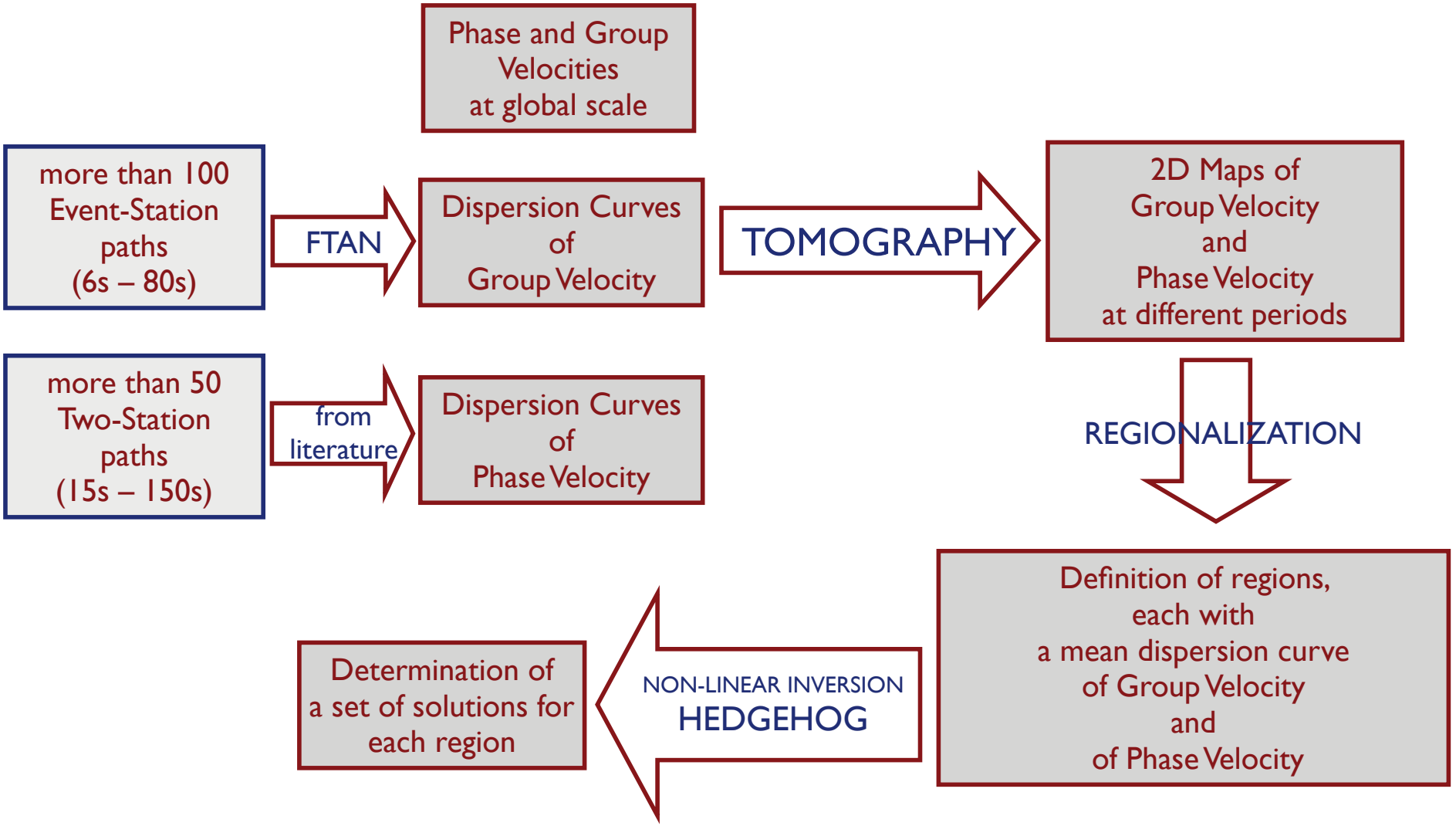

Studied region

The Italic region with studied cells sized 1°x1°. The main tectonic features and volcanoes are indicated. The colored areas indicate the grouping of cells which V_S models will be presented

Modified from Brandmayr et al., 2010

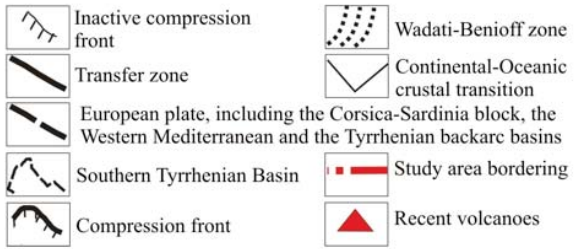

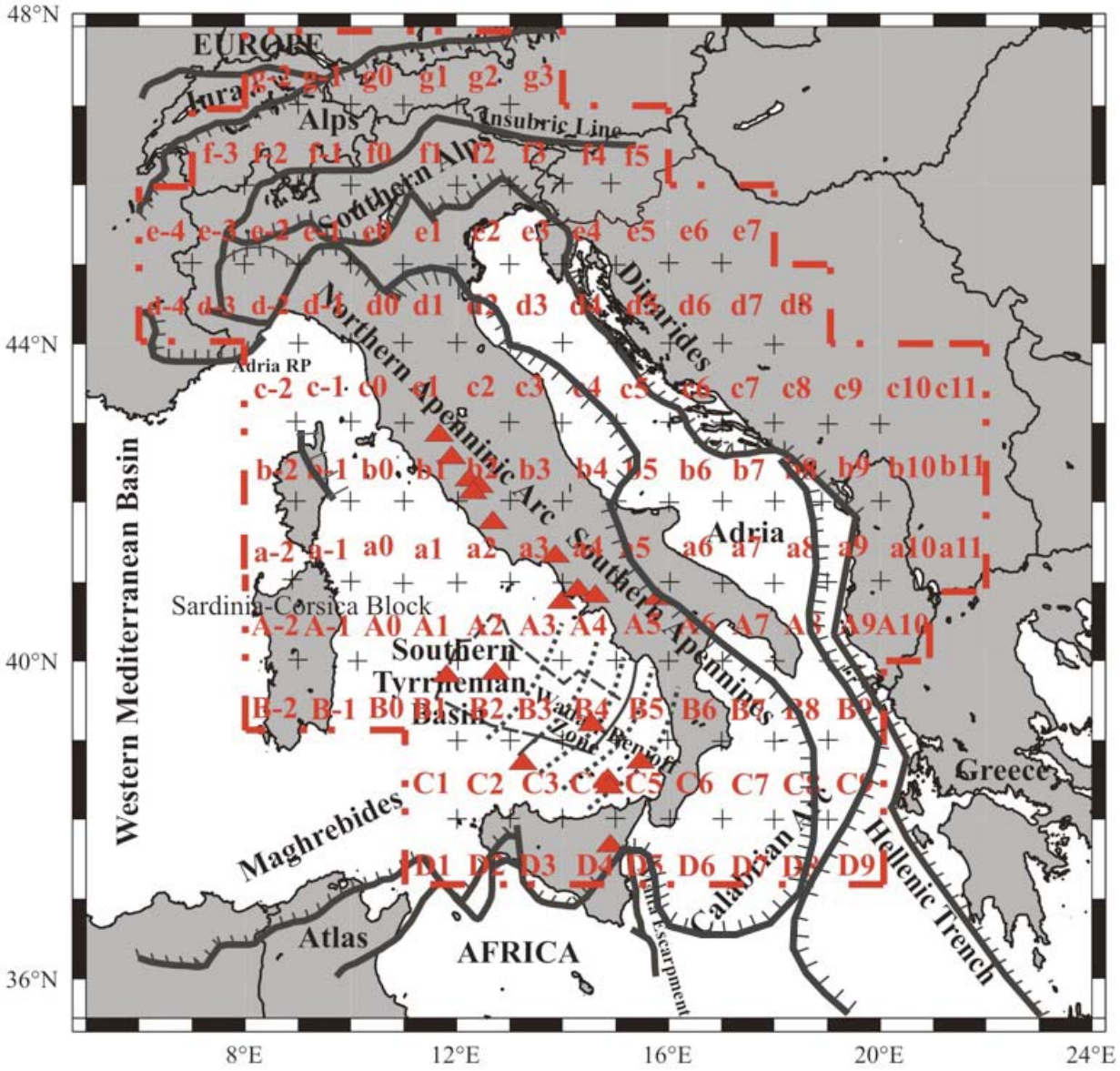

Paths...

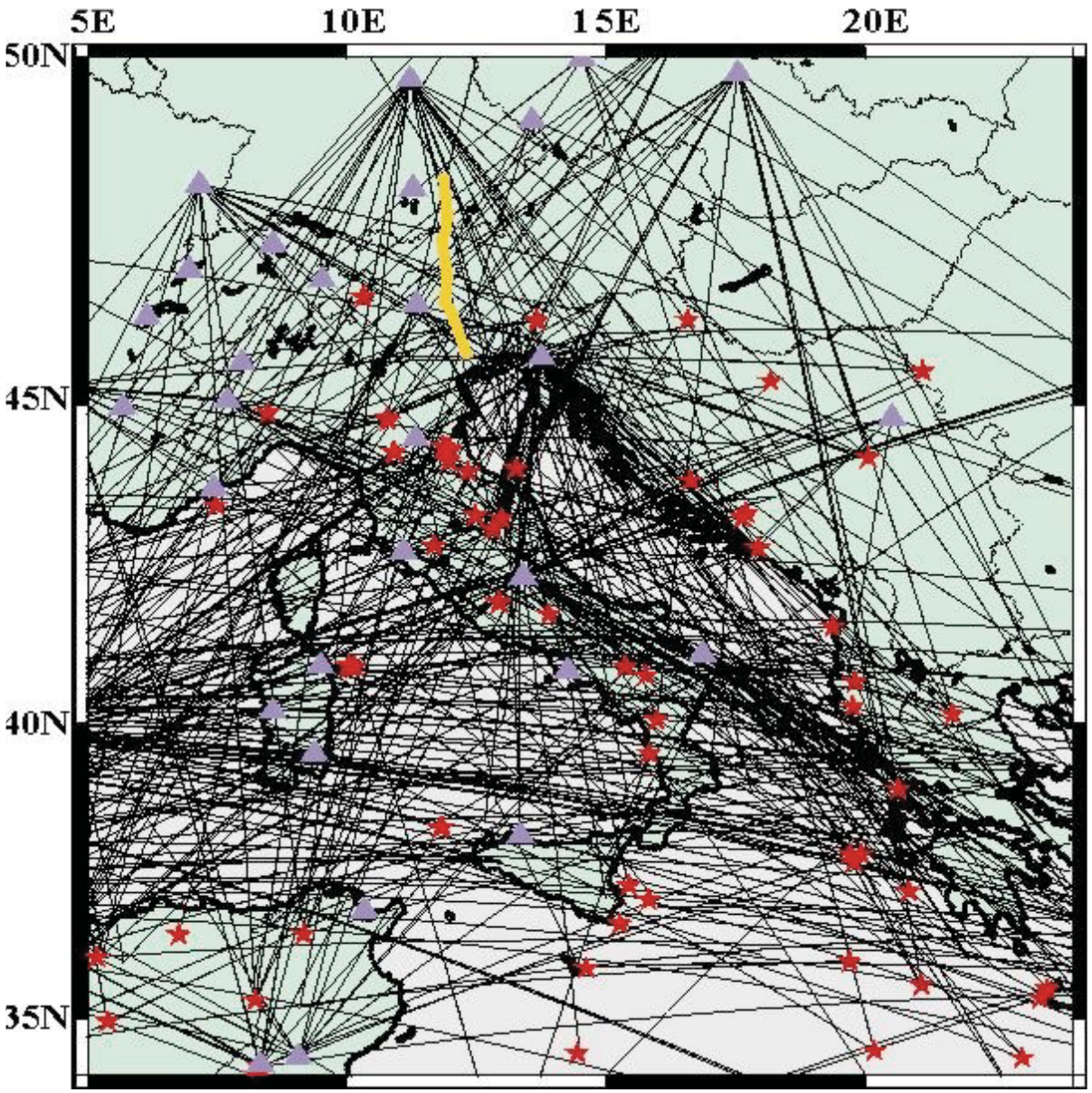

Paths from epicenters to stations in the study area

Transalp profile

Modified from Panza et al., 2007

FTAN

- Frequency-Time representation:
  - Gaussian filters; FTAN maps
  - Floating filters: Phase equalization

e.g. Levshin et al., 1972

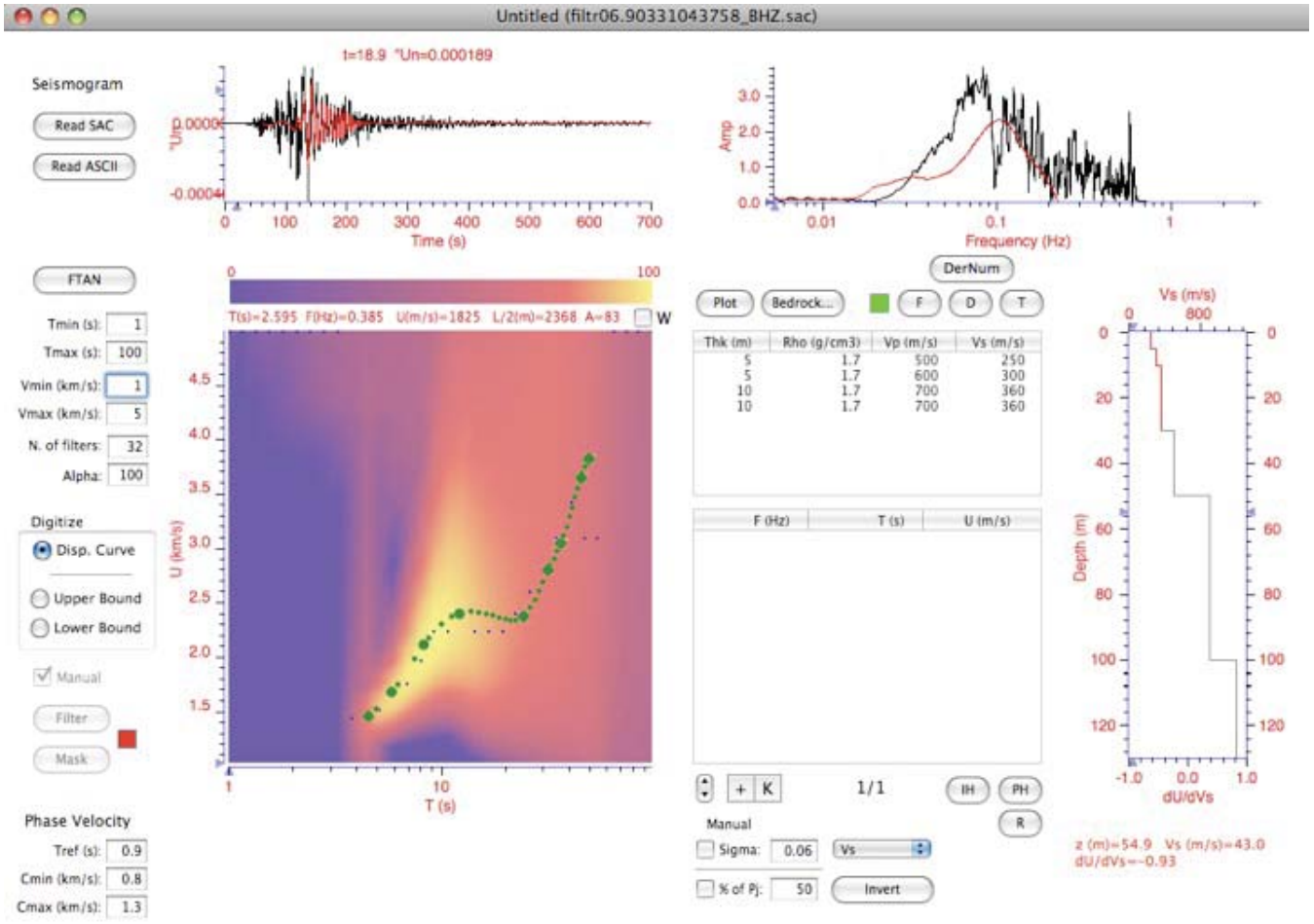

from XFTAN2012 (F. Vaccari)

FTAN - Tsunami signal

Untitled (japan10012.tsz.00001.ft)

Dist. (km): 269.39
Samples: 4096
dt (s): 24.414

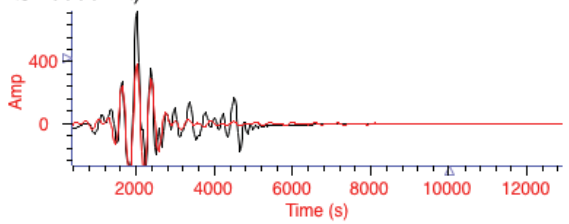

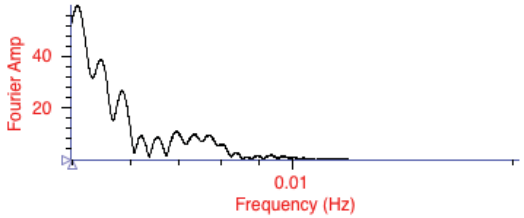

FTAN analysis

Tmin (s): 73.233
Tmax (s): 10000.
Umin (km/s): 0.055
Umax (km/s): 1.576
N. Filters: 32
Alpha: 100

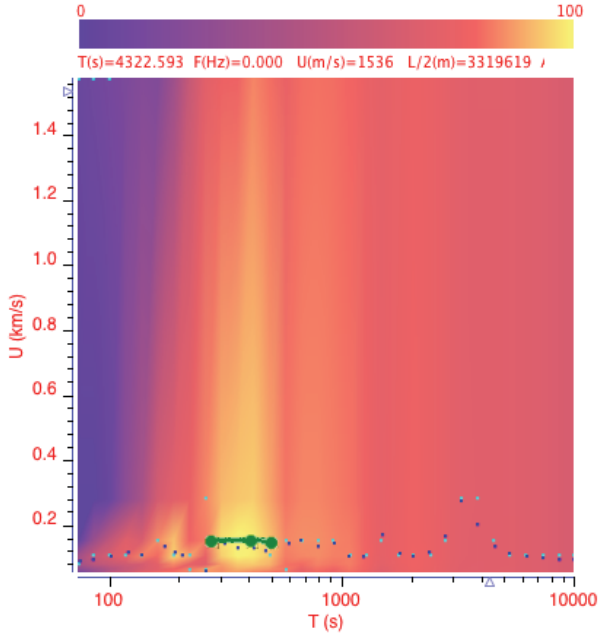

Structural Model

Depth (m)	Thk (m)	D (g/cm3)	Vp (m/s)	Vs (m/s)	Qp	Qs
5	5	1.7	500	250	220	100
10	5	1.7	600	300	220	100
20	10	1.7	700	350	220	100
30	10	1.7	800	400	220	100
50	20	1.8	900	500	220	100
100	50	1.9	1600	900	220	100
200	100	2	2000	1200	220	100
500	300	2.3	2250	1300	220	100
1000	500	2.3	2600	1500	220	100
1500	500	2.3	3200	1800	220	100
2000	500	2.3	3600	2100	220	100
2500	500	2.3	4000	2300	220	100
3000	500	2.3	4400	2500	220	100
3500	500	2.45	4800	2700	220	100
4000	500	2.5	5400	3100	220	100

Fundamental Mode

F (Hz)	T (s)	U (m/s)	C (m/s)

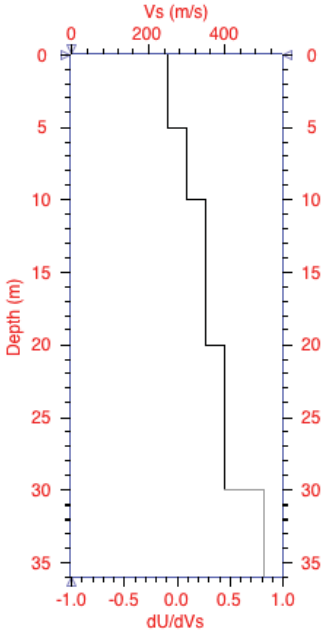

FTAN - Acoustic signal

nosed1 (edi.syz.00001.ft)

Dist. (km):	14.942
Samples:	8192
dt (s):	0.005

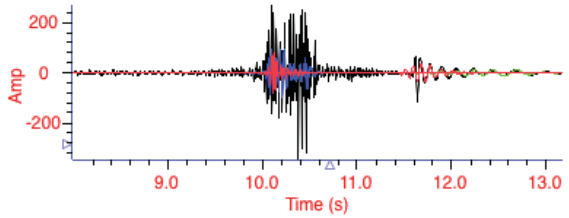

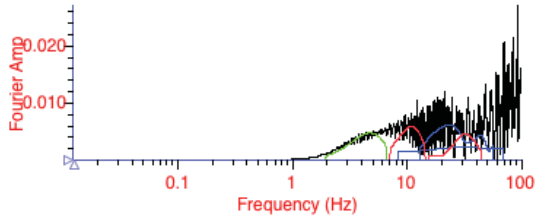

FTAN analysis

Tmin (s):	0.01
Tmax (s):	4.
Umin (km/s):	1.019
Umax (km/s):	2.
N. Filters:	32
Alpha:	100

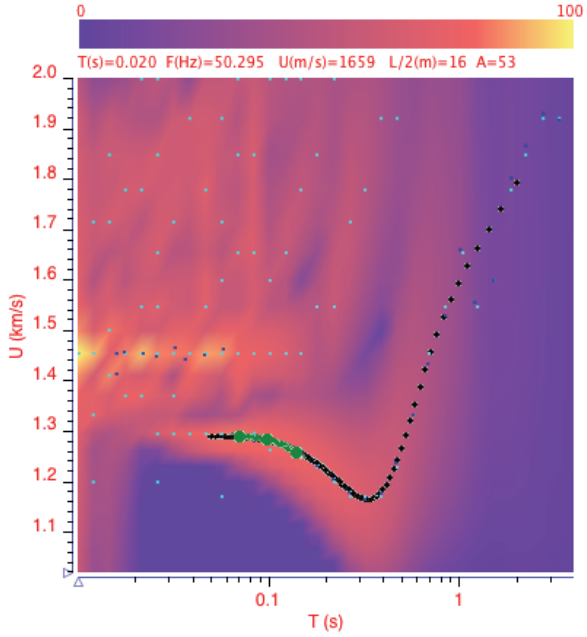

Structural Model

Depth (m)	Thk (m)	D (g/cm3)	Vp (m/s)	Vs (m/s)	Qp	Qs
130	130	1	1500	0	10000	10000
230	100	2.45	2800	1618	1000	500
330	100	2.45	3000	1734	1000	500
430	100	2.45	3400	1965	1000	500
530	100	2.45	3500	2023	1000	500
780	250	2.45	3600	2081	1000	500
1030	250	2.45	3700	2139	1000	500
1530	500	2.45	3800	2196	1000	500
2030	500	2.45	3900	2254	1000	500
3030	1000	2.45	4000	2312	1000	500

Fundamental Mode

F (Hz)	T (s)	U (m/s)	C (m/s)
0.5000	2.00000	1791	1949
0.6000	1.66667	1741	1916
0.7000	1.42857	1700	1885
0.8000	1.25000	1663	1857
0.9000	1.11111	1628	1831
1.0000	1.00000	1594	1806
1.1000	0.90909	1559	1782
1.2000	0.83333	1525	1759
1.3000	0.76923	1490	1737

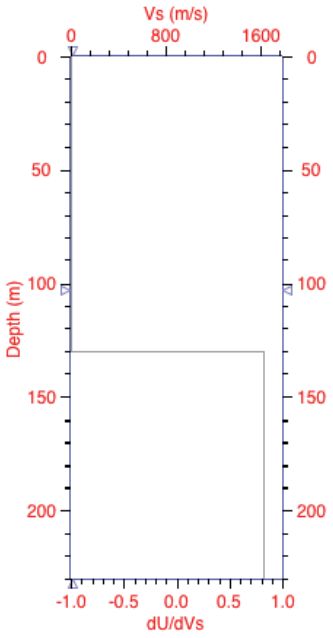

SW Tomography

- Phase velocity: 2 stations method

$$\delta\phi = \int \delta k ds = -\frac{\omega}{c^2}\int \delta c ds$$

- Group velocity: FTAN

$$\delta t = \int \delta\left(\frac{1}{u}\right) ds = -\frac{1}{u^2}\int \delta u ds$$

- Local velocity perturbation is obtained by tomographic inversion

$$\delta t_i = -\int_{L_{0i}} \frac{\delta u}{u_0^2} ds = \iint_{\Omega} G(r)m(r)dr$$

- Minimizing

$$\sum_i \left(\delta t_i - \iint_{\Omega} G(r)m(r)dr \right)^2 + \alpha \iint_{\Omega} \left|\Delta m(r)\right|^2 dr$$

- c(x,y,T) u(x,y,T)

e.g. Yanovskaya and Ditmar, 1990.

Phase Velocity Tomography

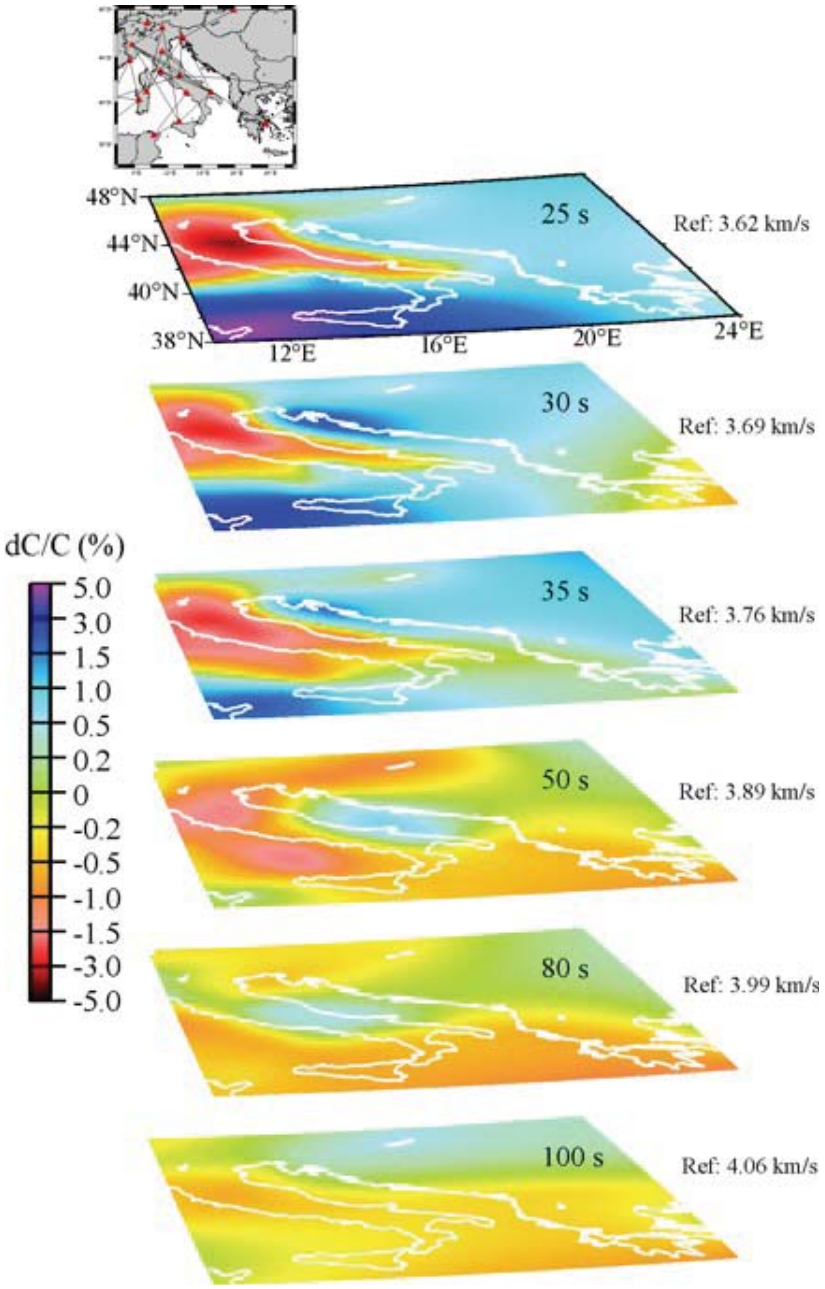

$$\left(\frac{dV(x,y)}{V(x,y)}\right)_T = \left(\frac{V_{mean} - V(x,y)}{V(x,y)}\right)_T$$

period range
25-100 s

Modified from Pontevivo and Panza, 2002

Group Velocity Tomography

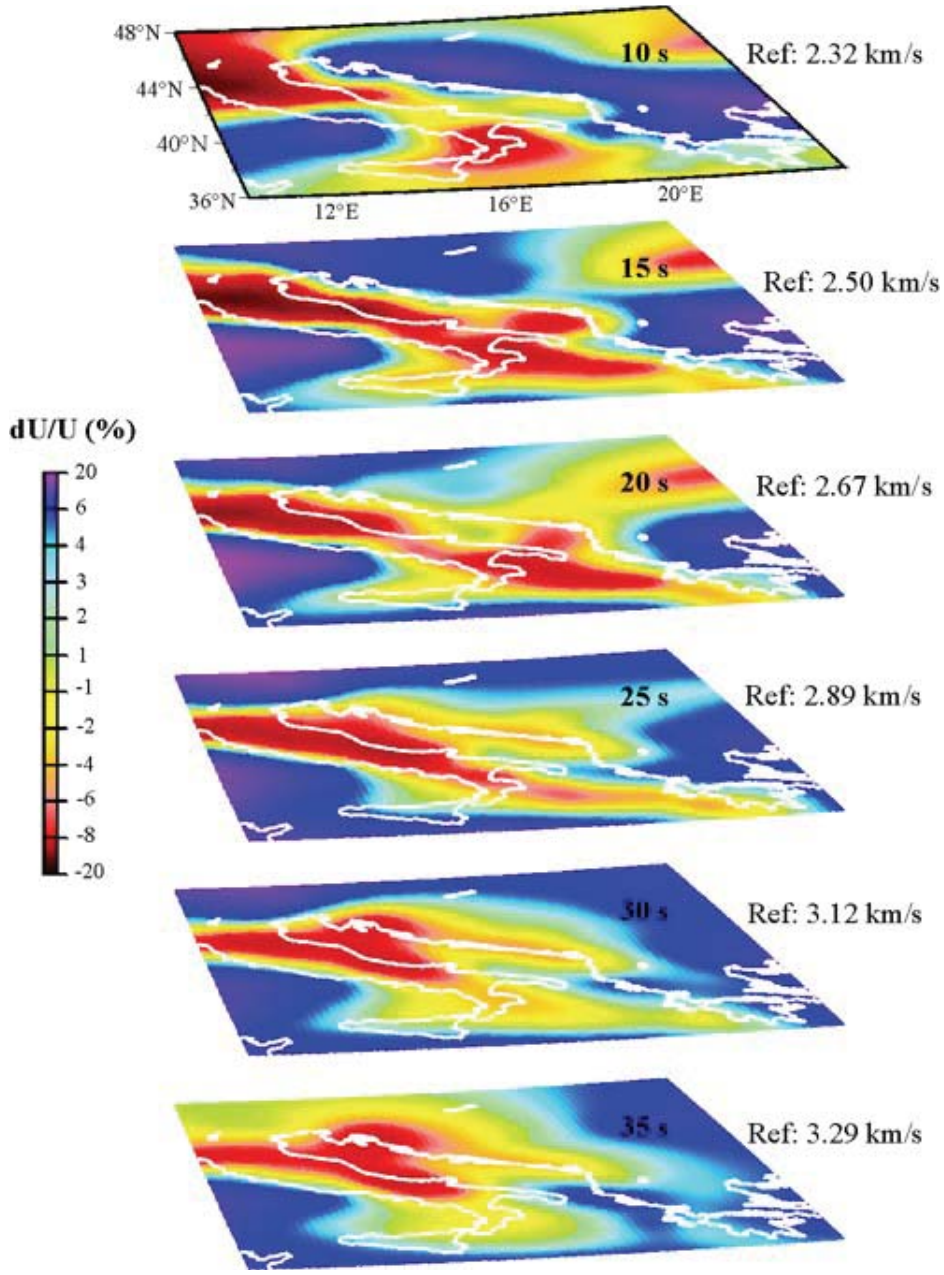

$$\left(\frac{dV(x,y)}{V(x,y)}\right)_T = \left(\frac{V_{mean} - V(x,y)}{V(x,y)}\right)_T$$

period range
10-35 s

Modified from Pontevivo and Panza, 2002

SW Tomography: resolution & grouping

- Density, azimuthal coverage and length of the paths control the lateral resolution of the data set and the maps can be discretized with a step consistent with the value of the lateral resolution length (200 km)

- Improvement of the lateral resolving power when some parameters of the uppermost part of the crust are fixed on the base of "a priori" independent geological and geophysical additional constraints: 1°× 1° grid

- To each cell of the grid is assigned an average dispersion curve, $U_j(T_i)$, obtained by averaging, for each T_i, the values of the group velocity at the four corners (knots) and single point errors $\sigma_{U_j}(T_i)$

- To regionalize the study area, the cellular dispersion curves can be grouped according to specific rules independently from any a priori geological assumption.

SW Tomography: cells

Gridding with a mesh comparable to the resolving power

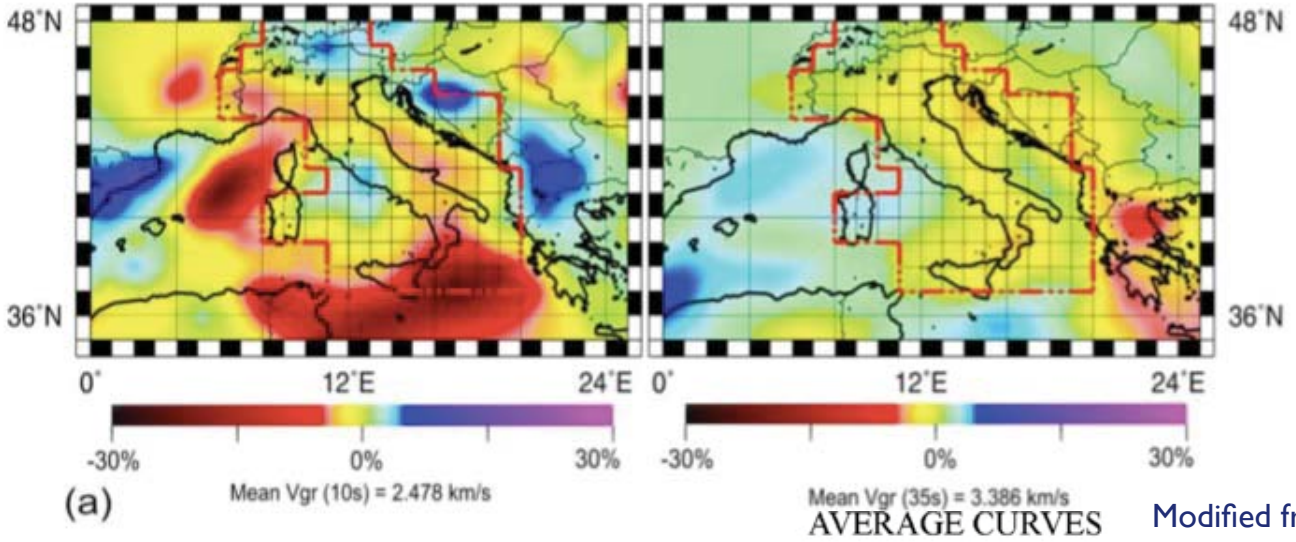

Modified from Panza et al., 2007

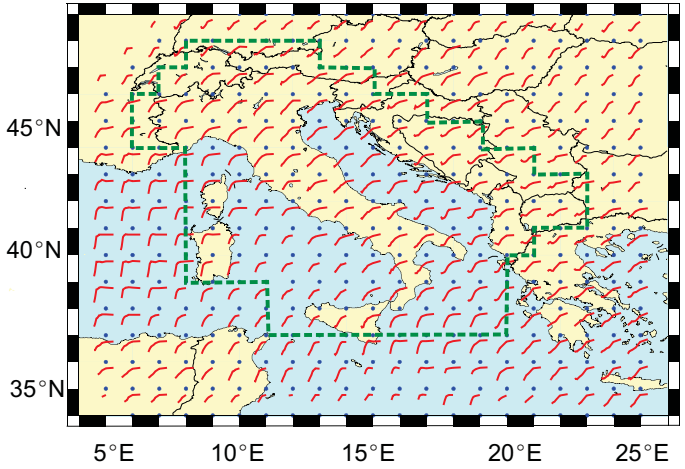

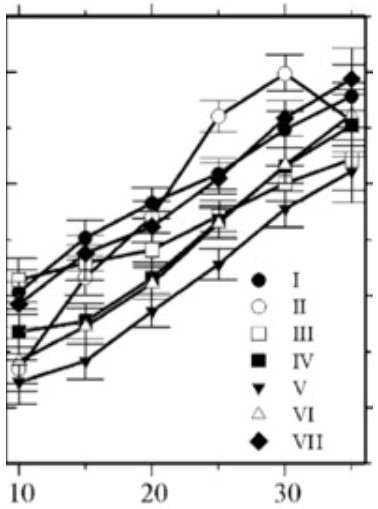

Characterization of each 1°x1° cell with local dispersion curves and their errors

Non-Linear Inversion (Hedgehog)

- The structure is modeled as a stack of N homogeneous isotropic layers each one defined by (V_P, V_S, ρ, th); any structural model is a point in the space of the unknown parameters $\{P_i\}$

- Optimized Monte Carlo search to find velocity depth distributions consistent with dispersion data (difference between computed and experimental values has to be less than measurement error)

- $x(P_i)$ is a single point of a minimum region: neighboring points $x'(P_i+a_i\delta P_i)$ are tried, with $a_i=0$ or 1; procedure is applied to every selected point until the whole region is covered

- Return is made to Monte Carlo technique, another minimum region is reached...

Hedgehog resolution

- Structure parametrization is made according to the resolving power of the data and "a priori" information (e.g. petrological, geophysical constraints)
- Parameters can be fixed, independent or dependent (e.g. Poissonian behaviour)
- Parameters and their steps can be used to represent the uncertainty of the inverted parameters
- Partial derivatives of the dispersion curves w.r.t. the considered parameter control the suitable steps in the inversion (act as a guiding criteria) and depth resolution

$$\left[\frac{1}{N}\sum_{i=1}^{N}\left(\frac{\partial V(T_i)}{\partial P_j}\right)^2\sigma^{-2}(T_i)\right]^{-\frac{1}{2}} \Rightarrow \delta P_j$$

Covariance matrix

$$\sum_j \left(\frac{\partial V(T_i)}{\partial P_j}\right)_{\text{minima}} \delta P_j = \sigma(T_i)$$

Partial derivatives

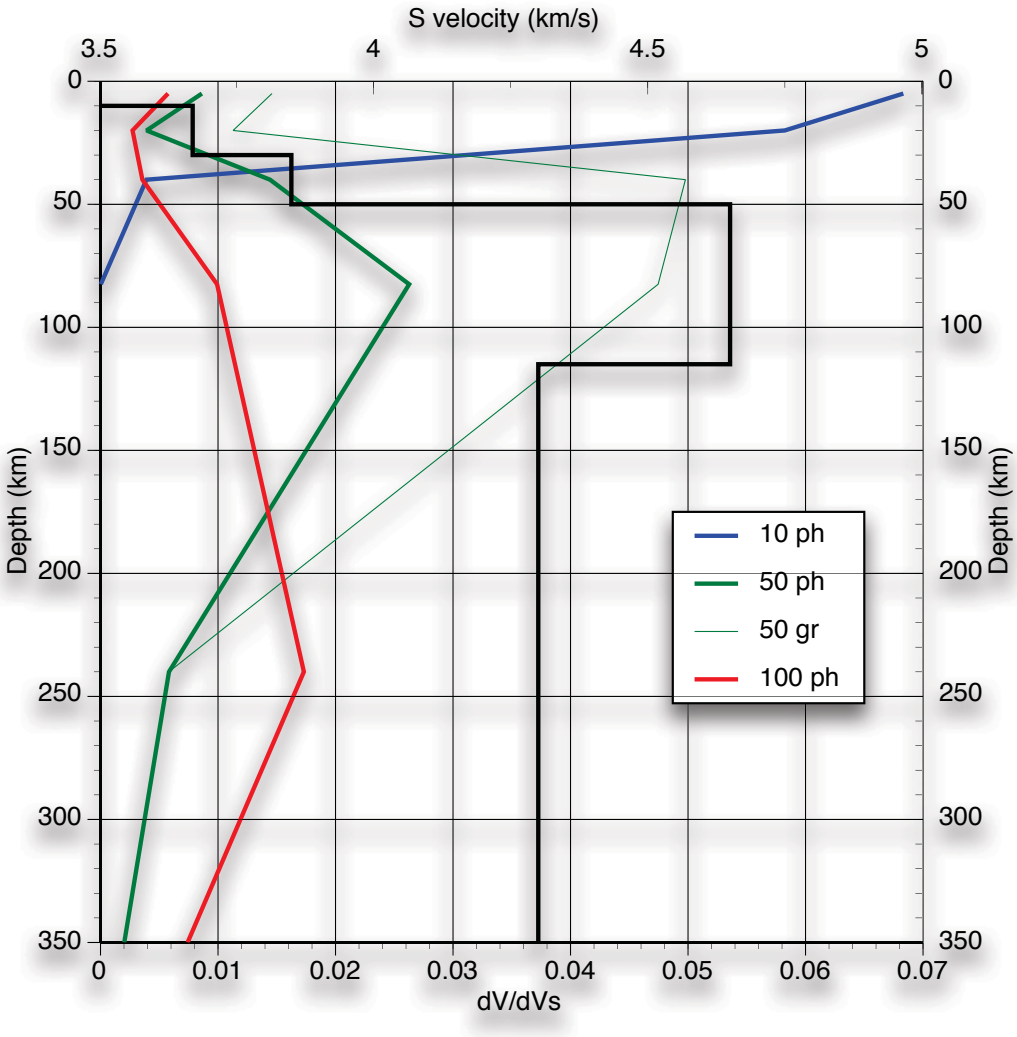

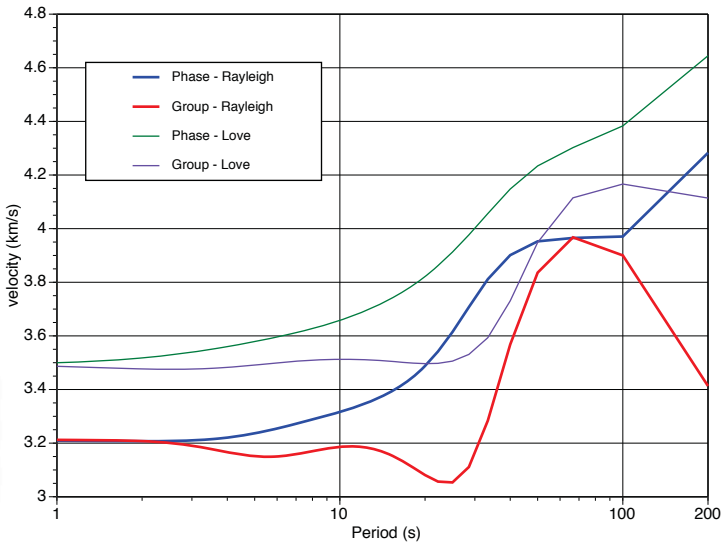

From the experiments of Panza (1981) on the resolving power of dispersion measurements with respect to structural parameters in the crust and in the upper mantle, for a given error, Rayleigh wave group velocities lead, in general, to a better resolution as compared with Rayleigh wave phase velocities. The results of the inversion experiments (Panza, 1981) clearly indicate that the sub-Moho Vs can be determined with a rather good accuracy using indifferently phase or group velocity data, while crustal parameters are better resolved by group velocities.

The representative solutions...

- The non-linear inversion of geophysical data in general does not yield a unique solution, but a single model representing the investigated field, and is preferred for an easy geological interpretation of observations.

- The analyzed region is constituted by a number of sub-regions where multi-valued non-linear inversion is applied, which leads to a multi-valued solution. Therefore, combining the values of the solution in each sub-region, many acceptable models are obtained for the entire region and this complicates the geological interpretation of geophysical investigations.

- New methodologies are presented, capable of selecting one model among all acceptable ones, that satisfies different criteria of smoothness in the explored space of solutions. We focus on the non-linear inversion of surface wave dispersion curves, which gives structural models of shear-wave velocity versus depth.

Looking for representativeness...

- Median model
  - may not be representative
- Minimum r.m.s.
  - may be affected by systematic errors
- the one with the r.m.s for phase and group velocities closest to the average r.m.s. for all the solutions
  - the range is decided by the parameter step
- Optimization procedures
  - consists in finding, for each cell, the representative solution so that the lateral velocity gradient between neighbouring cells is minimized, this means that the local shape of the physical field has to be as smooth as possible (Occam's razor)

Alps...

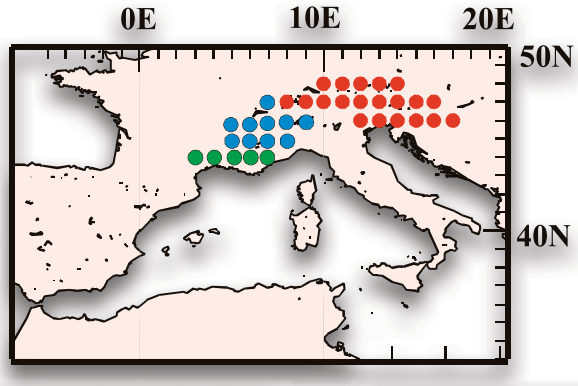

- EASTERN-CENTRAL ALPS
- CENTRAL-WESTERN ALPS
- WESTERN ALPS

Modified from Panza et al., 2003

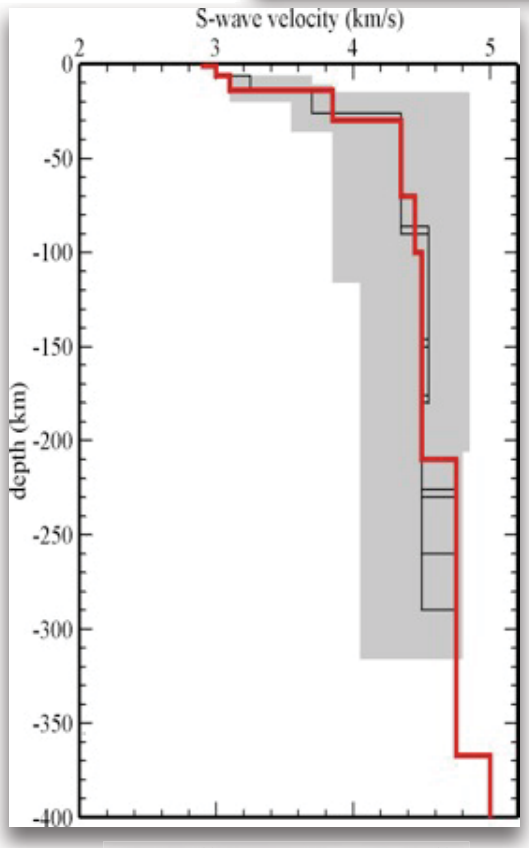

WESTERN ALPS

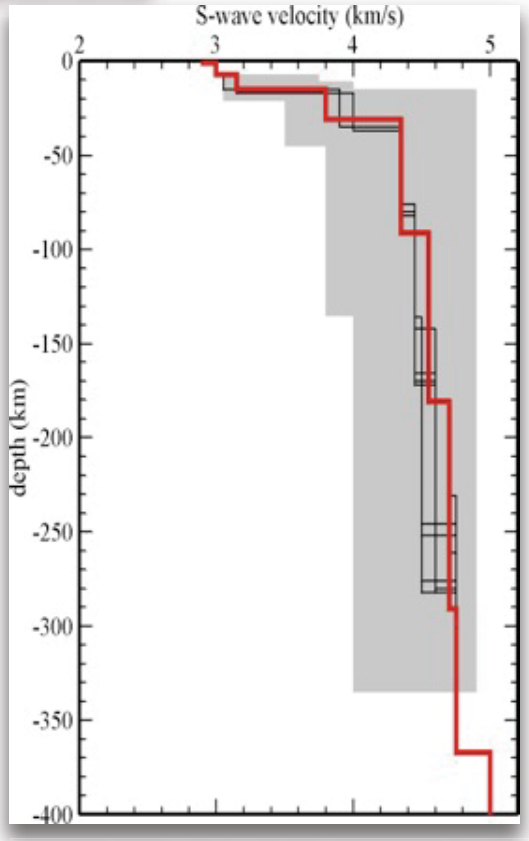

CENTRAL-WESTERN ALPS

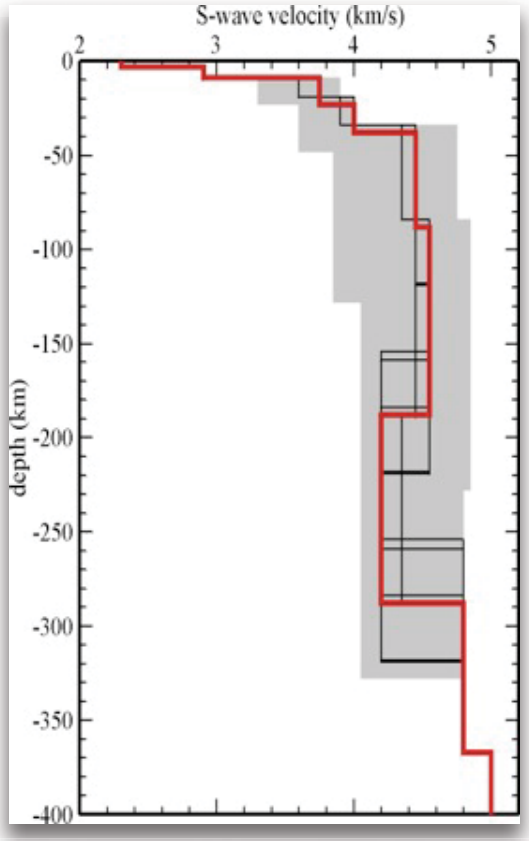

EASTERN-CENTRAL ALPS

Road map

- Methodology:
  - Surface wave dispersion analysis
  - Surface wave tomography
  - Non linear inversion of dispersion data
- Cellular models for the lithosphere-asthenosphere system
  - Optimization techniques
  - Scale level I: 1°x1° cells in the whole Italian region
  - Adding other geophysical constraints
  - Selected sections and geodynamic modelling

Criteria for optimality

- Local Smoothness Optimization (LSO): the optimized local solution of the inverse problem is the one that is searched for, cell by cell, considering only the neighbours of the selected cell and fixing the solution as the one which minimizes the norm between such neighbours.

- Global Flatness Optimization (GFO): the optimized global solution of the inverse problem with respect to the flatness criterion is the one with minimum global norm in-between the set.

- Global Smoothness Optimization (GSO): the optimized global solution of the inverse problem with respect to the smoothness criterion is the one with minimum norm in-between all the members of the set. The GSO is based on the idea of close neighbours (local smoothness) extended, in a way, to the whole study domain.

LSO steps

- the data pre-processing in which the different layering of the models of each cell and, therefore, of the whole domain, is considered and equalized;

- the choice of the starting cell among all the cells of the domain;
  - it has been decided to choose the one with the minimum "average distance" i.e. the dependence of the smoothing process on the initial solution is minimized.

- the optimization algorithm in which the final method is described and some definition are given.
  - a first iteration identifies the representative solution for the SC and a second iteration (with or without a priori constraints) identifies the representative solutions for all the other cells.

Consistency

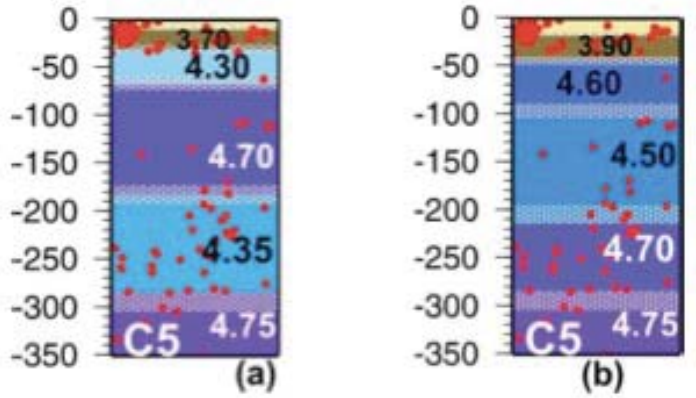

Among the hedgehog solutions for this cell, we choose the one, which agrees best with the distribution of the intermediate-depth seismicity falling in this cell. Thus in cell C5 a high velocity lid, with Vs of about 4.60 km/s sits on a fast asthenosphere, with Vs of about 4.50 km/s reaching a depth of about 200 km, where a fast mantle, with Vs of about 4.70 km/s is seen down to a depth of more than 300 km. With this solution fixed, we run the optimization again.

Modified from Panza et al., 2007

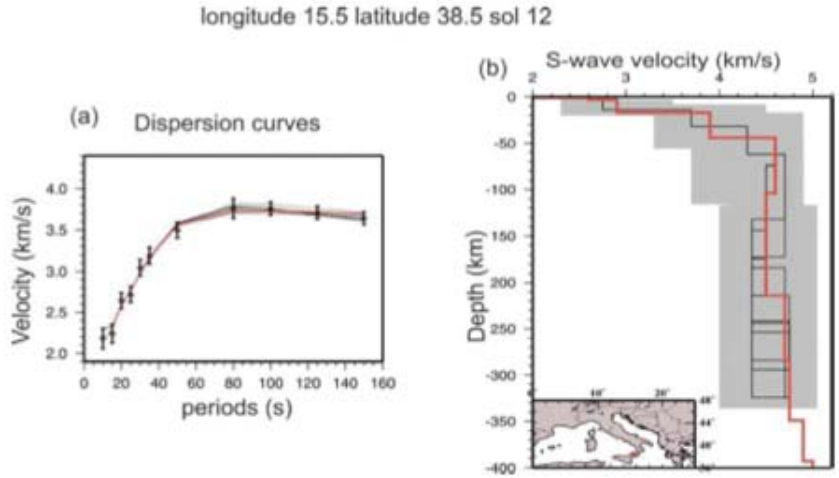

LSO for Western Alps

Cellular structural model extended down to 350 km depth for the western Alps area. Yellow to brown colors represent crustal layers, blue to violet colors indicate mantle layers. Red dots denote all seismic events collected by ISC with magnitude greater than 3 (1904-2006). For each layer VS variability range is reported. For the sake of clarity, in the uppermost crustal layers the values of VS are omitted. The uncertainty on thickness is represented by texture.

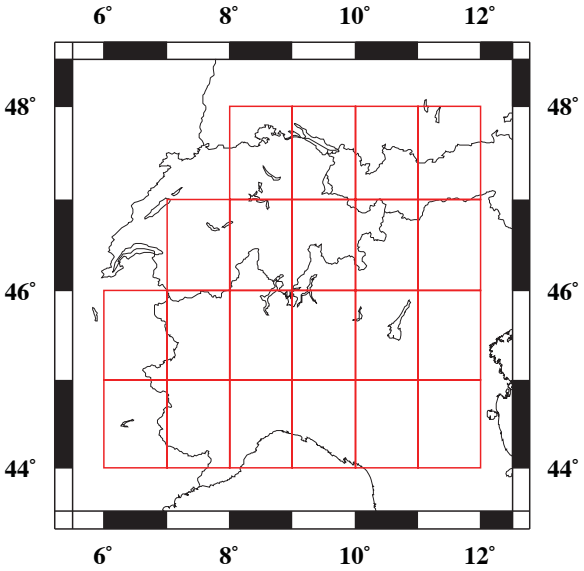

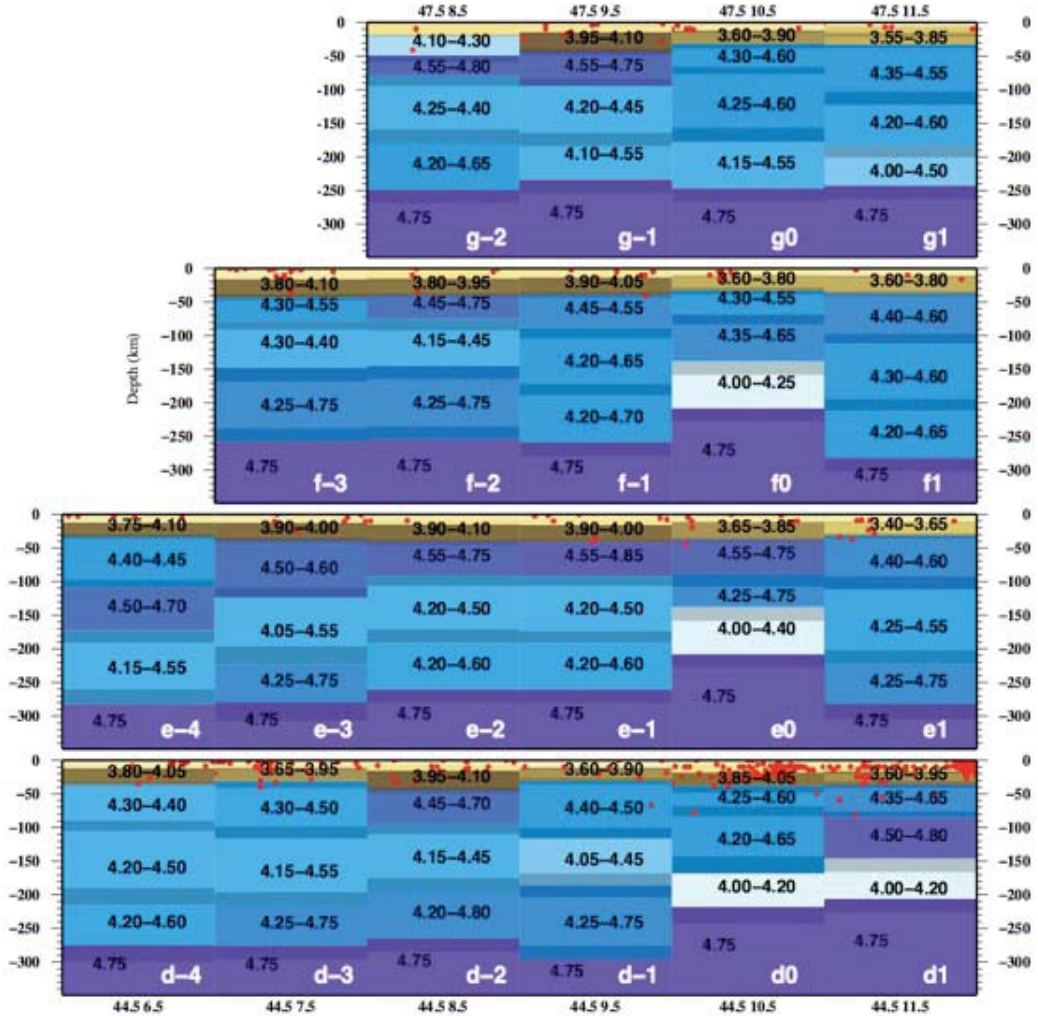

GFO for Western Alps

Cellular structural model extended down to 350 km depth for the western Alps area. Yellow to brown colors represent crustal layers, blue to violet colors indicate mantle layers. Red dots denote all seismic events collected by ISC with magnitude greater than 3 (1904-2006). For each layer VS variability range is reported. For the sake of clarity, in the uppermost crustal layers the values of VS are omitted. The uncertainty on thickness is represented by texture.

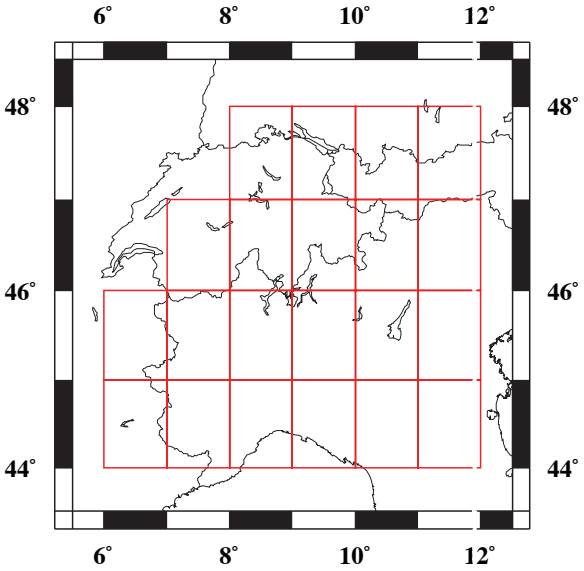

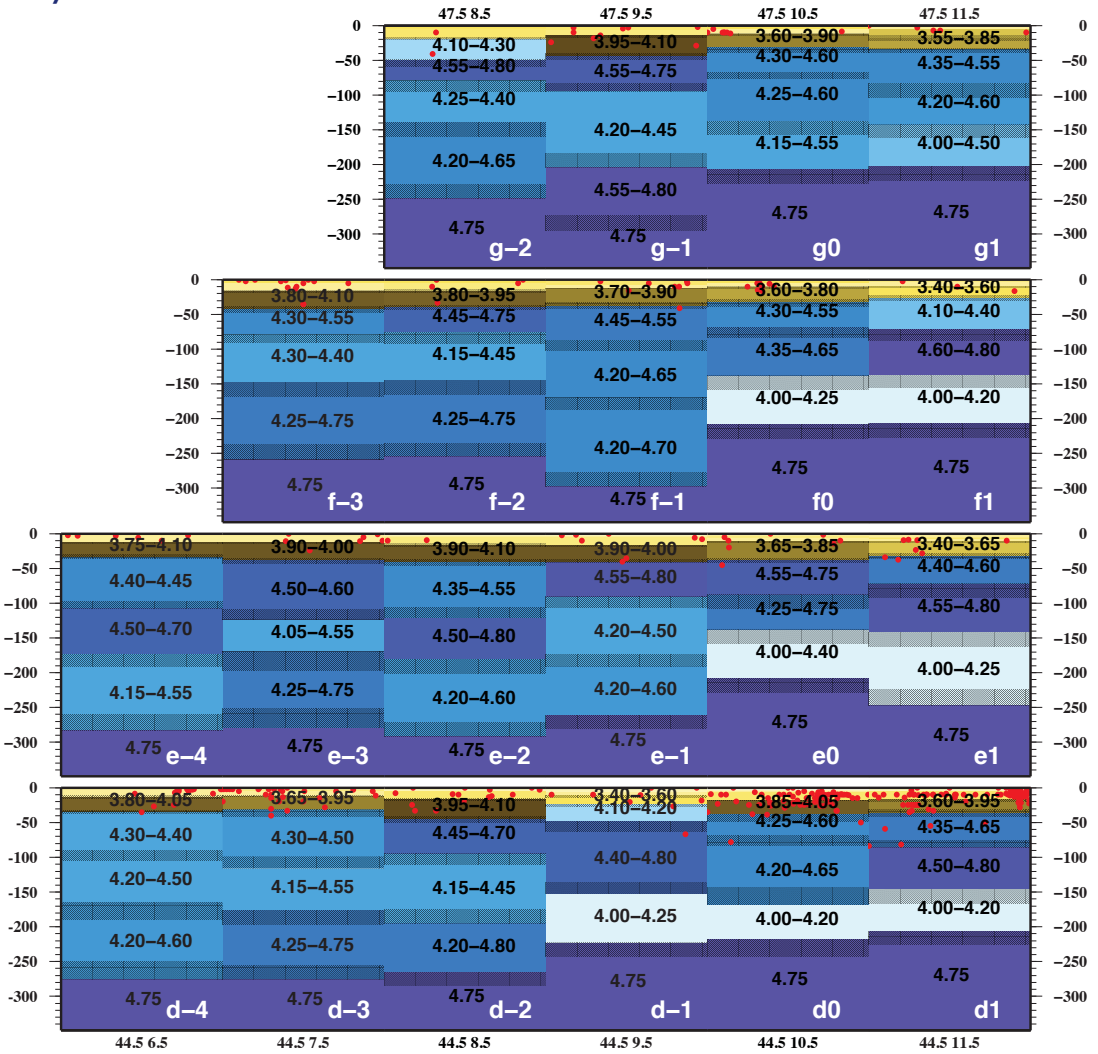

Alps refined

Alpine refined cellular model. Cellular structural model extended down to 350 km depth for the Alpine area, refined with GSO and GFO optimization algorithms, with splitting of some cells to 1°x0.5° or 0.5°x1.0°, along profiles where additional crustal information were available.

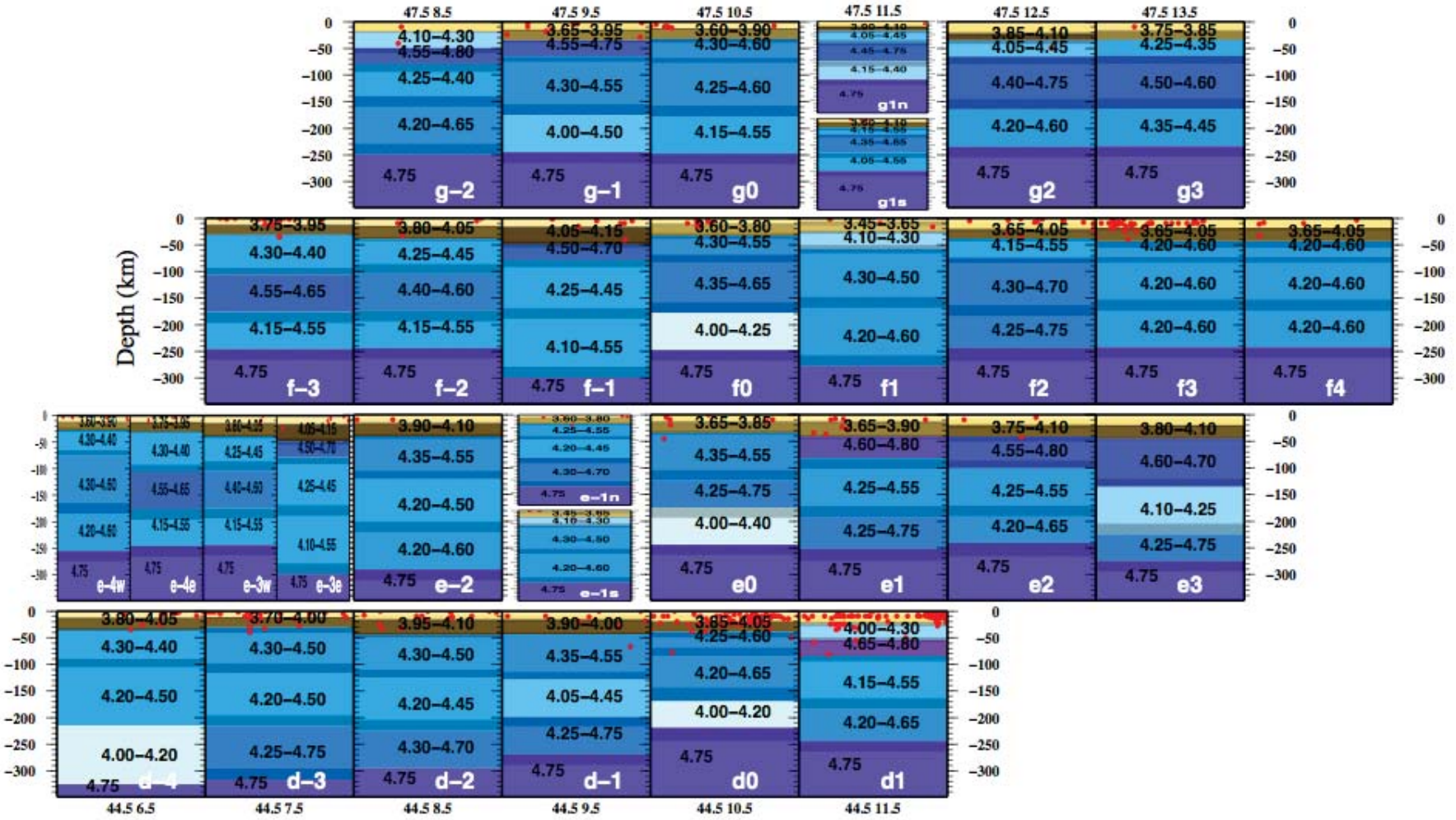

V_S models and geophysical constraints

- Since the non-linear inversion and its smoothing optimization guarantee only the mathematical validity of the solution of the inverse problem, the optimization procedure can be repeated whenever necessary.

- Including additional geophysical constrains, such as Moho depth, seismic energy distribution versus depth, presented magmatism, heat flow, etc., until the appraisal of the selected models against well-known and constrained structural features gives an agreement comparable with the model's uncertainties

V_S models and geophysical constraints

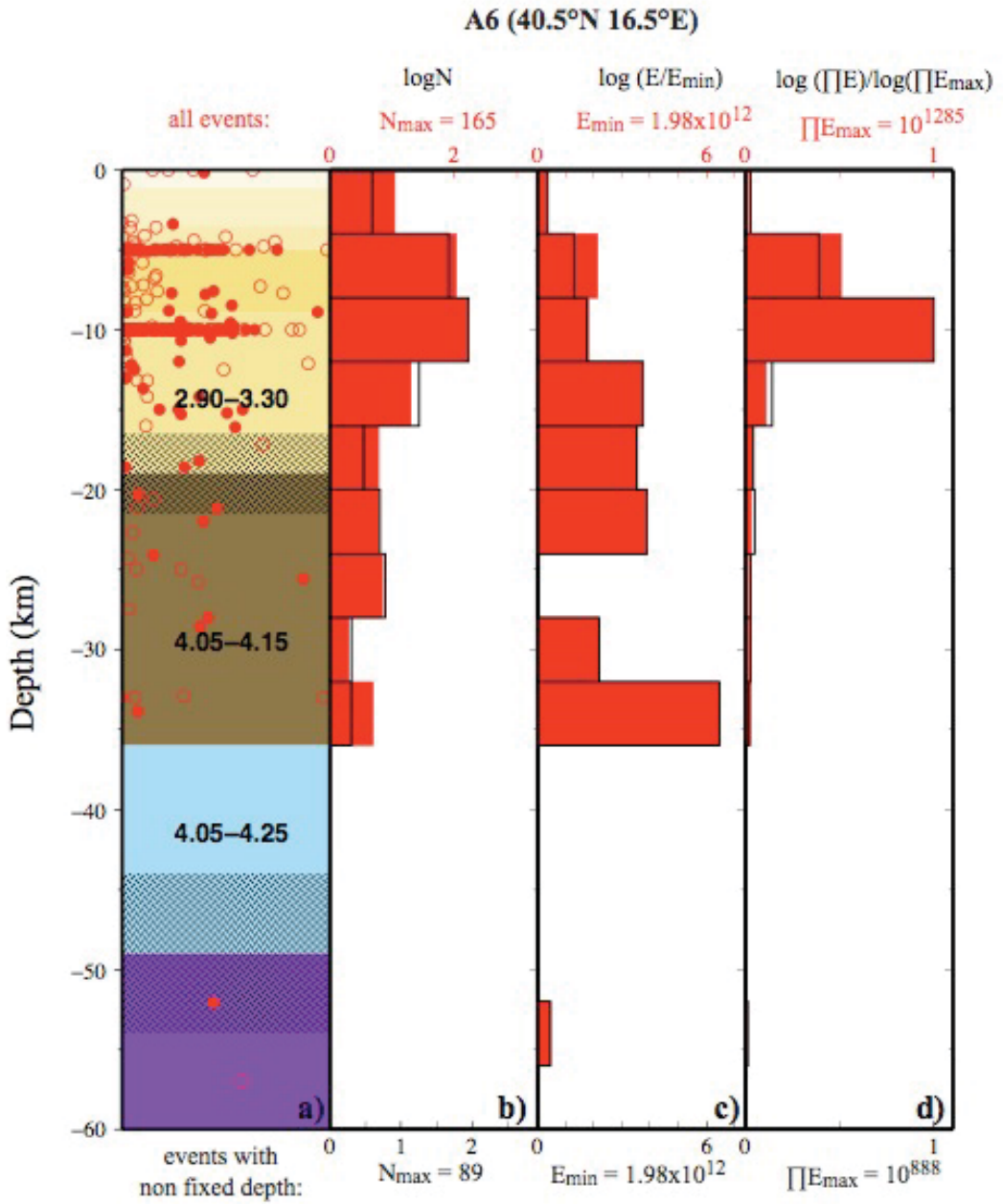

Analyzing the presented seismicity-depth distributions the clear stop of the seismicity at about 36 km is observed and thus we define the Moho depth at this depth. So the lower 17 km thick lower crust with VS range of 4.05-4.15 km/s is followed by 13 km thick soft mantle layer with VS range of 4.05-4.25 km/s. The presence of this shallow, thin, and soft mantle layer can be related to the elevated local heat flow data (up to 90 mW/m2

INPAR methodology

Linear step

Extraction of Green's function computed by modal summation

Dynamic relocation of the hypocentre

Computing the base function for a set of hypocentral coordinates and structural models and the differences between observed and synthetic records

Retrieval of MTRF

Non linear step

Reduction of MTRF to a constant moment tensor with the corresponding STF taking only the correlated part from each of them

Comparison of our results with CMT and RCMT

Contribution of our results to the general tectonic picture

Period range used by different methods

CMT	RCMT	INPAR
long period body waves T>45 T>135	intermediate period surface waves 35-135 s	waveforms at a regional distance >10 s

Improved resolving power for M_{zx} and M_{zy} components

Reliable estimation even of shallow earthquake's mechanisms

CMT solutions

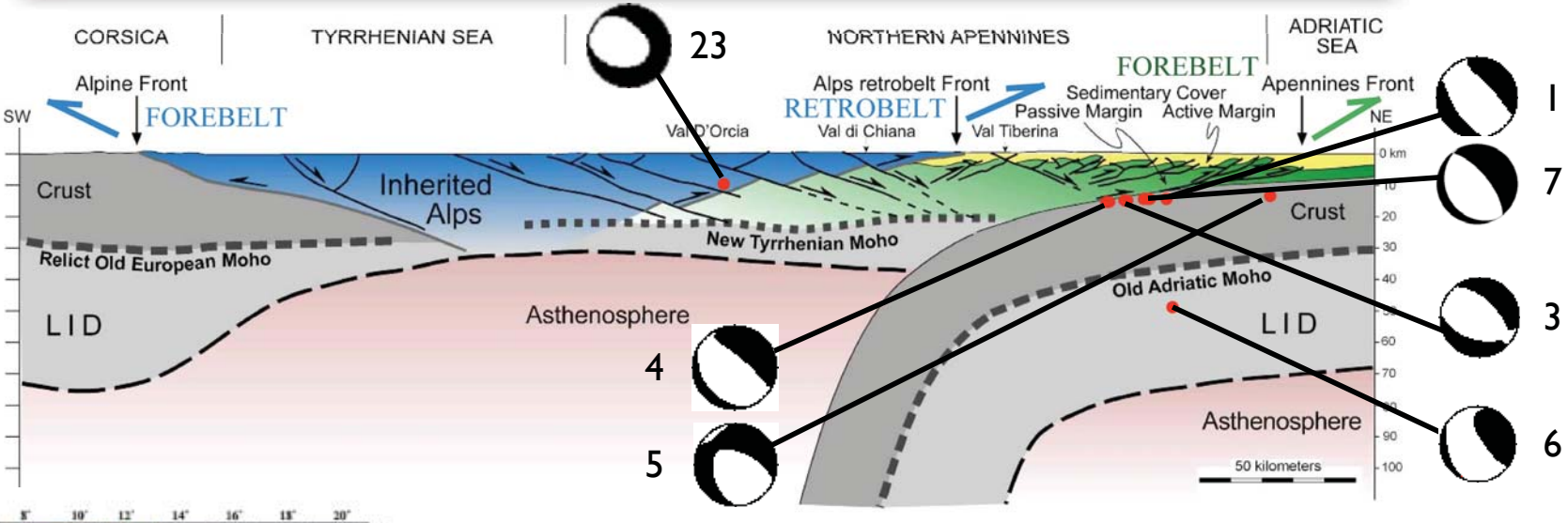

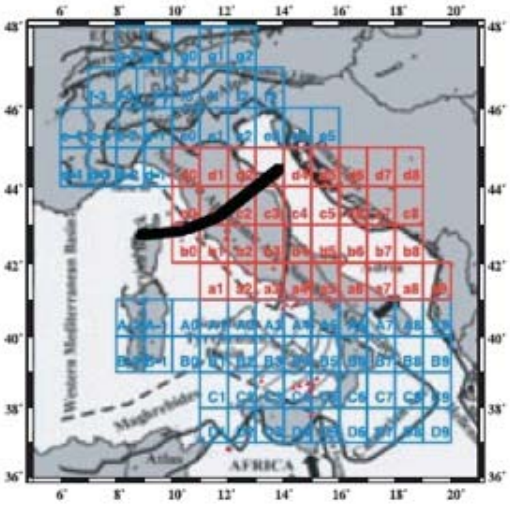

The hypocentres are located in the following cells

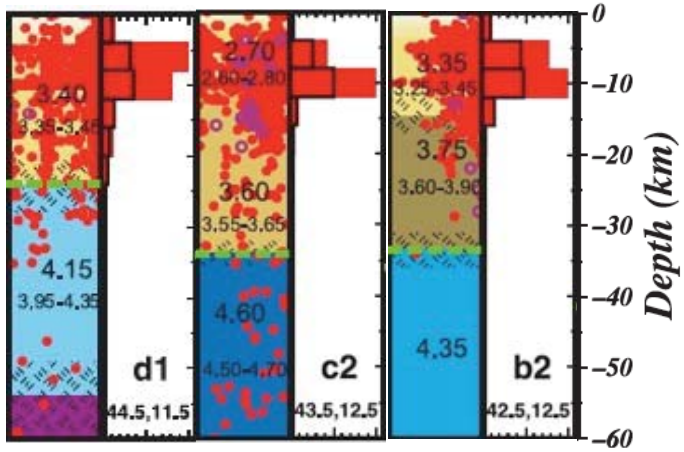

INPAR solutions

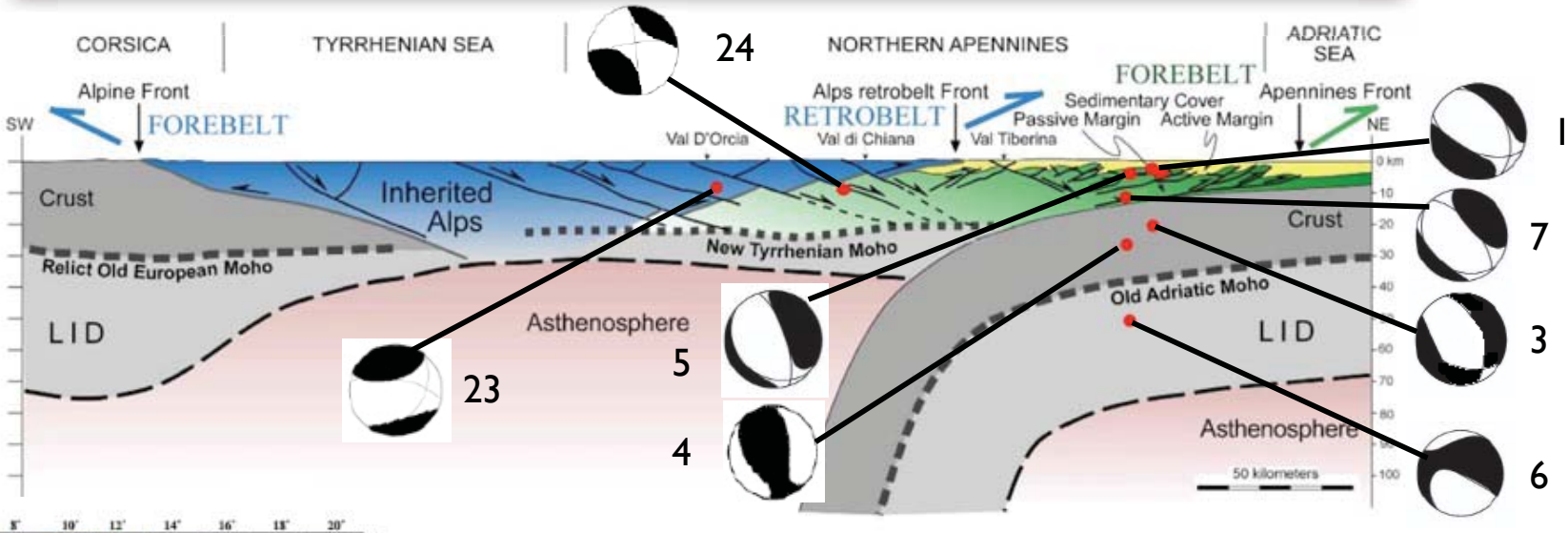

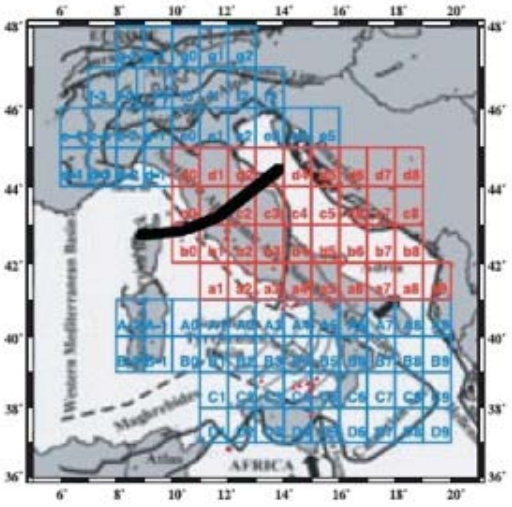

The hypocentres are located in the following cells

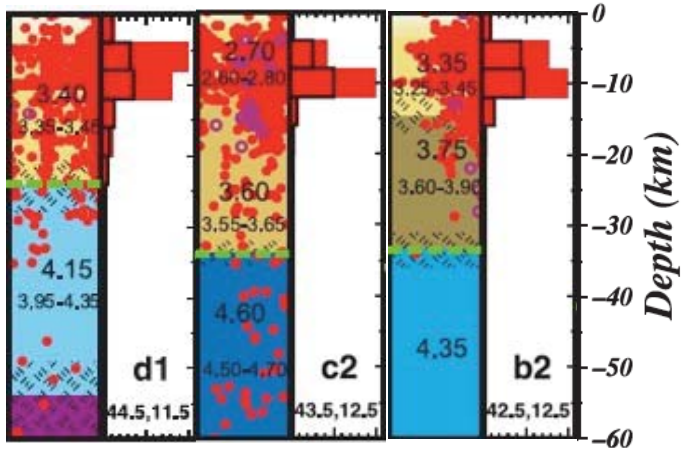

CROP03 section

Top: cellular model of the drown section along CROP03 profile. Yellow to brown colors represent crustal layers, blue to violet colors indicate mantle layers.

Centre: interpretation of the model, modified after Carminati et Scrocca (2004). The V_S value reported may not necessarily fall in the centre of the V_S range gained from inversion. The plotted hypocenters, and their focal mechanisms (on the right side), are retrieved by INPAR moment tensor inversion.

Bottom: heat flow (mWm^{-2} ,red full circles) and gravimetric anomaly (mGal, green triangles) data along profile used to support our interpretation.

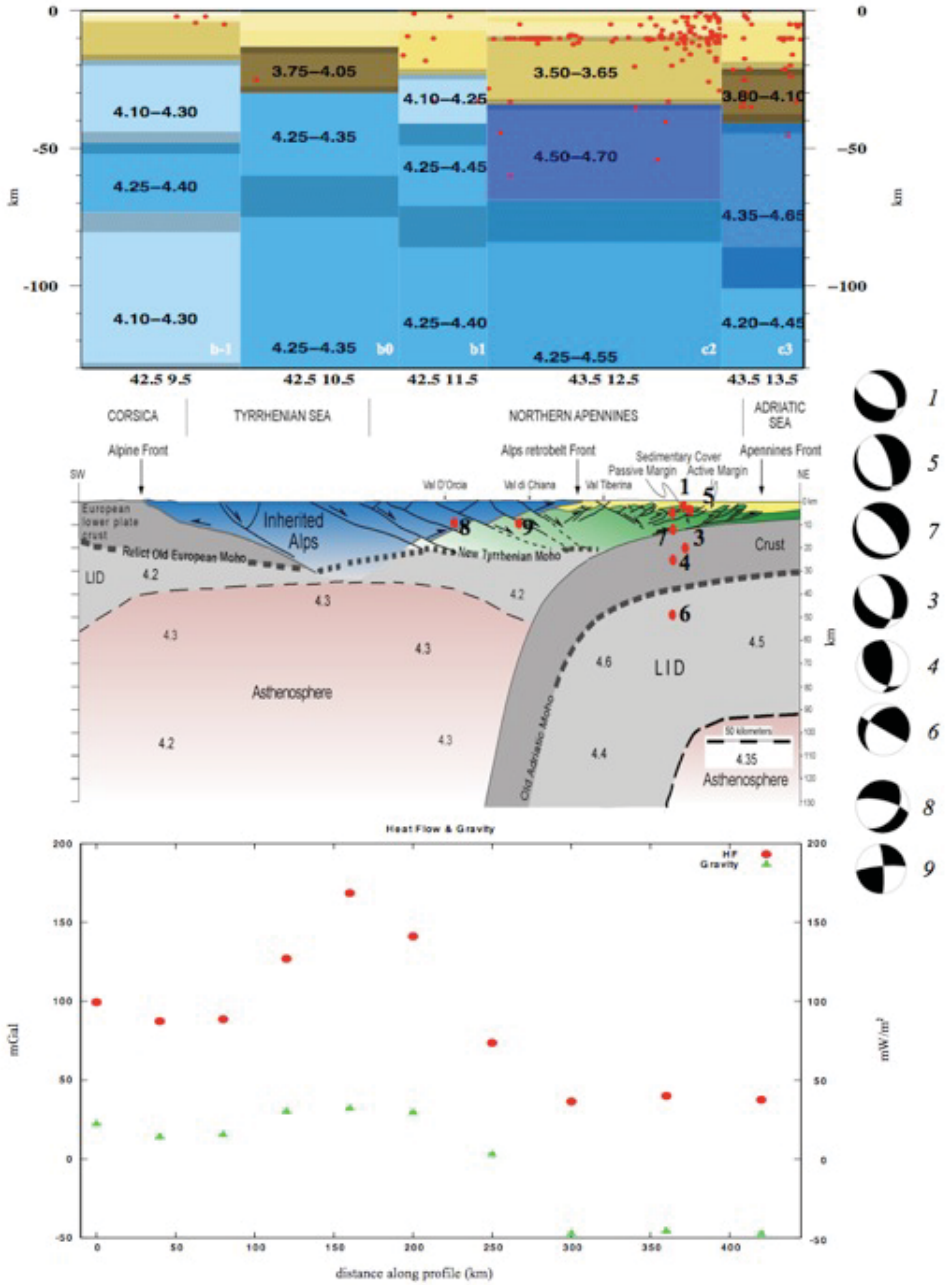

Cellular models

- A cell-by-cell database has been compiled to complete the obtained results with some independent data (VP, attenuation and density) to create an easier way to access the data. All collected information for each cell is stored in a table.
- The V_P data are taken from Piromallo et al. (2003) where a P-wave tomography study of the whole Mediterranean region is provided on a grid of 50 km in both horizontal and vertical directions down to a depth of 1000 km. The calculated V_P value for each layer in our cellular models permits to reduce the uncertainty ranges of V_S, in the mantle, as far as the V_P/V_S ratio in the mantle is kept as close as possible to 1.82 (Kennet et al., 1995).
- The database is completed with S-wave attenuation (Q_S) data given in recent studies of Martinez et al. (2009, 2010) for the Mediterranean at latitude less than 45°N. Using averaging and linear interpolation, the value of Q_S is calculated for the centre of each layer in our cellular solutions. The Q_S data for the rest of the cells are taken from Craglietto et al. (1989). The values of P-wave attenuation (Q_P) has been derived using the relation $Q_P = 2.2Q_S$ (Anderson, 2007). All V_S values are rounded to 0.05 km/s, according to the precision of our modelled data.
- In some cases, as in the cell presented in example, a V_S inversion is modelled in the upper 20 km. Whether this is a real structural feature or an artefact of the inversion, will be a matter to be settled performing the inversion using the receiver functions data to better constrain the upper fixed crust.

Cited references can be found in Brandmayr et al., 2010

- The values (respect to a reference model) obtained from P wave tomography (Piromallo e Morelli, 2003) have been translated into absolute ones.

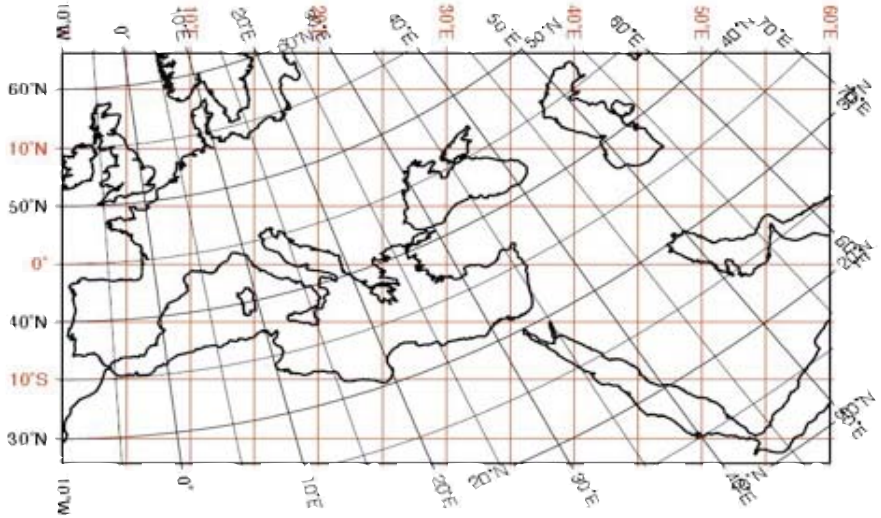

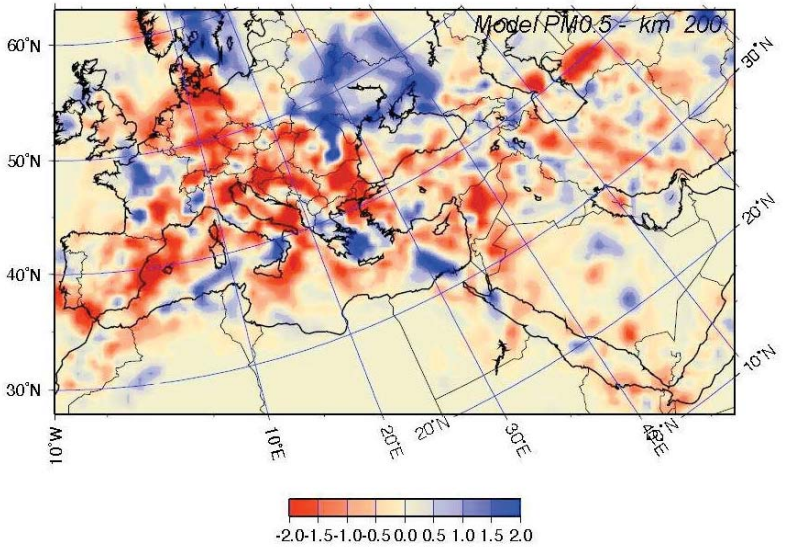

Example cell: b3

H	DENS	V_P	VS	Q_P	Q_S	Z	Lon	Lat	Delta V_S+	Delta V_S-	V_P/V_S
1.20	2.30	2.70	1.55	440.00	200.00	1.20	13.50	42.50	0.00	0.00	1.74
0.80	2.50	3.70	2.13	418.00	190.00	2.00	13.50	42.50	0.00	0.00	1.74
1.50	2.60	5.35	3.10	418.00	190.00	3.50	13.50	42.50	0.00	0.00	1.73
12.00	2.75	5.70	3.30	330.00	150.00	15.50	13.50	42.50	0.05	0.05	1.73
20.00	2.80	6.40	3.70	198.00	90.00	35.50	13.50	42.50	0.15	0.10	1.73
60.00	3.30	7.90	4.40	176.00	80.00	95.50	13.50	42.50	0.15	0.00	1.80
60.00	3.30	8.00	4.35	176.00	80.00	155.50	13.50	42.50	0.00	0.15	1.84
110.00	3.30	8.70	4.60	220.00	100.00	265.50	13.50	42.50	0.00	0.20	1.89
84.50	3.60	8.95	4.75	330.00	150.00	350.00	13.50	42.50	0.00	0.00	1.88

H - Thickness (km); DENS - Density (g/cm3); V_P - P-wave velocity (km/s); V_S - S-wave velocity (km/s); Q_P - Quality factor for P-wave; Q_S - Quality factor for S-wave; Z - Depth of the lowest interface (km); Lon, Lat - Geographical coordinates (°); Delta V_S+ Delta V_S- - Variation range for Vs (km/s); Delta H+ Delta H- - Variation range for H (km). The boundaries between layers can well be transition zones in their own right. Black bold lines separate fixed ("a priori") and inverted layers; red bold line indicates the Moho.

Two cross sections: EW

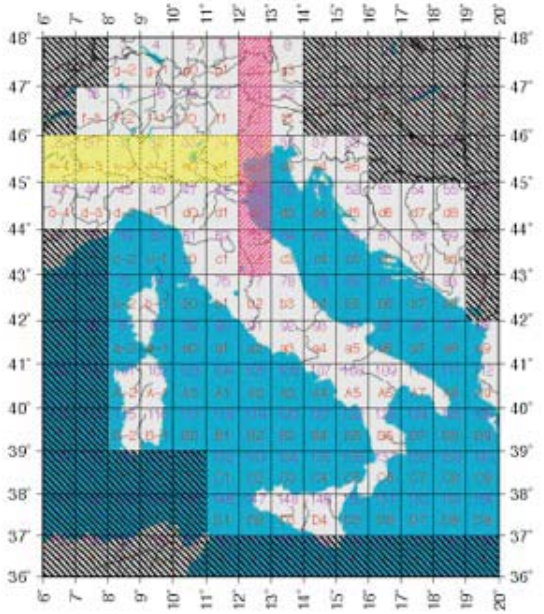

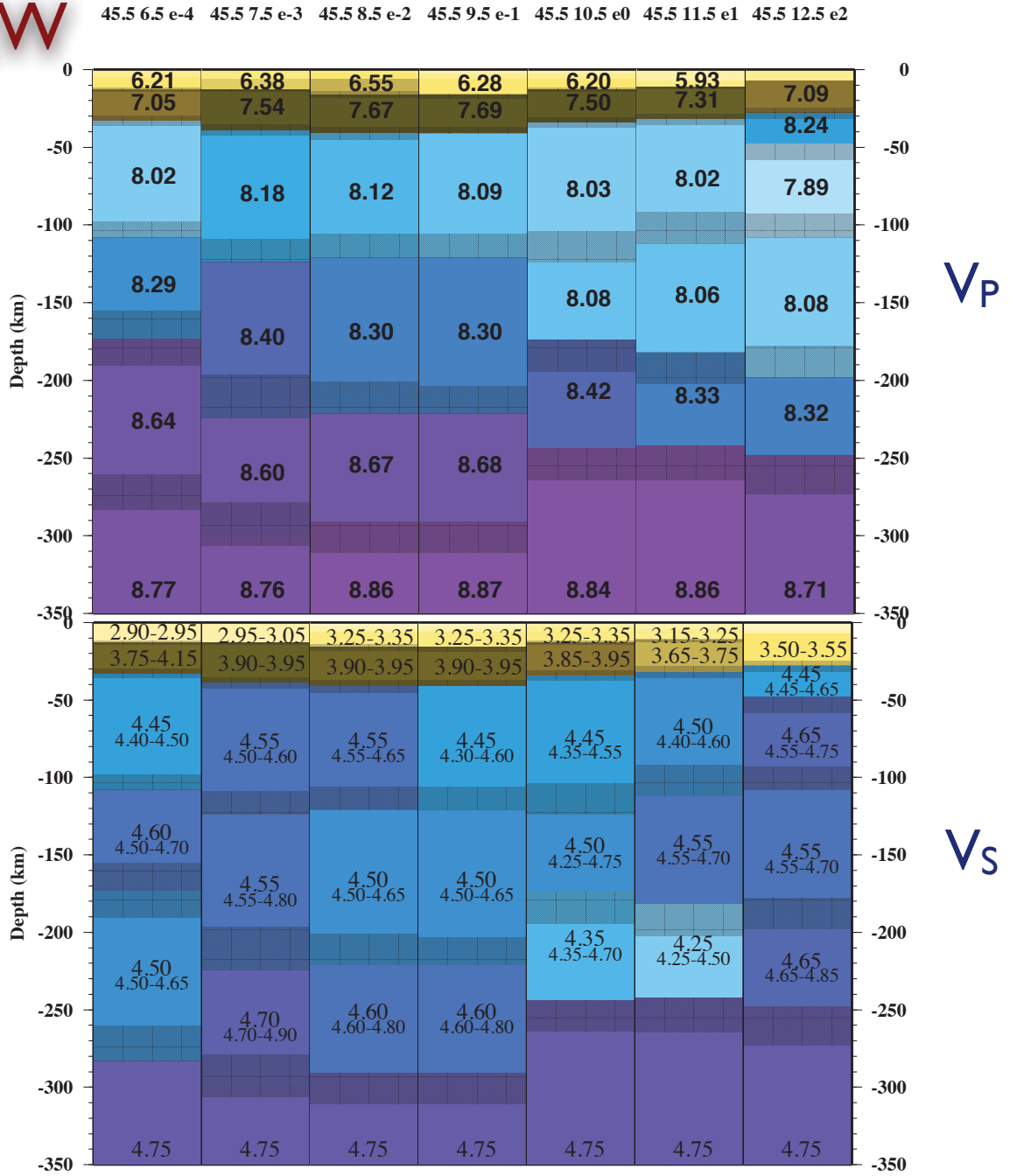

V_P

V_S

Method
Cells
Applications

Two cross sections: NS

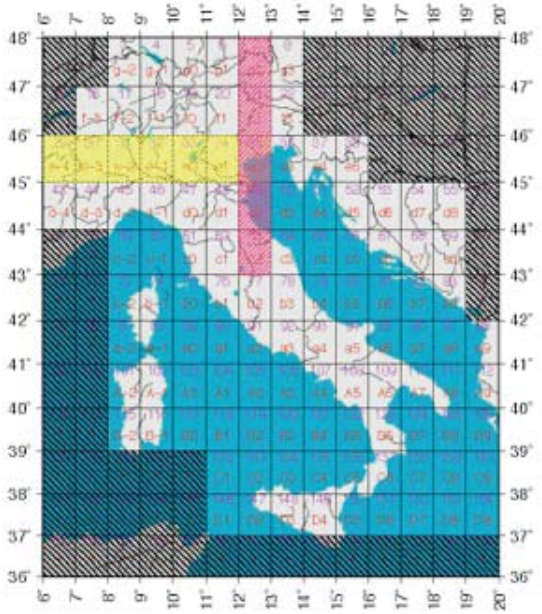

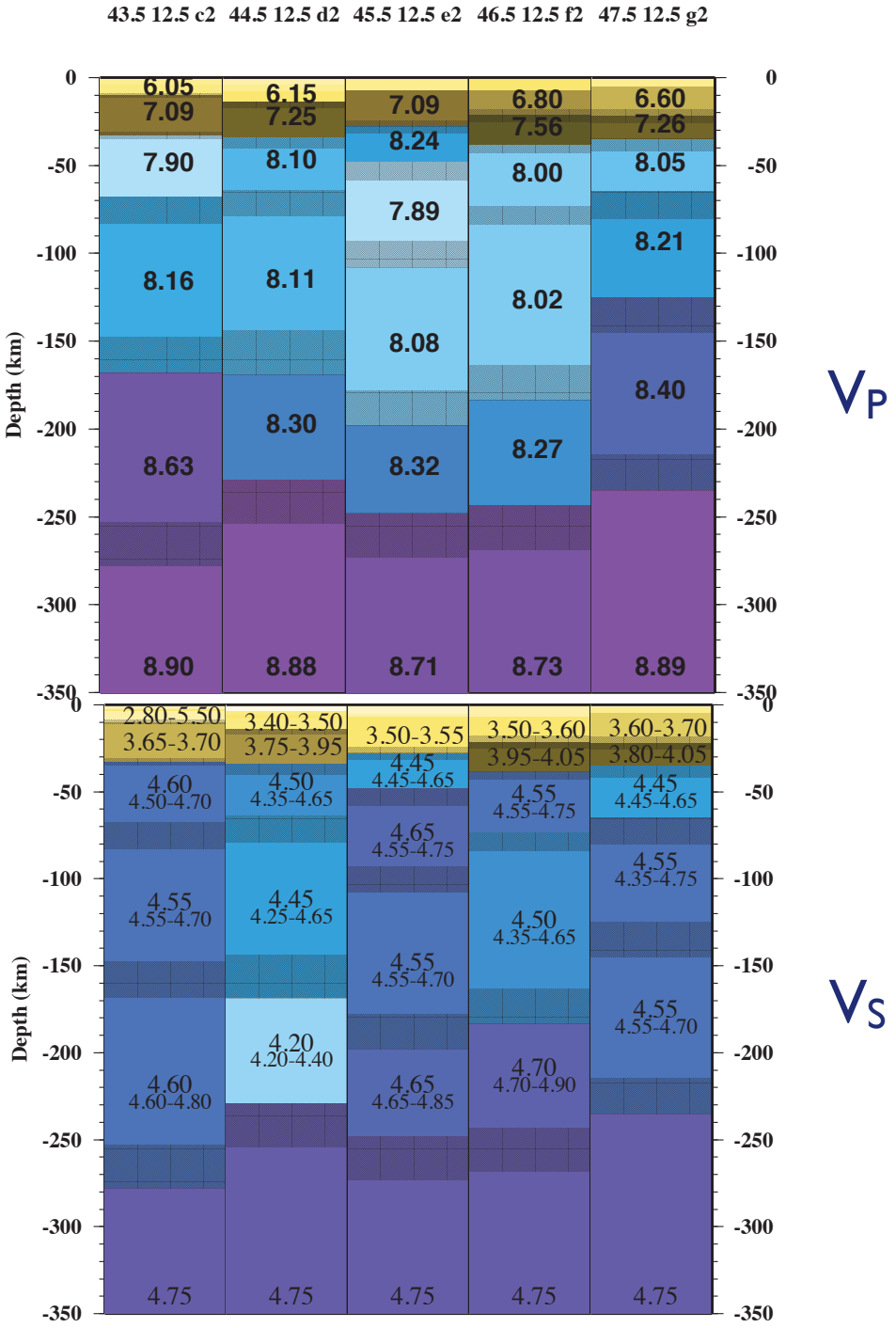

Definition of Φ

Bulk Sound Speed: $$\Phi = \sqrt{V_P^2 - \frac{4}{3}V_S^2} = \sqrt{\frac{k}{\rho}}$$

the ratio may have the power, according to its sign, if the mantle anomalies (respect to a reference model) have a thermal or different (e.g. chemical) origin

$$\frac{\partial\Phi}{\Phi} \Big/ \frac{\partial V_S}{V_S}$$

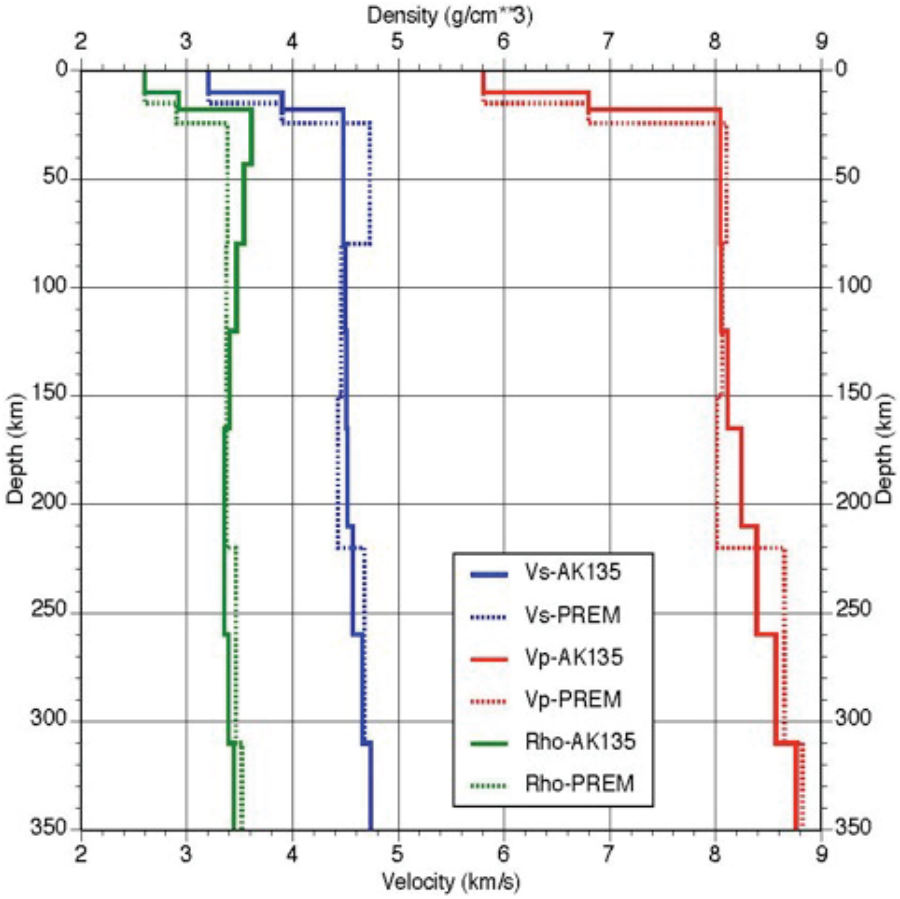

two reference models that have been used are:

- **AK135** Kennett et al. (1995)
- **PREM** Dziewonski & Anderson (1981).

AK135 – PREM Comparison (I)

- **g2:** both models reveal a thermal anomaly starting from LID; PREM shows an interruption about 50 Km thick
- **f2:** both models reveal a deep anomaly
- **e2:** PREM reveals two thermal anomalies
- **d2:** PREM reveals two thermal anomalies marking upper and lower border of a LVZ; AK135 reveals only the shallower one
- **c2:** both models reveal a thermal anomaly in the asthenosphere (more evident for AK135)

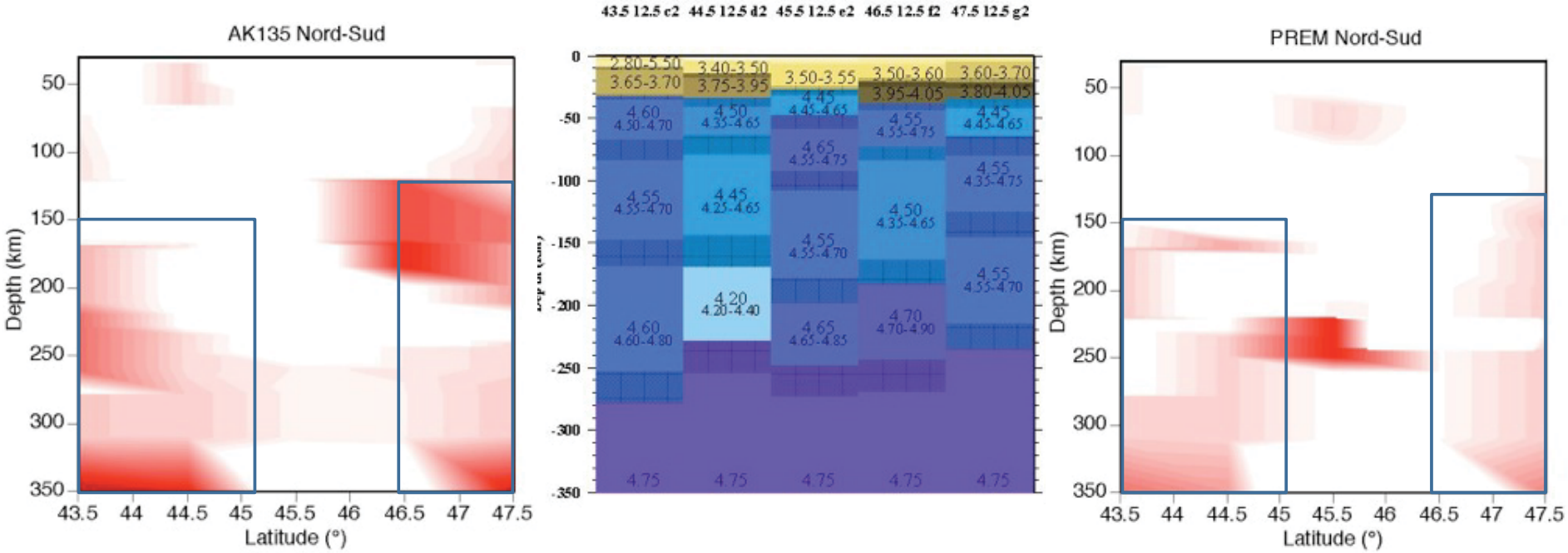

AK135 – PREM Comparison (II)

- **e-4:** both models reveal a thermal anomaly (but at different depths)
- **e-3:** anomaly revealed by AK135 involves almost the whole column; PREM involves part of LID and of asthenosphere
- **e-2:** both models reveal two anomalies in the asthenosphere (more evident for AK135)
- **e-1:** both models reveal two anomalies (more evident for AK135)
- **e0:** PREM reveals two anomalies in the LID and in the asthenosphere near LVZ; AK135 reveals only one in the upper asthenosphere and a much deeper one
- **e1:** both models reveal a thermal anomaly in the asthenosphere
- **e2:** only PREM reveals anomalies

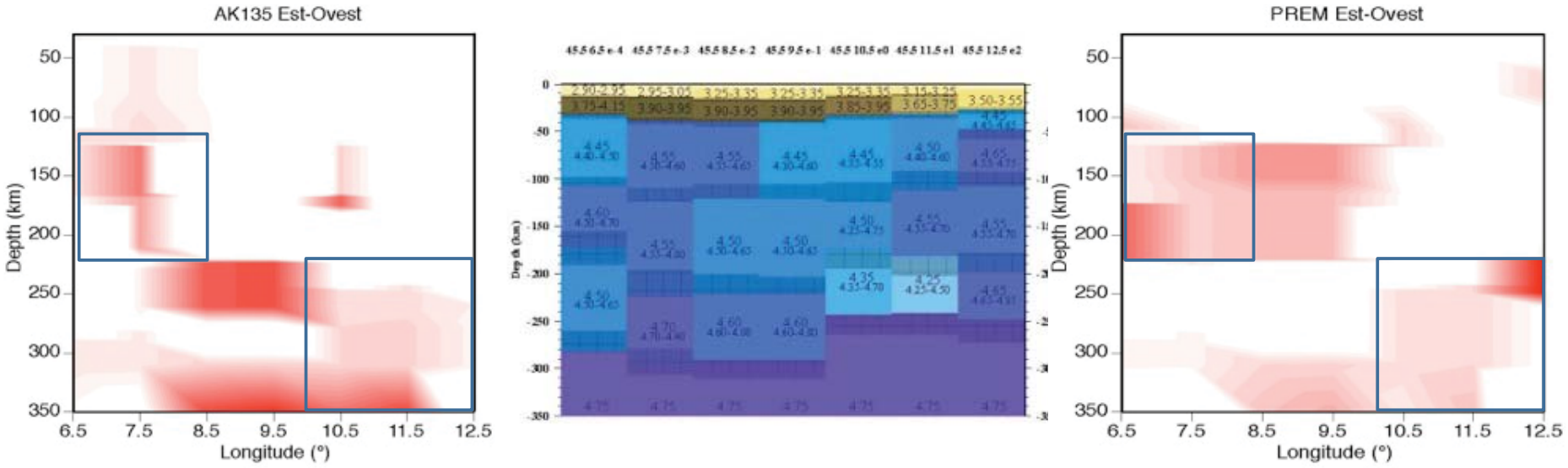

Lithosphere density model

- The velocity structure obtained through nonlinear inversion of dispersion curves and the smoothing optimization method to choose the representative cellular model, whose layering is used as fixed (a priori) information to obtain a density model by means of linear inversion of gravimetric data.

- Seismicity and heat flow are used as independent constraints in outlining both the crustal and the seismic lid thickness; the nonlinear moment tensor inversion of recent damaging earthquakes allows some insight in the ongoing kinematic processes.

- Asymmetry between west-directed (Apennines) and east-directed (Alps, Dinarides) subductions is a robust feature of the velocity model, while density model reveals that slabs are not denser than the ambient mantle, thus supplies no evidence for slab pull.

Brandmayr et al., 2011

Lithosphere density model

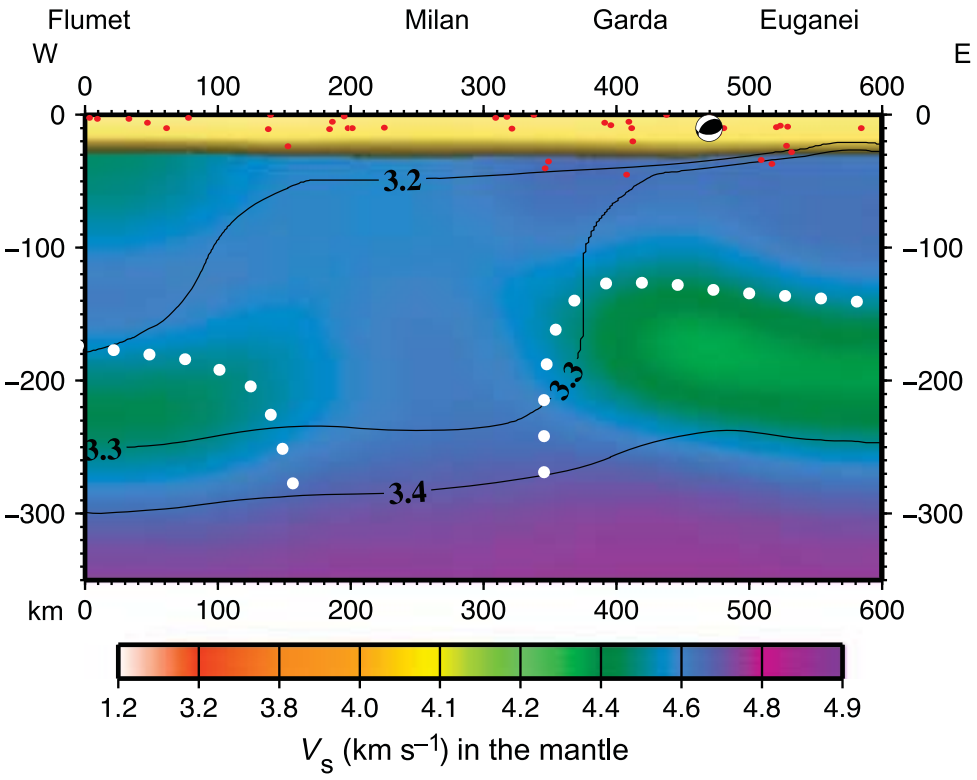

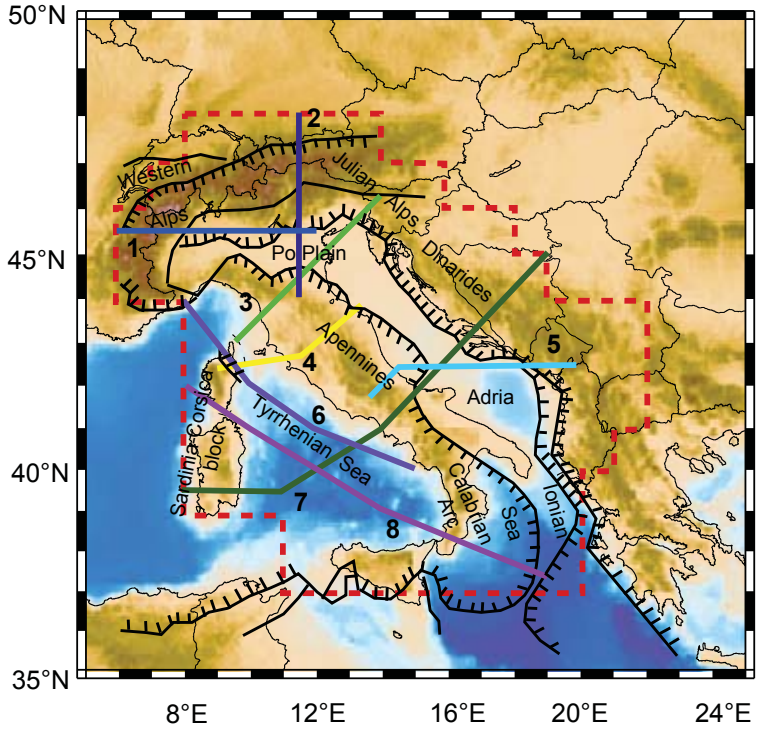

1. Ecors section: Flumet (western Alps) to Euganei Hills.

Striking feature of the section is the subduction of the European plate below the Adriatic plate, with deep Ôlithospheric rootsÕ below Milan, represented by high-velocity lid, well in agreement with what was shown by Mueller and Panza (1986). In contrast to Apennines subduction, no intermediate depth seismicity is observed in western Alps. To the West the LVZ is found at a depth of about 180 km. To the East, a prominent LVZ marks the Euganei Hills magmatic zone below a depth of about 130 km. The subducting lid is characterized by negative density anomaly, whereas a positive density anomaly is seen beneath Euganei Hills, as shallow as 30 km.

Lithosphere density model

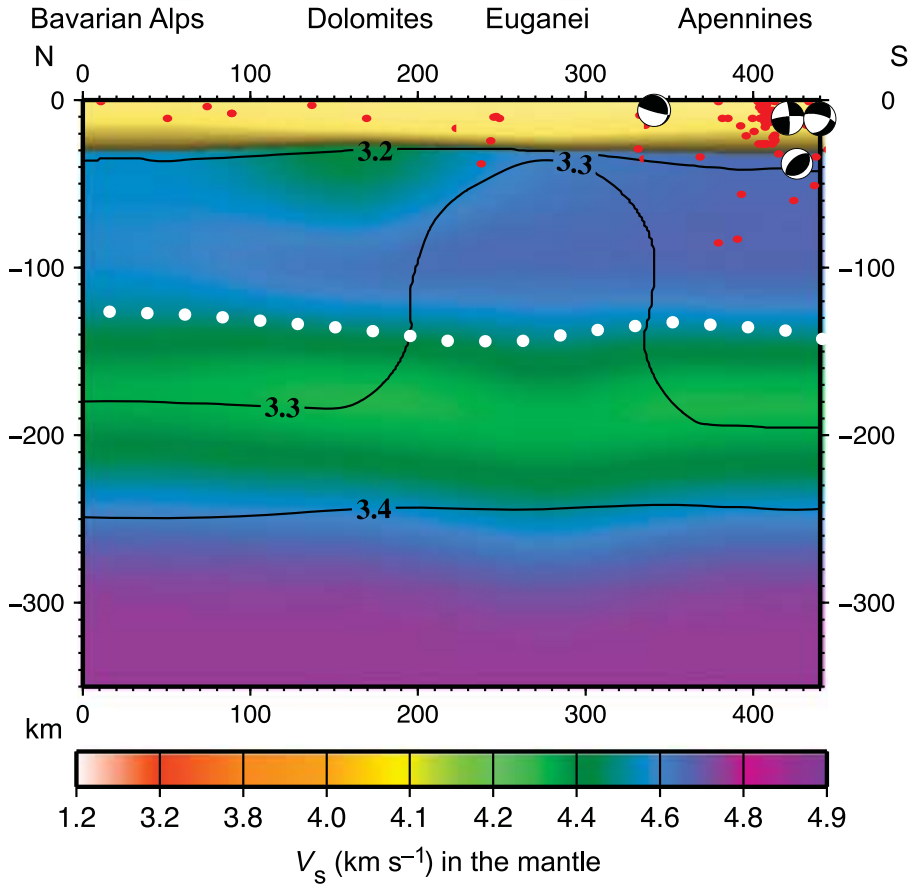

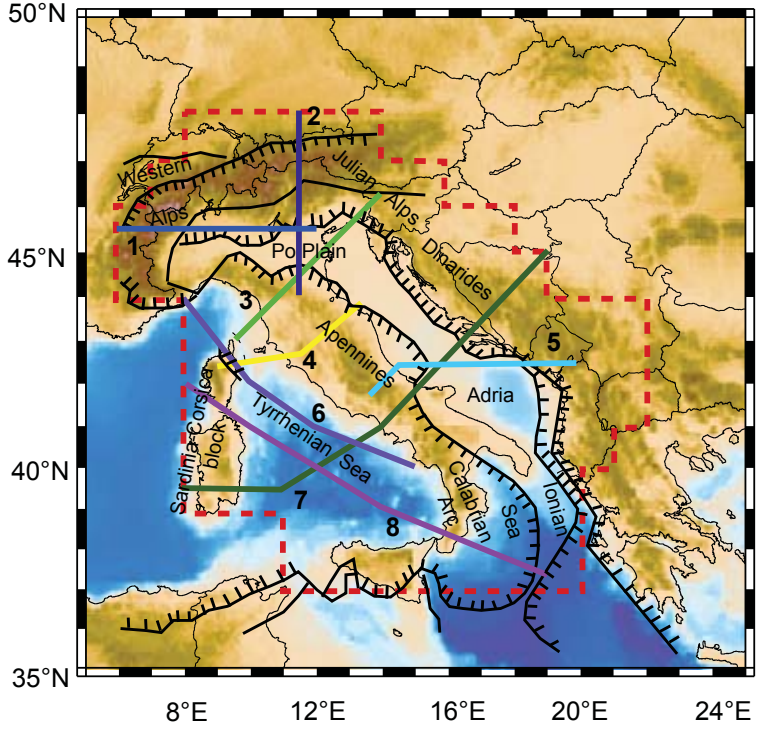

2. Transalp section: from Bavarian Alps to Apennines

The low-angle subduction of the European plate below the Adriatic plate is fairly well evidenced by gently N–S dipping high-velocity lid and in accordance with scarce shallow seismicity and almost absent intermediate depth seismicity, as seen in Ecors section. A relatively low velocity lid is found beneath Dolomites, just below the Moho. The bottom of the lid is found at about 120–140 km of depth and overlies a well-marked LVZ in the asthenosphere. In the southernmost part of the section, Apennines subduction is delineated by high seismicity that reaches intermediate depth. The prominent high- density body, as shallow as 40 km of depth, below Venetian plain, may be a signature of the Euganei Hills magmatic activity.

Lithosphere density model

- The asymmetry between E-verging and W-verging subduction zones, clearly evidenced by VS model, sup- ports the hypothesis of an eastward mantle flow, especially in the LVZ, between 120 and 200 km of depth, that is likely to represent the decou- pling between the lithosphere and the underlying mantle at global scale (Panza et al., 2010).

- The flow is very shallow in the active Tyrrhenian basin due to mantle compensation induced by the eastward migration of the Apennines subduction. High densities (>3.3 g cm)3) in the mantle seem to be strictly related to the eastward flow itself and to its ascent beneath the back-arc basin or to other extensional tectonics or to volcanism.

- On the contrary, slabs are not denser than the ambient mantle, but they appear to be slightly lighter; this evidence conflicts with the concept of "slab pull" and thus calls for different actors in subduction dynamics (e.g. Doglioni et al., 2007).

Seismic sequence January 2012

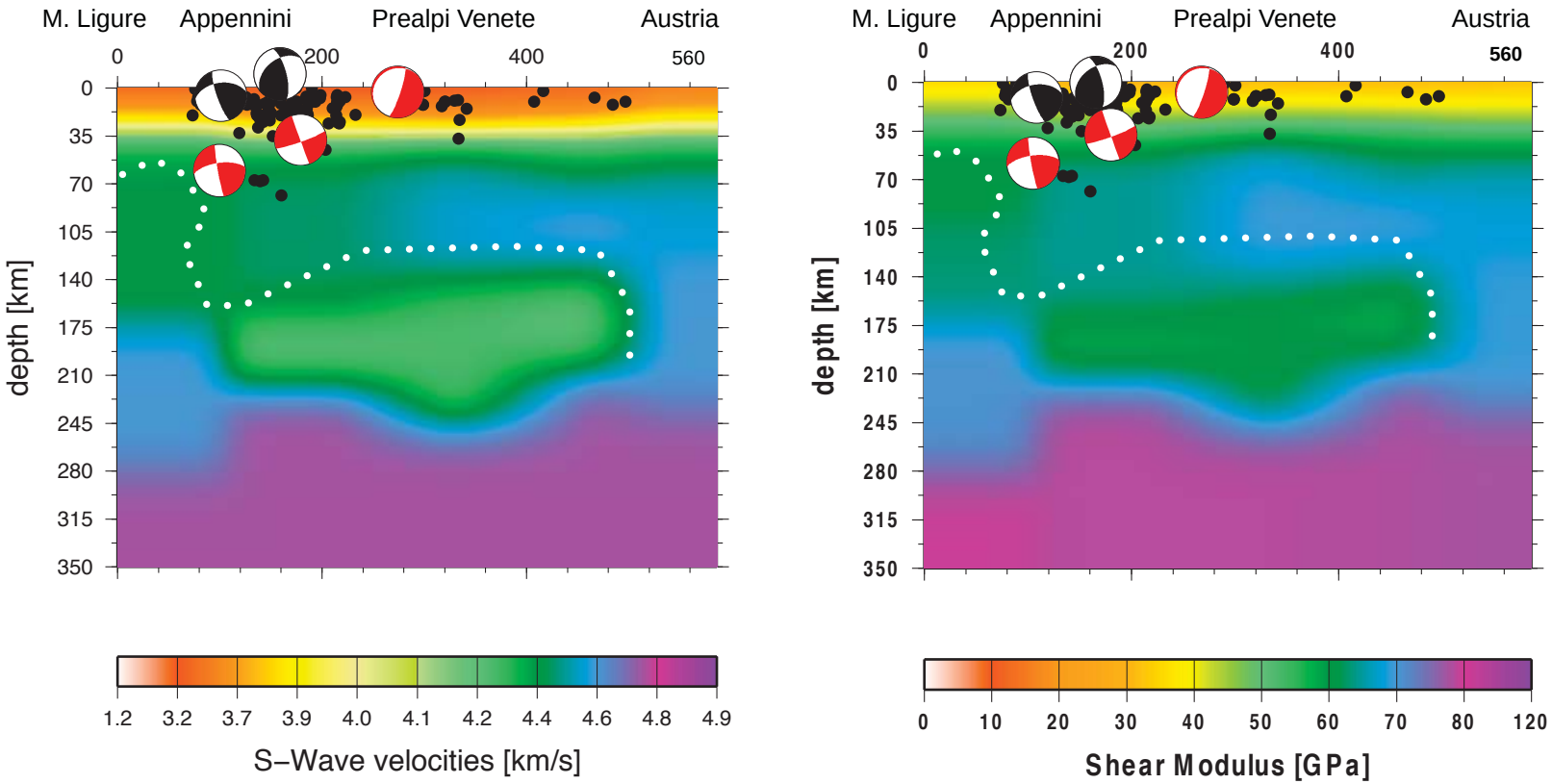

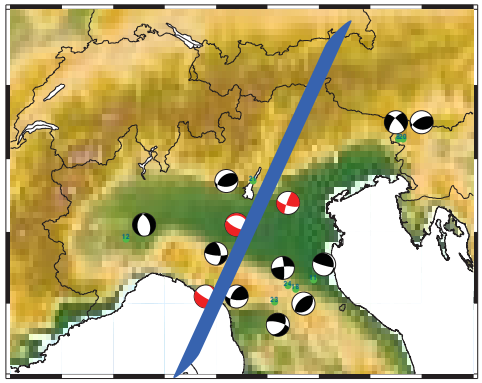

Courtesy of E. Brandmayr

http://140.105.54.18/geoweb/index.php

Seismological web-based data application

Seismic sequence January 2012

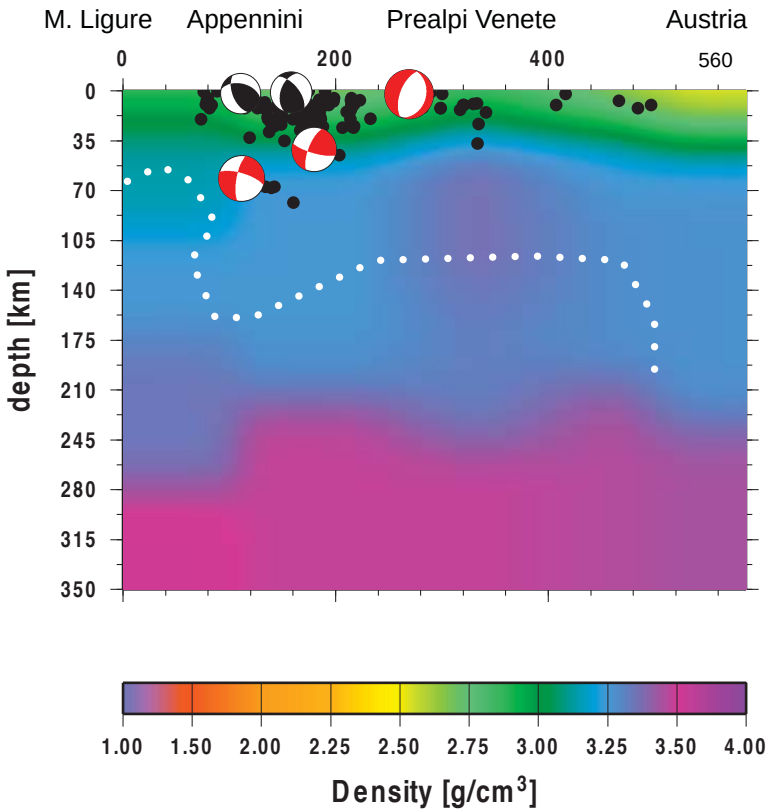

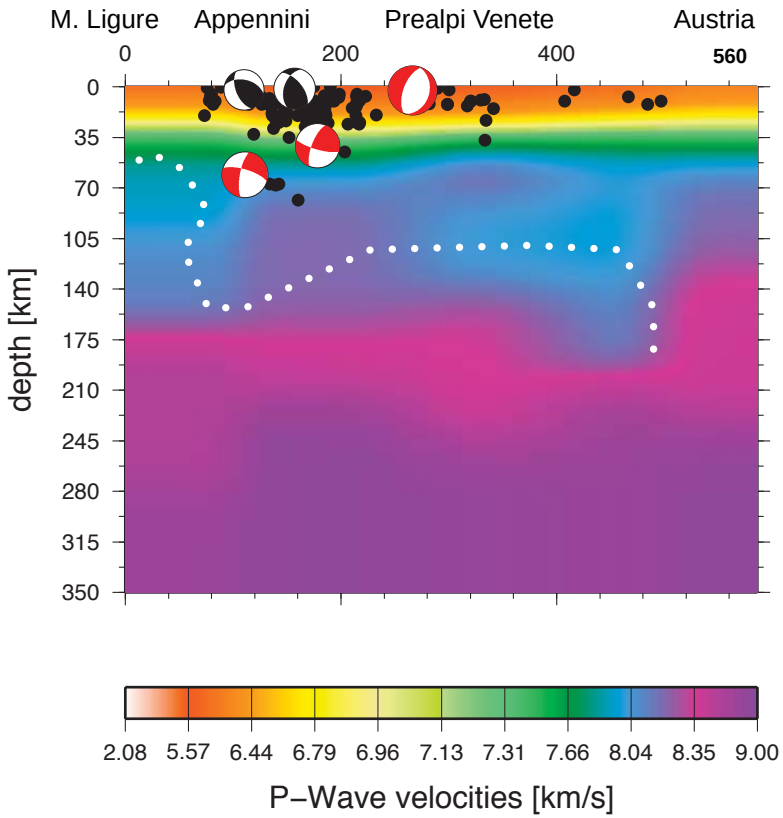

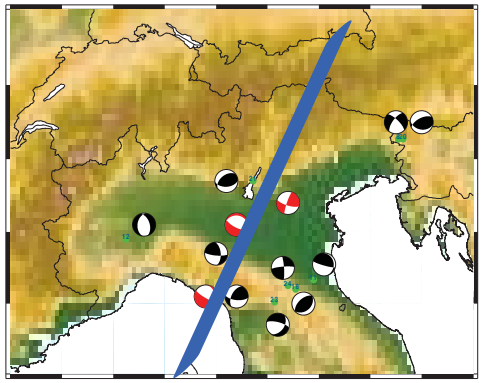

Courtesy of E. Brandmayr

http://140.105.54.18/geoweb/index.php

Seismological web-based data application

Road map

- Methodology:
  - Surface wave dispersion analysis
  - Surface wave tomography
  - Non linear inversion of dispersion data
- Cellular models for the lithosphere-asthenosphere system
  - Optimization techniques
  - Scale level I: 1°x1° cells in the whole Italian region
  - Adding other geophysical constraints
  - Selected sections and geodynamic modelling
- Possible applications
  - Joint inversion
  - Seismic hazard studies

Joint inversion

- Surface waves provide valuable information on the absolute S-wave velocity (Vs) but are relatively insensitive to sharp vertical velocity contrasts.
- On the other hand, Receiver Functions are sensitive to S-wave velocity contrasts, which give rise to converted phases, but allows for substantial trade-off between the depth and velocity above an impedance change.
- Combining both kind of information in a joint inversion fills the resolution gaps associated with each individual data set

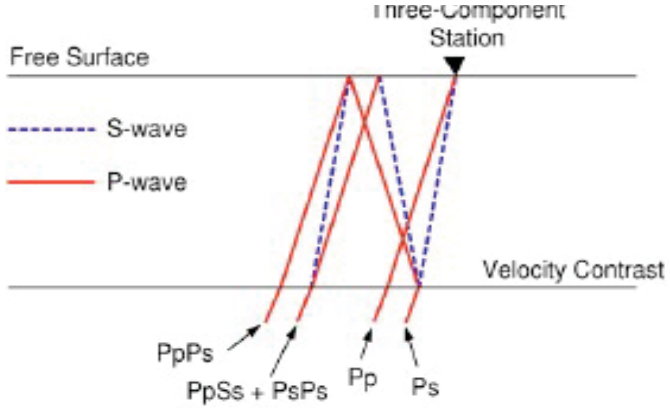

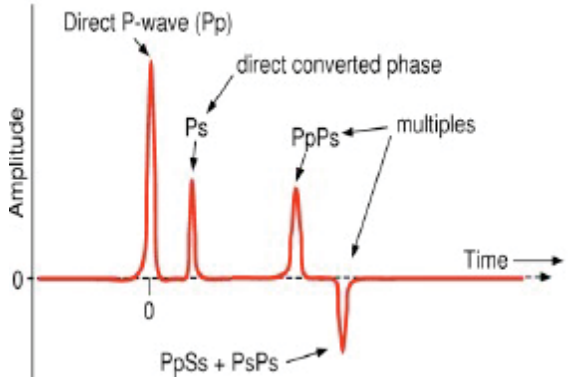

RF are time-series computed from three-component body-wave seismograms and sensitive to the earth structure below the receiver. They are computed deconvolving the vertical component of the selected earthquake signal from the corresponding horizontal component. The main conditions to be satisfied by the seismic events to be selected at a given receiver are: epicentral distance ranging from 30^0 to 90^0 and a good signal to noise ratio.

Joint inversion

As starting models of the linear inversion procedure, we used the set of models determined by the non-linear inversion of the dispersion curves of the Caribbean region (Gonzalez et al. 2011) corresponding to the cells where the stations are located.

Such models were chosen because they fulfill the following conditions:

a) The stations are located in cells, with adequate resolution, for the study region of surface wave tomography made by Gonzalez et al., (2011).

b) These models are the solutions for the dispersion curves from a broad search of possible models.

c) Each model belonging to the set of the accepted solutions for one cell, differs from the others by at least $\pm \Delta Pi$ for one parameter Pi (thickness, Vs), where ΔPi is consistent with the resolving power of the dispersion data, as described by Panza, (1981).

d) They minimize the drawbacks intrinsic in the linearization of a non-linear inverse problem.

Joint inversion - Caribbean stations

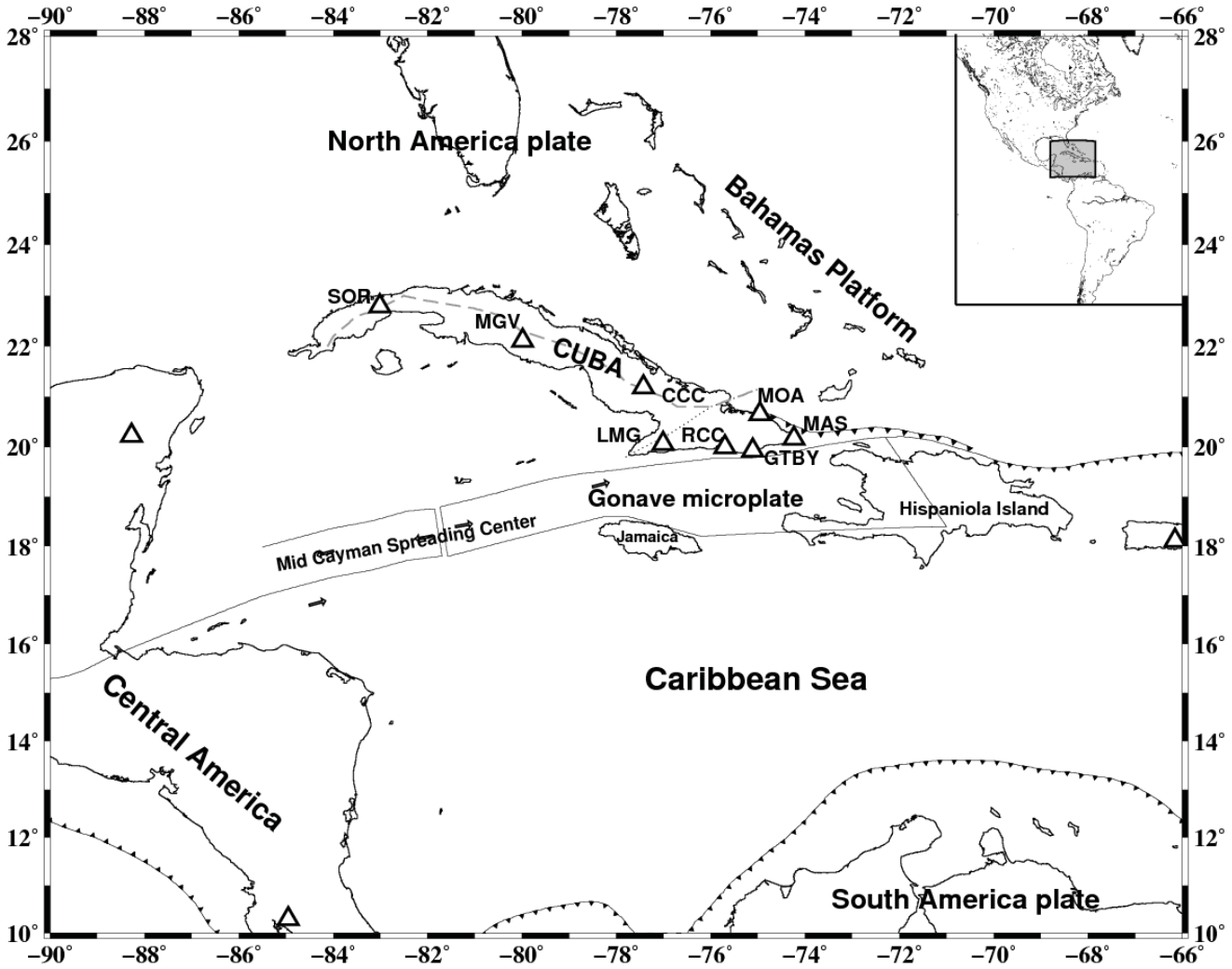

Location of seismic stations. Triangles represent the seismic stations used in this study; the dashed line represents the "Axial fault"; the dotted line represent the "Cauto Nipe fault"; barbed lines represent plate boundaries.

Gonalez et al., 2012

Joint inversion - Cascorro station

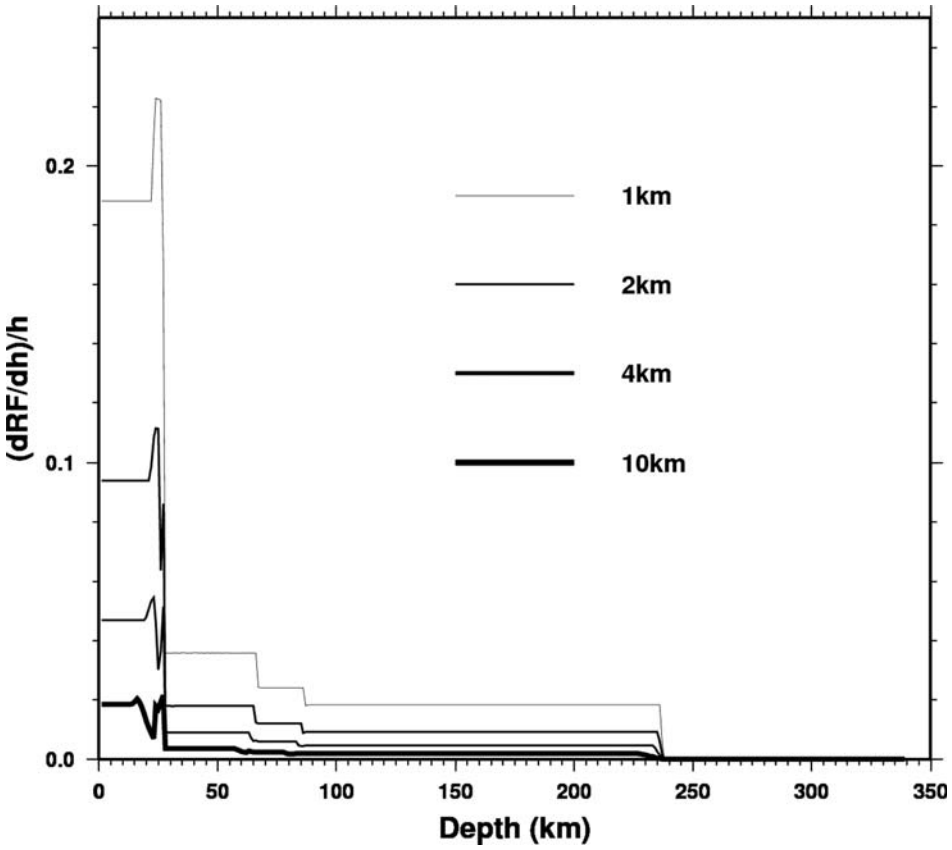

The layering of the initial models is consistent with the resolving power of the surface wave data but, in order to determine the optimum layering for the RF data, the partial derivatives of the RF with respect to the thickness of the layers (for values equal to 1, 2, 4, and 10 km) until the (final) depth of 350 km been calculated

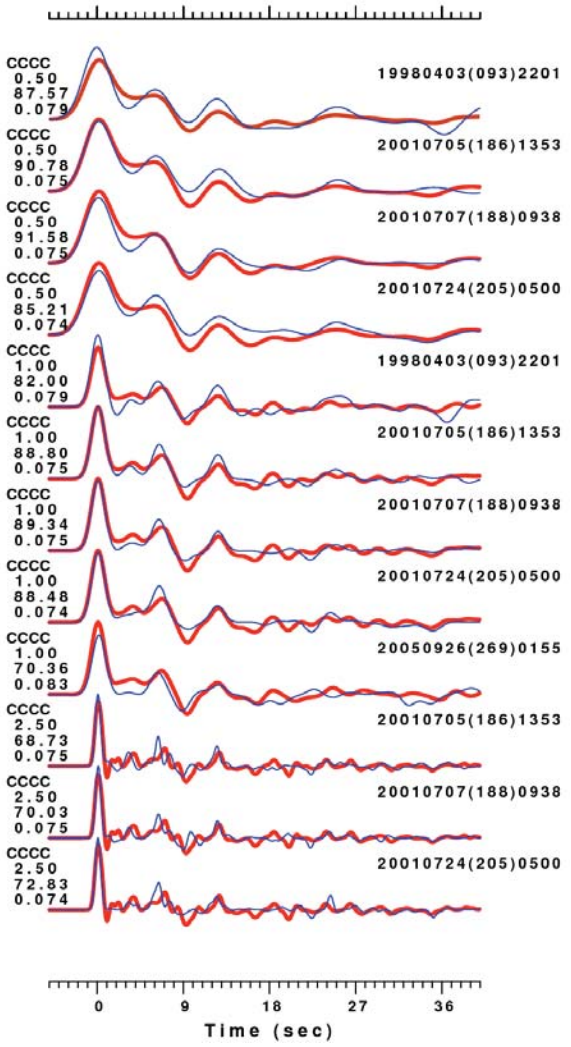

Example of fit for receiver functions in Cascorro station (CCC) resulting from the joint inversion (using Gaussian factors at 0.5, 1.0 and 2.5). Thin blue lines represent the experimental data and thicker red lines indicate the chosen solution corresponding to the best percent of fit (86%).

Gonalez et al., 2012

Joint inversion - Results

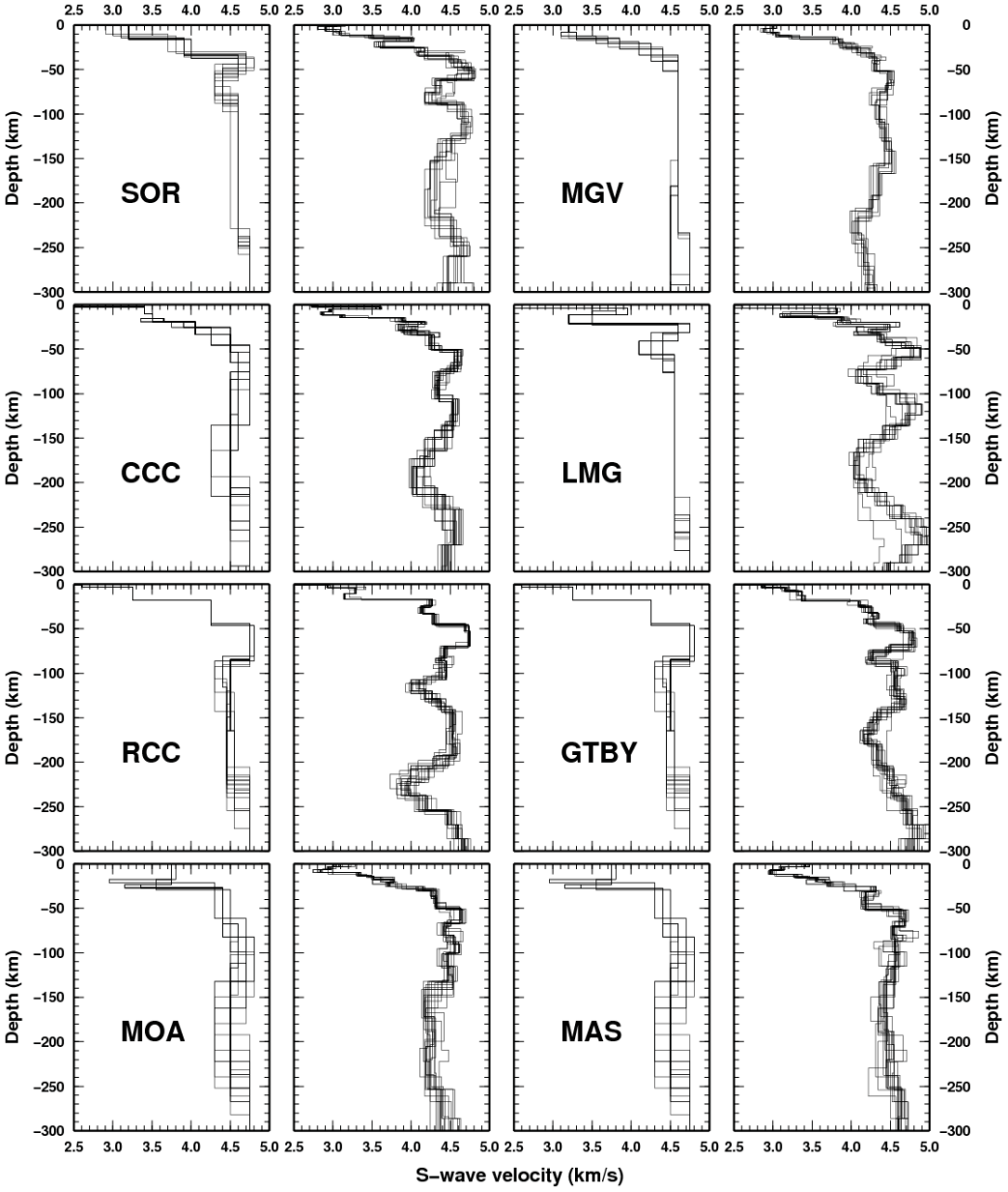

For each station, the initial models, from their corresponding cell of 2°x2° and final models, coming from the joint inversion procedure, are shown on the left and right side, respectively

Gonalez et al., 2012

Joint inversion - Chosen solution

The final model for each station is chosen according to the following two criteria:

(i) it is the solution with the best percentage of fit for the RFs, and

(ii) it corresponds to a dispersion curve whose difference with the experimental data at each period is within their corresponding experimental errors and the standard error with respect to observed group velocities

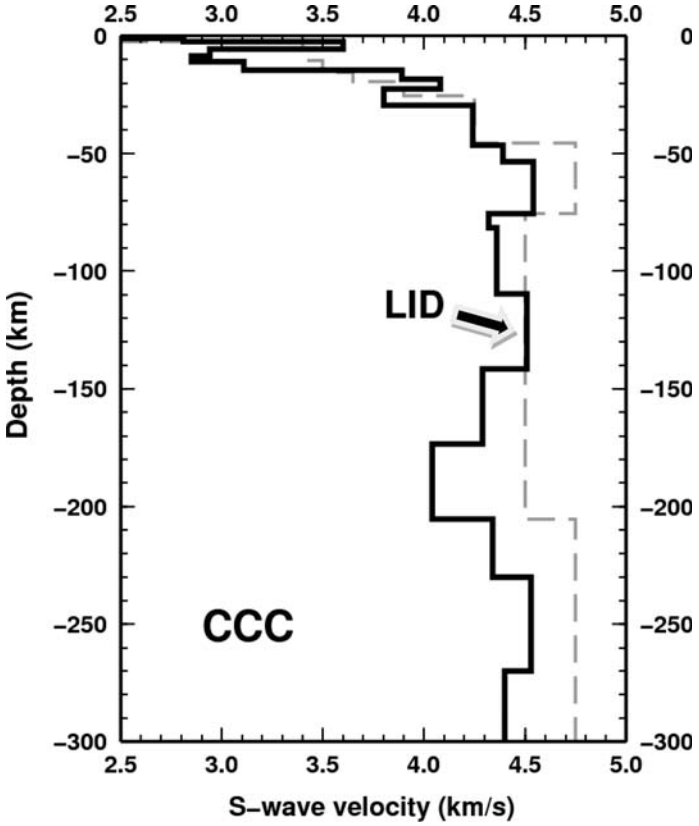

Chosen solution (thick solid black line) and initial model (gray dashed line) for Cascorro station (CCC), result of the joint inversion of RFs (using Gaussian factors at 0.5, 1.0 and 2.5) and dispersion data. The high velocity LID, centred at a depth of about 125 km, seems to reveal the presence of a subducted slab.

The resulting model for this station shows a crustal thickness of about 30 km, consistent with the values proposed by previous studies in the zone . In the crust, pronounced low velocity layers are present, which could be motivated by the obduction by earlier overthrusting of the Bahamas platform by the Cuban island arc; this feature, and a lithospheric thickness of ~75 km, are consistent with the presence of an accretionary type of crust. There is evidence of a subducted slab in the mantle, from ~110 to ~140 km depth.

Gonalez et al., 2012

Application to SHA: DGA

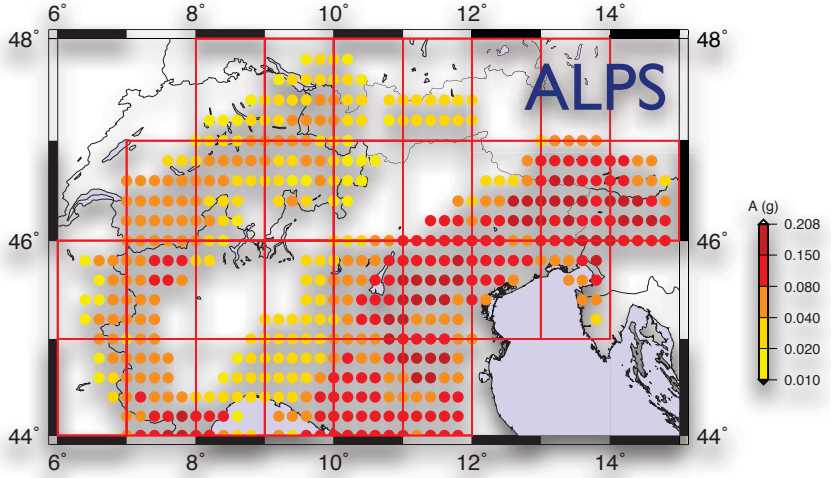

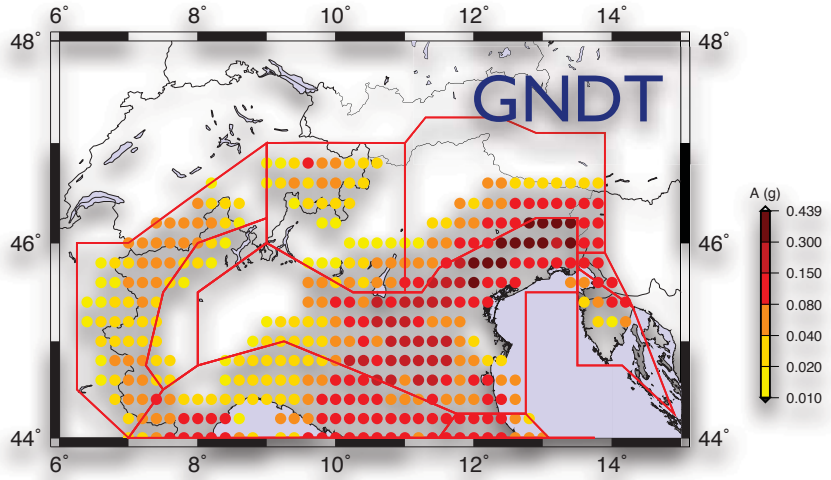

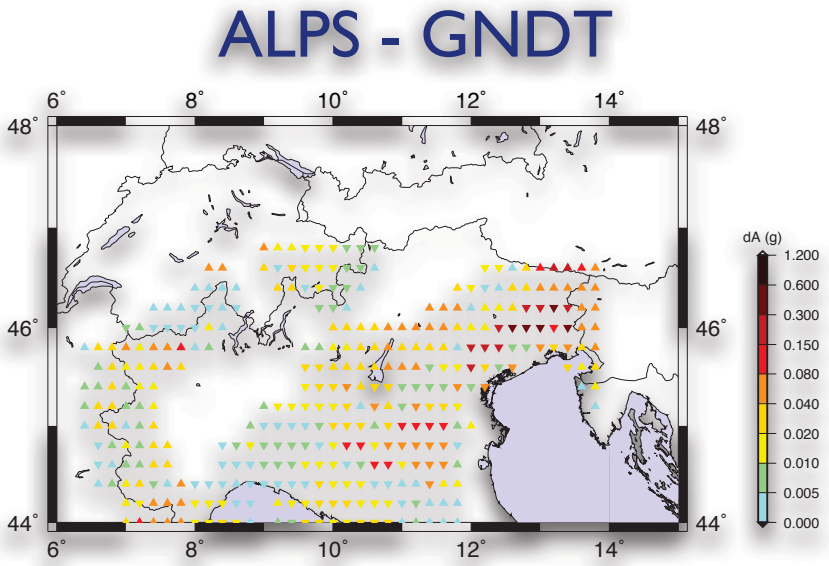

NDSHA - Multi scenario based - Regional scale

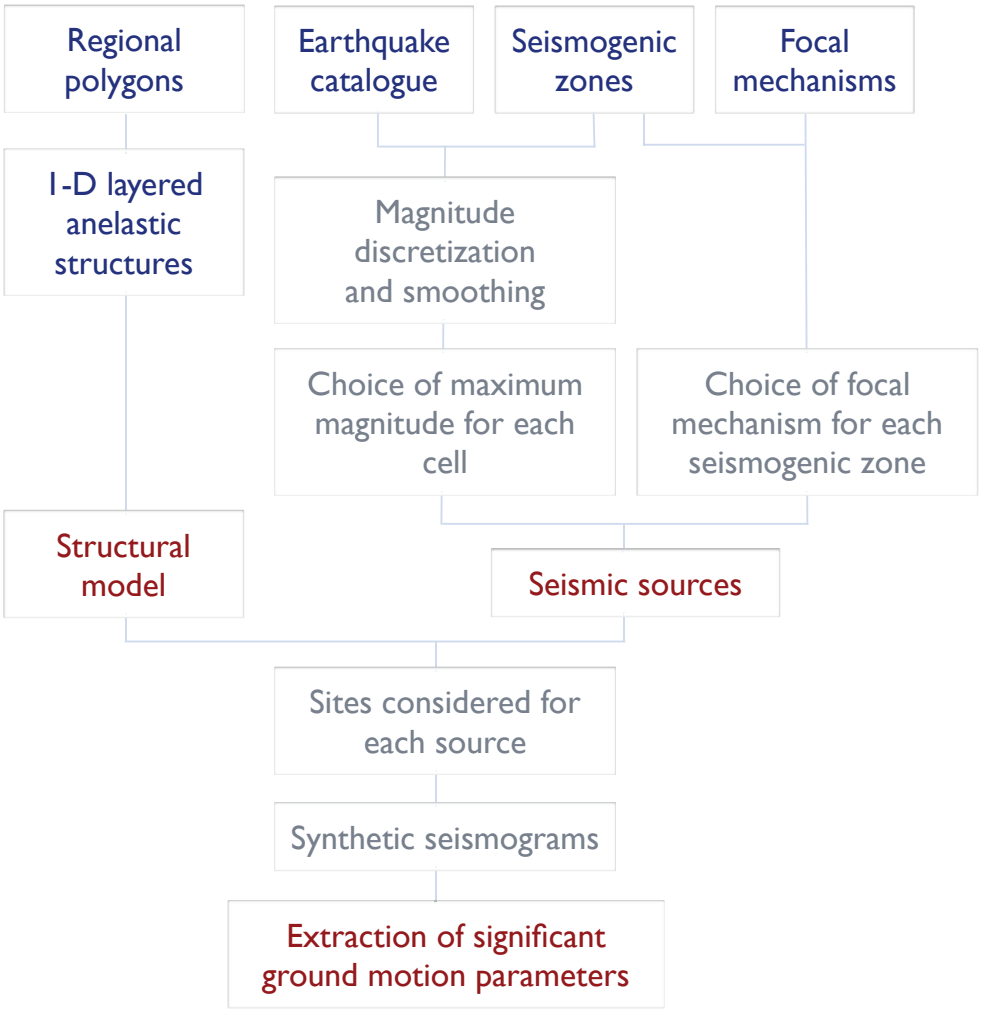

- Seismic zonation based on the computation of synthetic seismograms on the nodes of a grid that covers the study area
- Average structural properties
- Simple source model (scaled point source)
- Cut-off frequency 1 Hz
- Maps of peak displacement, velocity and Design Ground Acceleration

NDSHA - Multi scenario based - Structural models

Regional polygons

Earthquake catalogue

Seismogenic zones

Focal mechanisms

1-D layered anelastic structures

Magnitude discretization and smoothing

Choice of maximum magnitude for each cell

Choice of focal mechanism for each seismogenic zone

Structural model

Seismic sources

Sites considered for each source

Synthetic seismograms

Extraction of significant ground motion parameters

NDSHA - Multi scenario based - 1D models

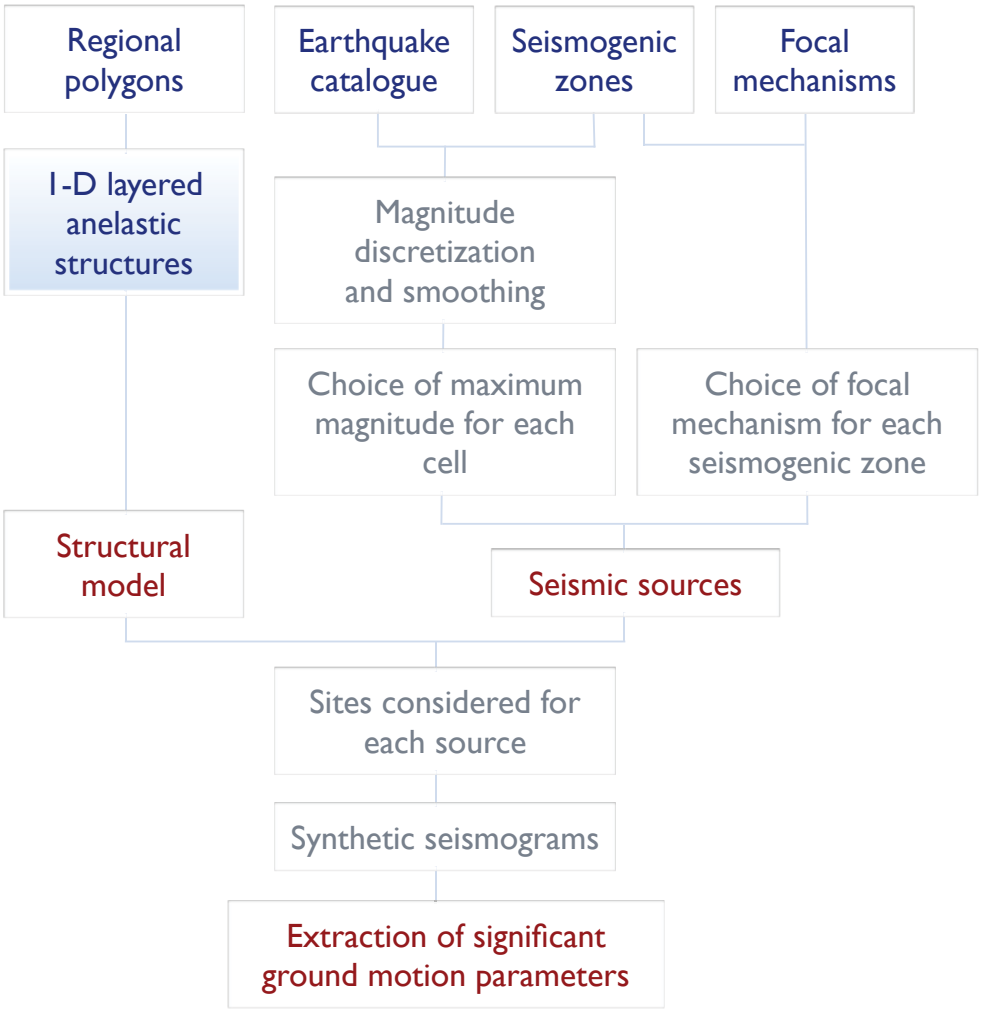

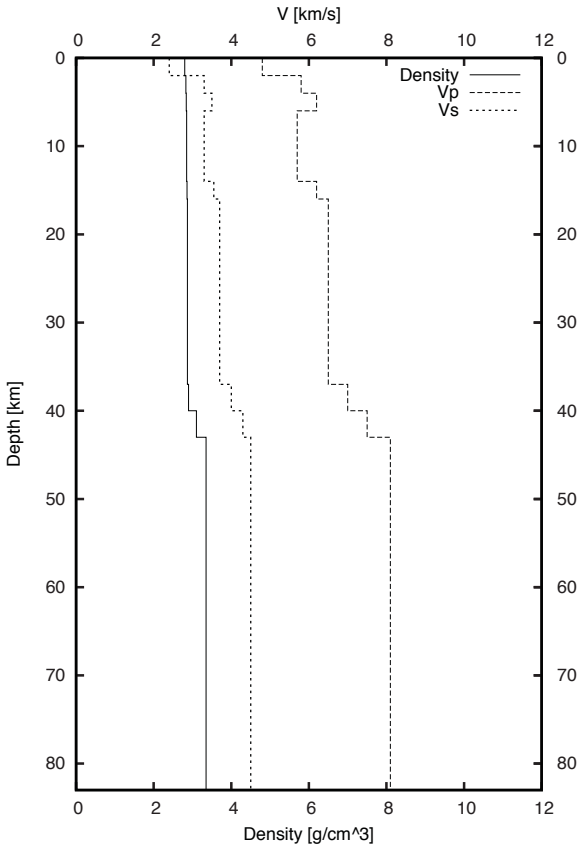

NDSHA - Multi scenario based - Historical seismicity

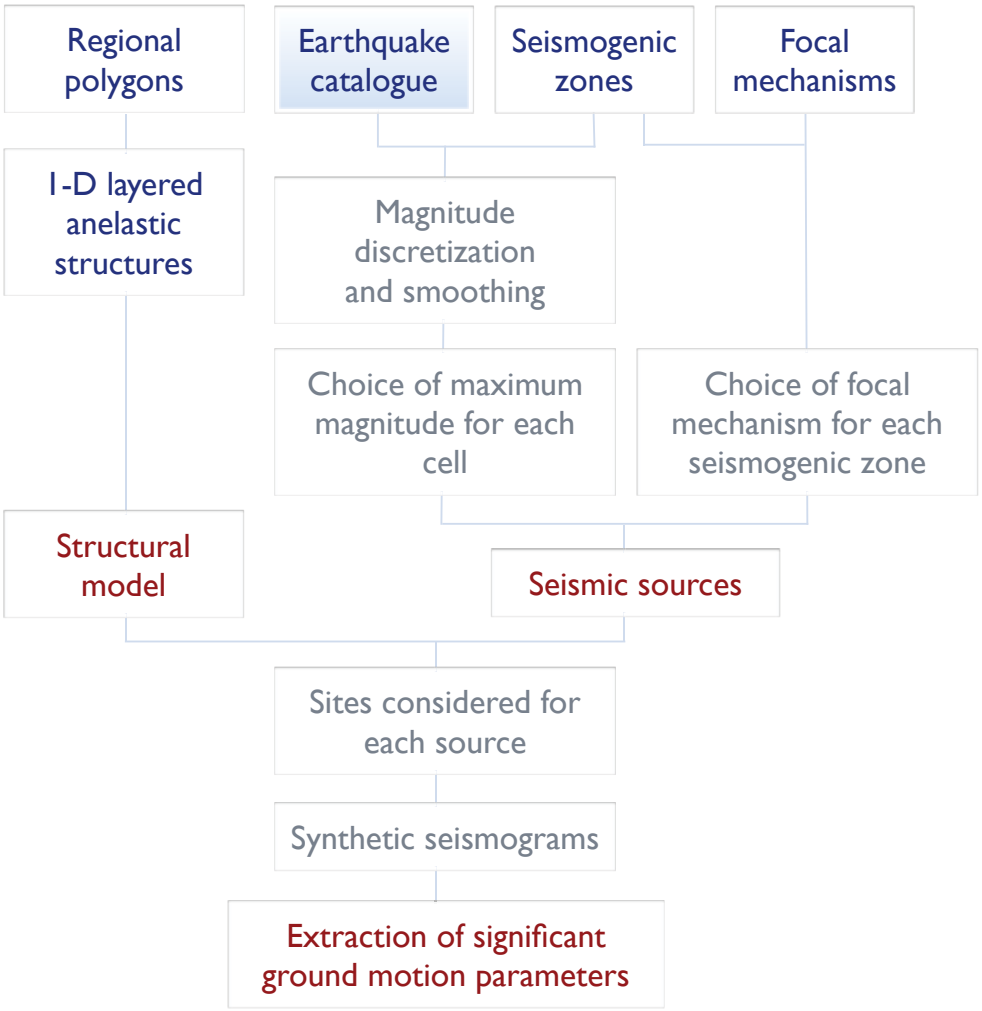

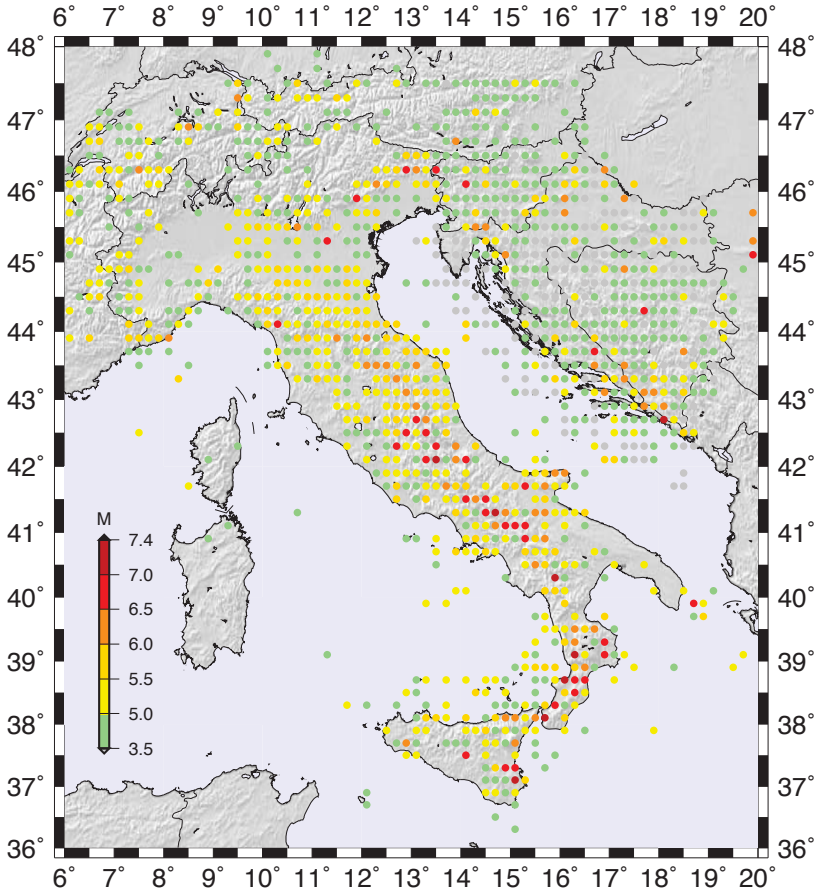

NDSHA - Multi scenario based - Tectonic setting

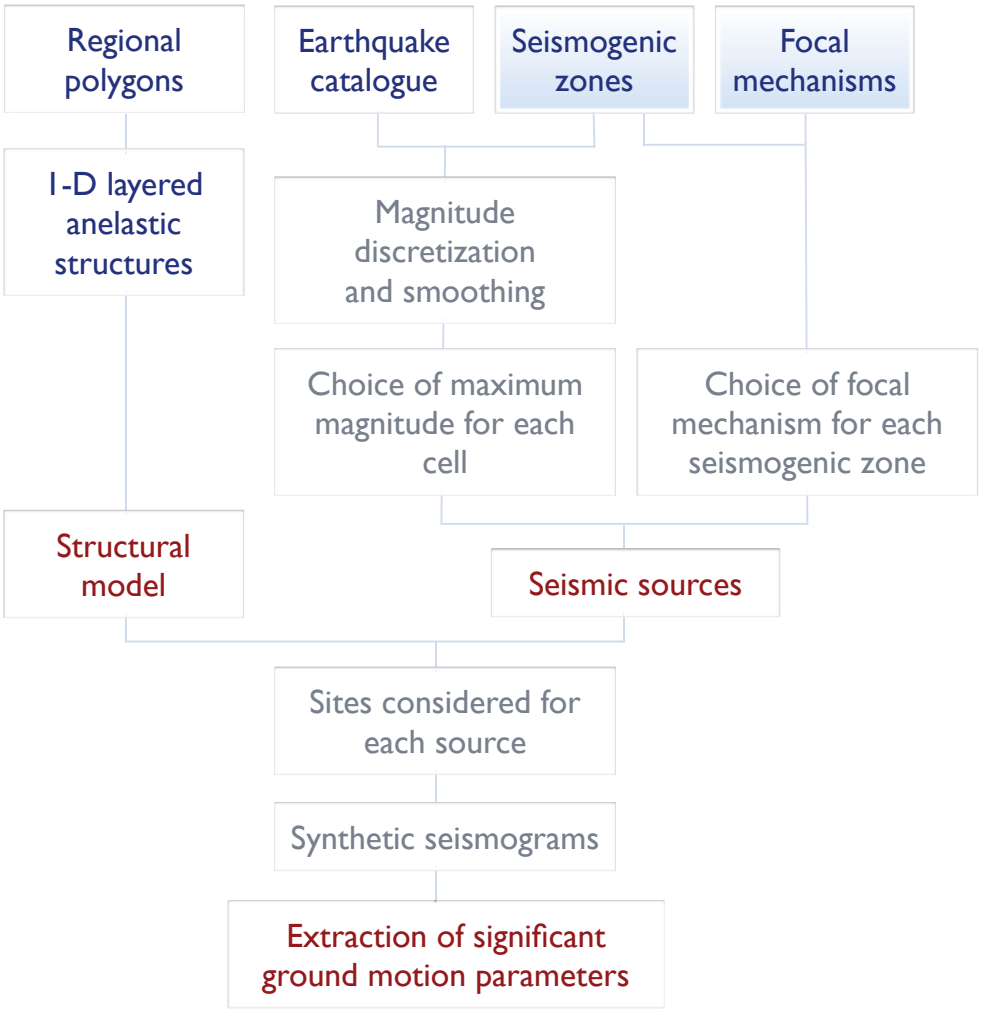

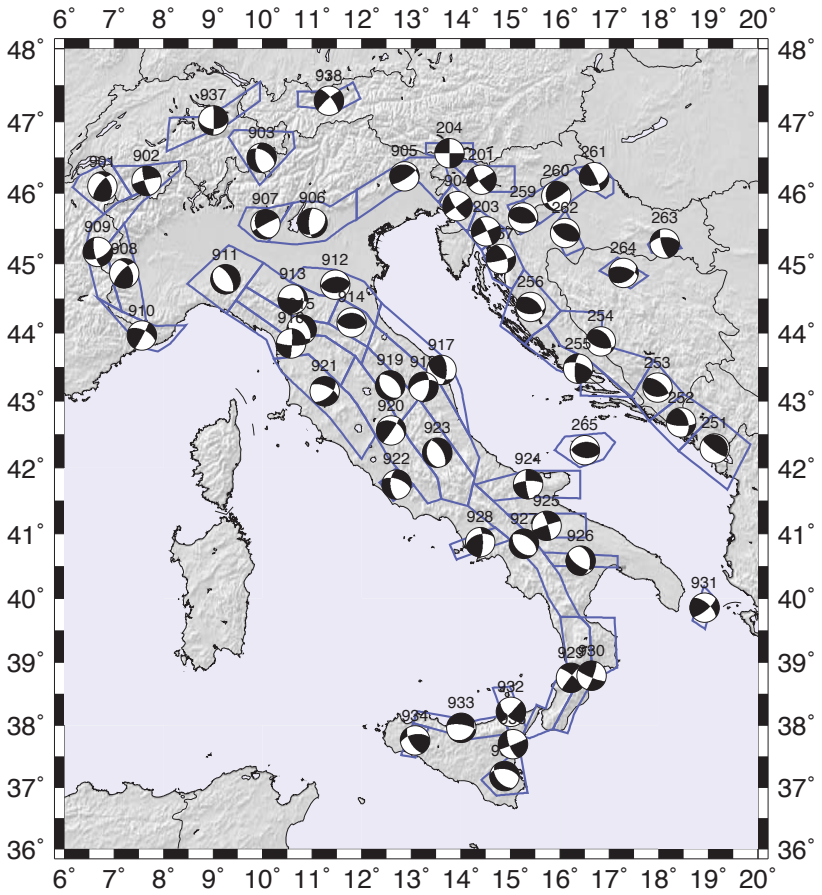

NDSHA - Multi scenario based - Signals

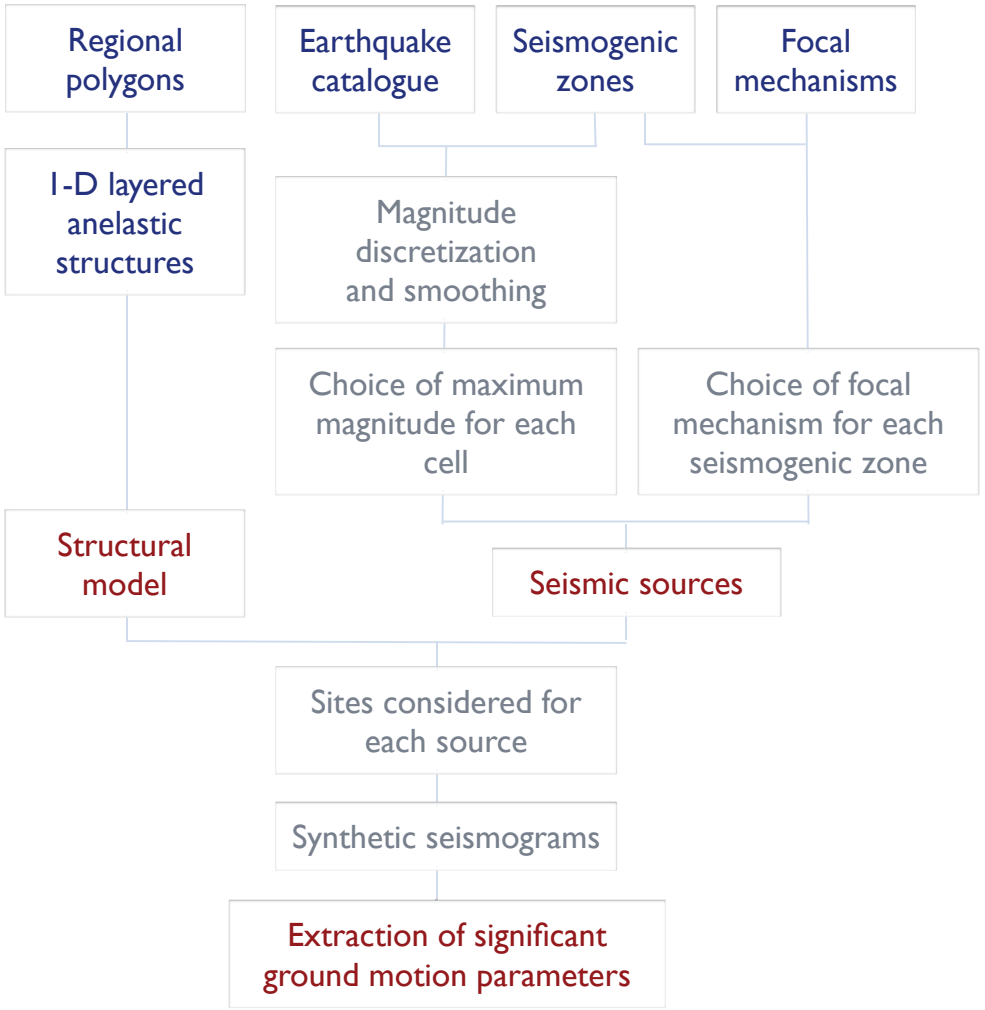

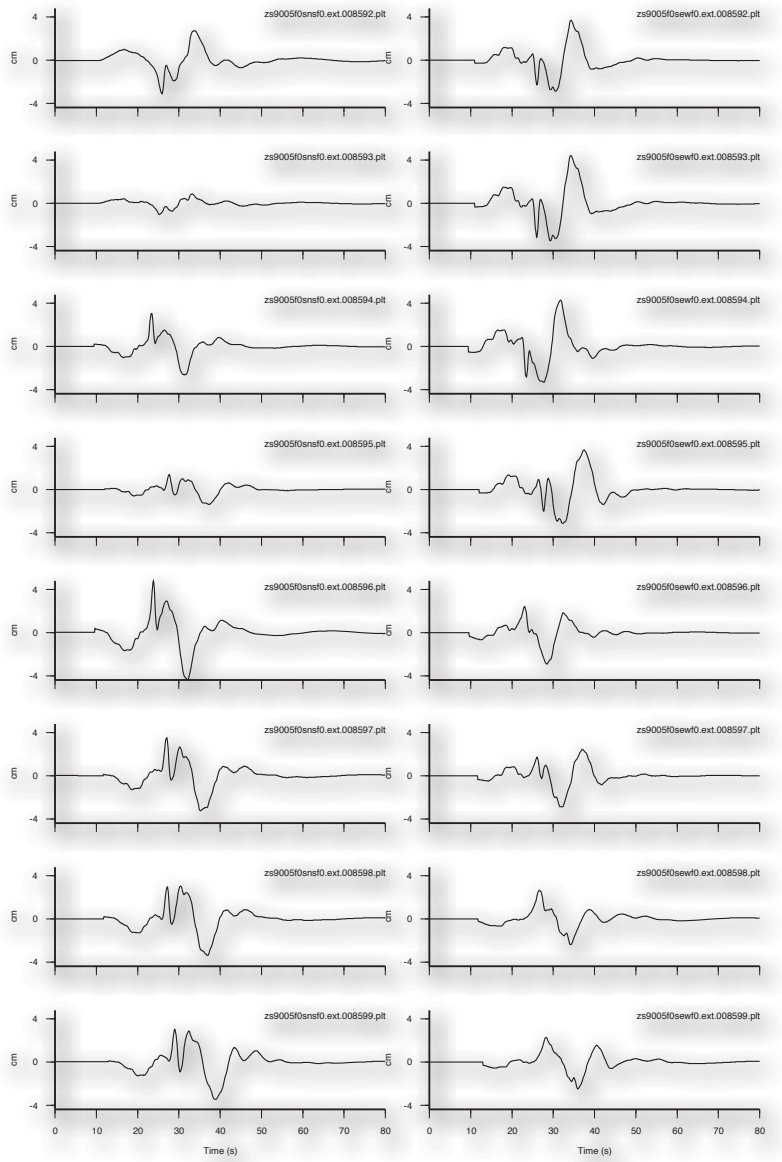

Displacement - Italy

Amplitude of Peaks from Time Series (1Hz)

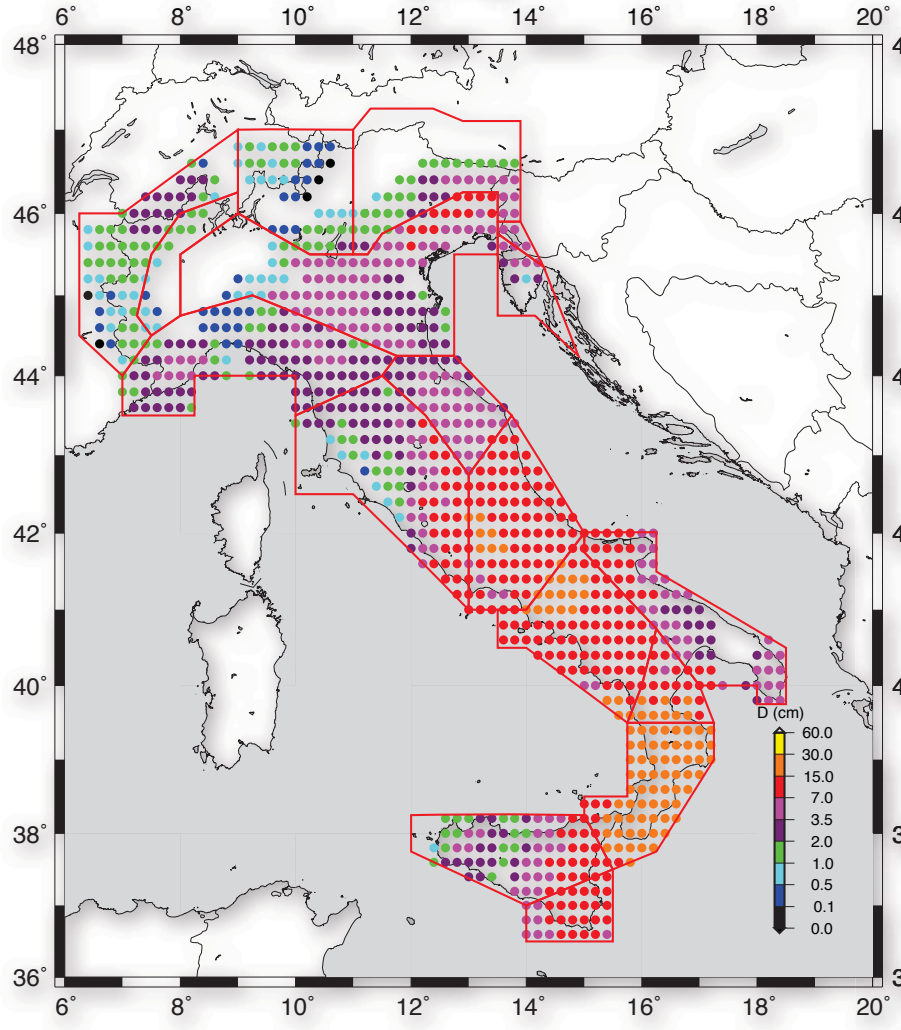

T of Peaks from Fourier Spectra

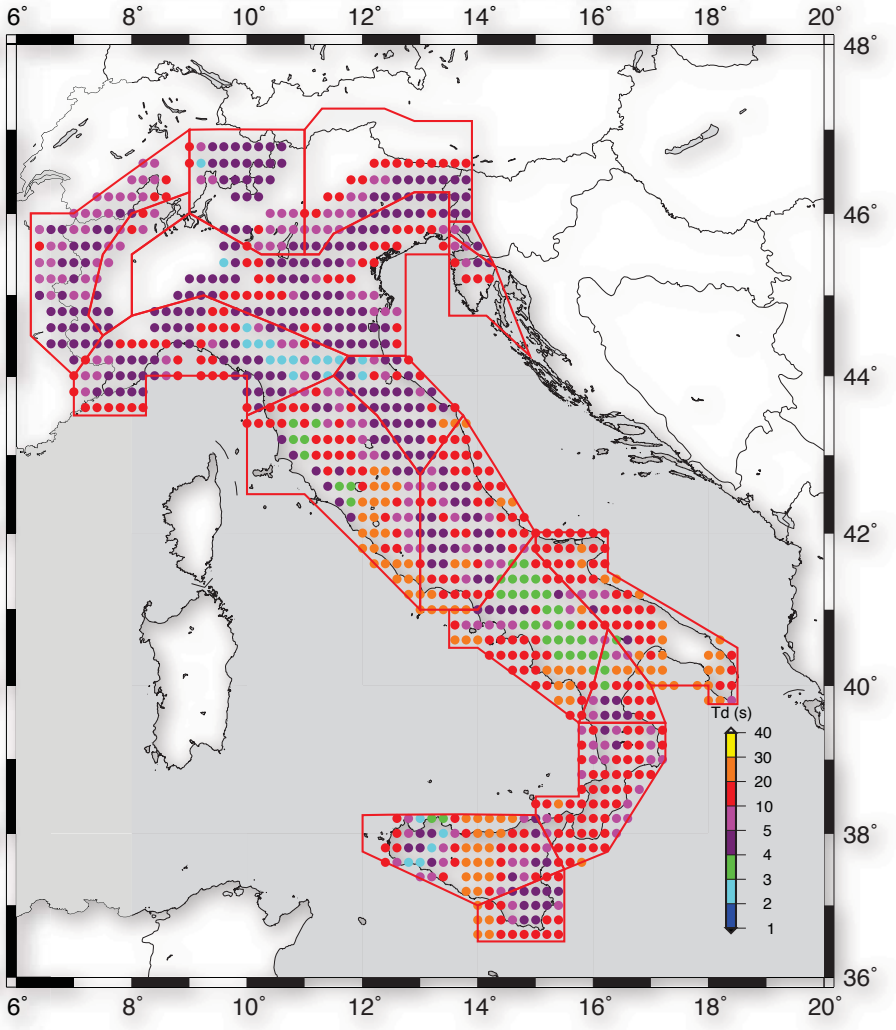

NDSHA - Multi scenario based - Structural models

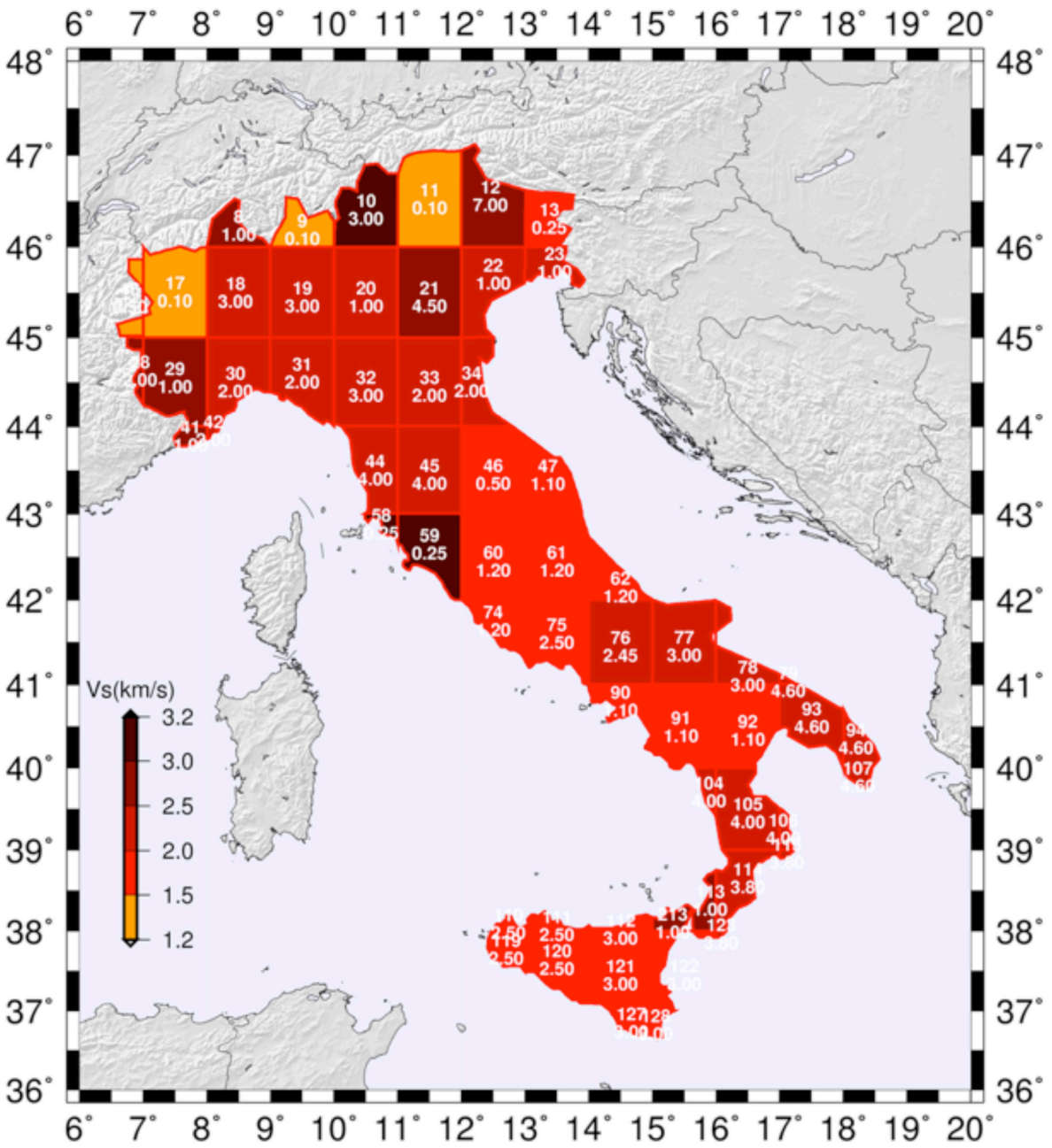

Displacement - Italy

Panza et al., 2012

References

Brandmayr, E., Raykova, R., Zuri, M., Romanelli, F., Doglioni, C., Panza, G. 2010. The lithosphere in Italy: structure and seismicity. In: (Eds.) Marco Beltrando, Angelo Peccerillo, Massimo Mattei, Sandro Conticelli, and Carlo Doglioni, Journal of the Virtual Explorer, volume 36, paper 1, doi: 10.3809/jvirtex.2009.00224.

Brandmayr E., Marson I., Romanelli F., Panza G.F., 2011. Lithosphere density model in Italy: no hint for slab pull. TERRA NOVA (ISSN:1365-3121), pp. 292- 299, Vol. 23/2011.

Boyadzhiev, G., Brandmayr, E., Pinat, T., and Panza, G.F., 2008. Optimization for non-linear inverse problems. Rendiconti Lincei 19, 17 – 43

Carminati E., Doglioni C. , Scrocca D., 2004. Alps Vs Apennines. Special Volume of the Italian Geological Society for the IGC 32 Florence-2004, 141-151.

Chimera, G., Aoudia, A., Saraò, A., and Panza, G.F., 2003. Active tectonics in Central Italy: constraints from surface wave tomography and source moment tensor inversion. Phys. Earth Planet. Int., 138, 241-262.

Eaton DW, Darbyshire F, Evans RL, Grütter H, Jones AG, Yuan X, 2009. The elusive lithosphere-asthenosphere boundary (LAB) beneath cratons, Lithos 109, 1-22, DOI:10.1016/j.lithos.2008.05.009.

González, O., Moreno, B., Romanelli, F. and Panza, G. F., 2012. Lithospheric structure below seismic stations in Cuba from the joint inversion of Rayleigh surface waves dispersion and receiver functions. Geophysical Journal International, 189: 1047–1059. doi: 10.1111/j.1365-246X.2012.05410.x

Kennett, Brian L.N., and Hans-Peter Bunge, 2008, Geophysical Continua, Cambridge University Press.

Levshin, A.L., Pisarenko, V.F., and Pogrebinsky, G.A., 1972. On a frequency time analysis of oscillations. Annales Geophysicae, 28: 211-218.

Panza, G.F., 1981. The resolving power of seismic surface waves with respect to crust and upper mantle structural models. In: The solution of the inverse problem in geophysical interpretation. Cassinis R. ed., Plenum Publ. Corp., 39-77.

Panza, G. F., Pontevivo A., Chimera, G., Raykova, R. and Aoudia, A., 2003. The Lithosphere-Asthenosphere: Italy and surroundings. Episodes, Vol. 26, n. 3, pp. 169-174.

Panza, G.F., Peccerillo, A., Aoudia, A., and Farina, B., 2007. Geophysical and petrological modelling of the structure and composition of the crust and upper mantle in complex geodynamic settings: the Tyrrhenian Sea and surroundings, Earth-Science Reviews, 80, 1-46.

Panza, G.F. and Raykova, R., 2008. Structure and rheology of lithosphere in Italy and surrounding. Terra Nova, Vol 20, No. 3, 194–199.

Panza G.F., La Mura C., Peresan A., Romanelli F., Vaccari F. (2012). Seismic Hazard Scenarios as Preventive Tools for a Disaster Resilient Society. Advances In Geophysics (ISSN:0065-2687), pp.93- 165, Vol. 53/2012.

Pontevivo A. and Panza, G.F., 2002. Group velocity tomography and regionalization in Italy and bordering areas, PEPI, 134, 1-15.

Pontevivo, A. and Panza, G.F., 2006. The Lithosphere-Asthenosphere System in the Calabrian Arc and surrounding seas – Southern Italy. PAGEOPH, 163 1617–1659.

Piromallo C., Morelli A., 2003. P wave tomography of the mantle under the Alpine-Mediterranean area. Journal of geophysical research, 108 (B2), 2065 – 2088.

Schmerr, N., (2012), The Gutenberg Discontinuity: Melt at the Lithosphere-Asthenosphere Boundary, Science, 335, 1480-1483.

Valyus, V.P., 1972. Determining seismic profiles from a set of observations. In: Computational Seismology. Keilis-Borok ed., Consult. Bureau, New-York, 114-118.

Yanovskaya, T.B. and Ditmar, P.G., 1990. Smoothness criteria in surface-wave tomography, Geophys. J. Int. 102, 63–72.

Zuri, M., 2009. Proprietà meccaniche cellulari della litosfera della regione italica, Tesi di Laurea in Geologia, Università degli Studi di Trieste.